

2443-27

**Winter College on Optics: Trends in Laser Development and Multidisciplinary
Applications to Science and Industry**

4 - 15 February 2013

Data capture and tomographic reconstruction of phase microobjects

M. Kujawinska
WUT
Poland



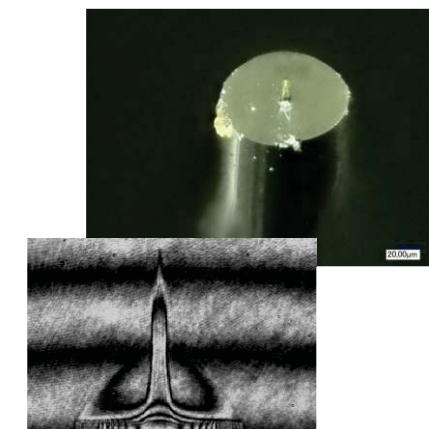
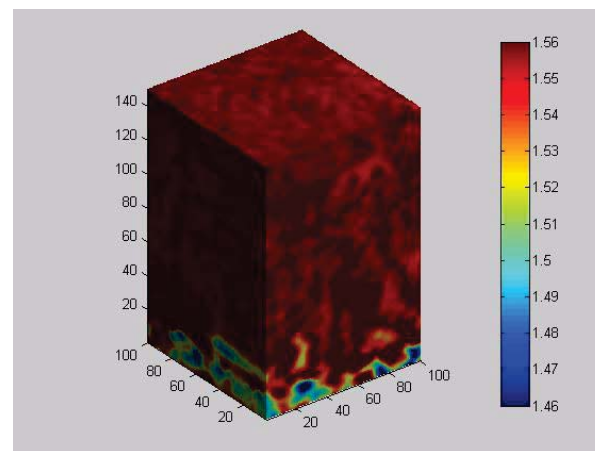
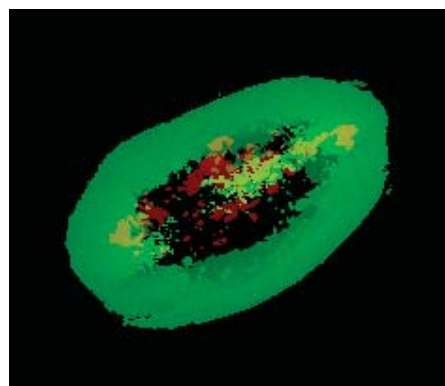
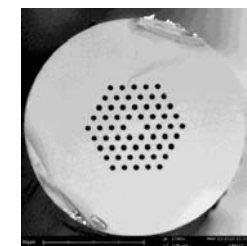
Winter College on Optics, ICTP, February 2013



Data capture and tomographic reconstruction of phase microobjects

M. Kujawińska

Warsaw University of Technology



INNOVATIVE ECONOMY
NATIONAL COHESION STRATEGY

FNP
Foundation for Polish Science

EUROPEAN UNION
EUROPEAN REGIONAL
DEVELOPMENT FUND





Outline

- Introduction: basic algorithms for tomography
- Tomography as the tool for investigation of internal structure of microelements
 - interferometric/holographic tomography
 - elastooptics tomography
- Diffraction tomography of biological microobjects - *tomorrow*



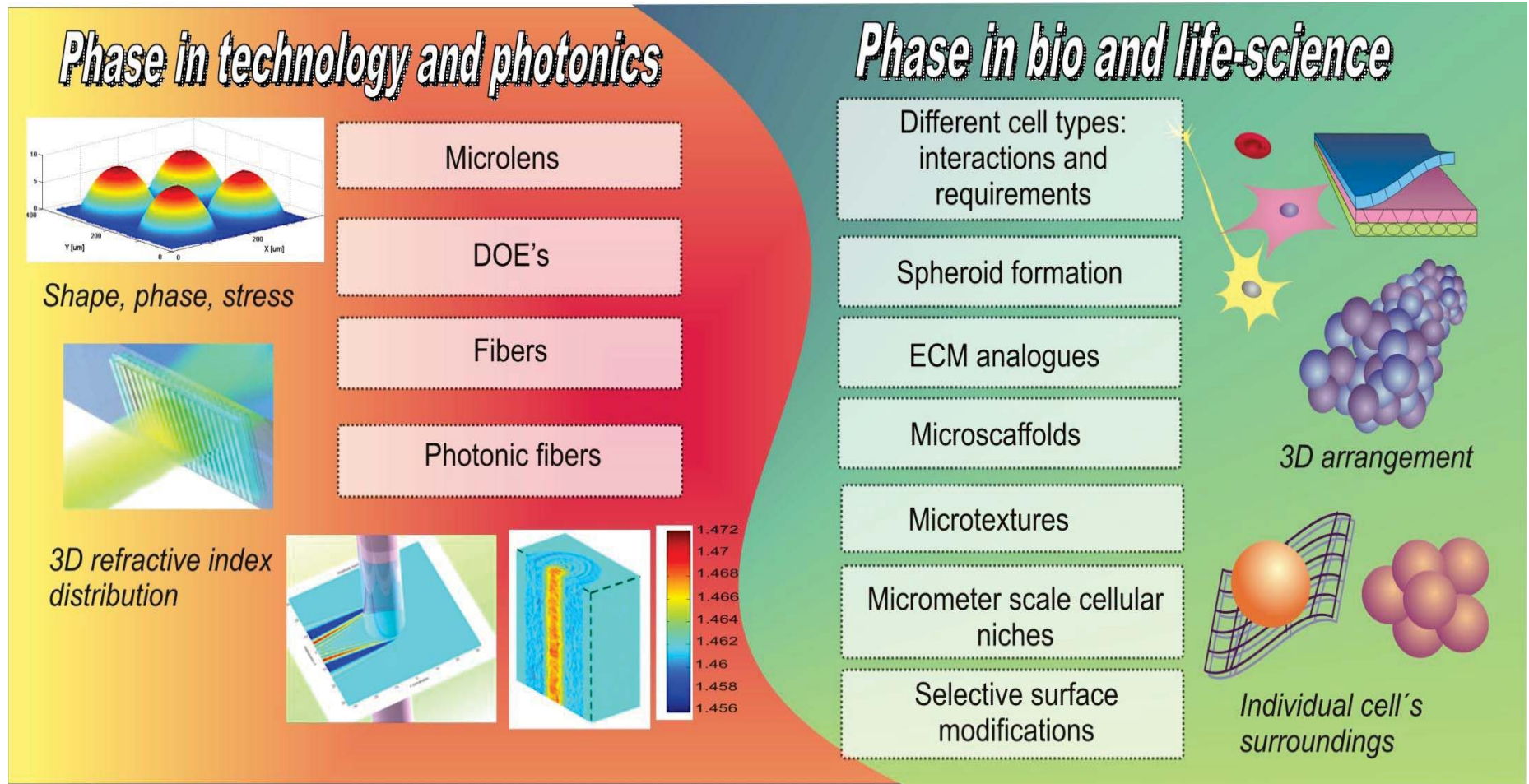
INNOVATIVE ECONOMY
NATIONAL COHESION STRATEGY



EUROPEAN UNION
EUROPEAN REGIONAL
DEVELOPMENT FUND

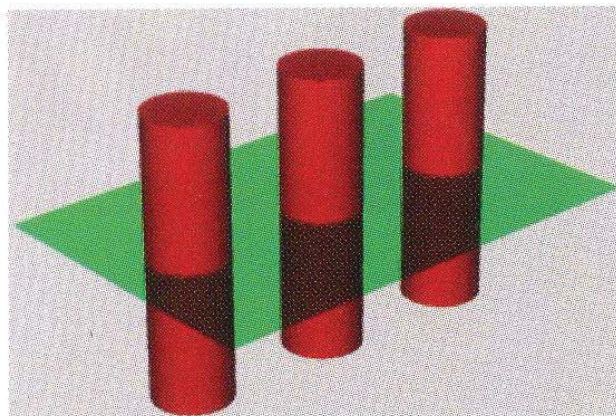


Phase information in technology and biology

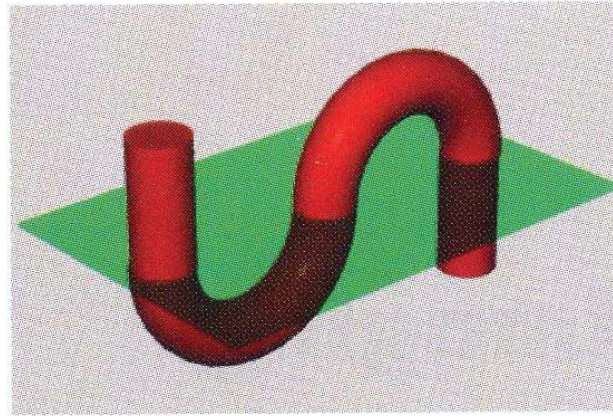


Objective for many research groups:
Develop tool for quantitative characterization of 3D and 4D phase
techno and bio samples in micro scale

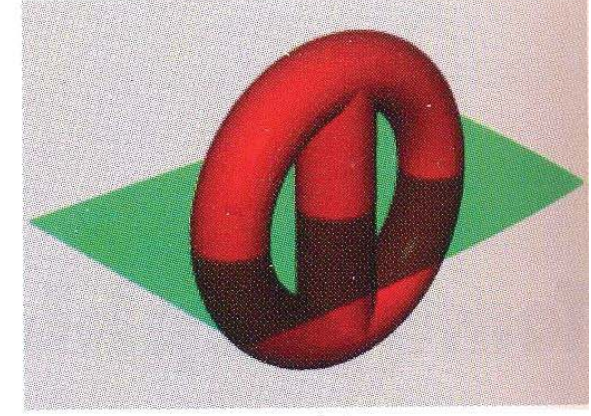
Why single projection is not sufficient



(a)



(b)

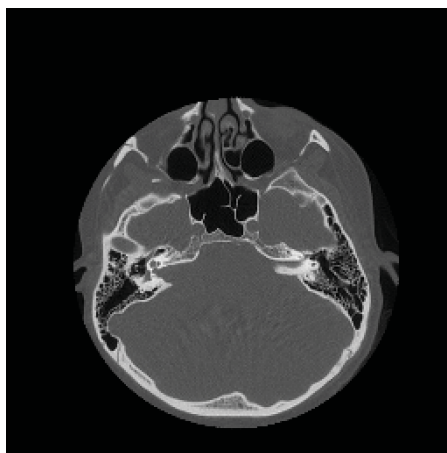


(c)

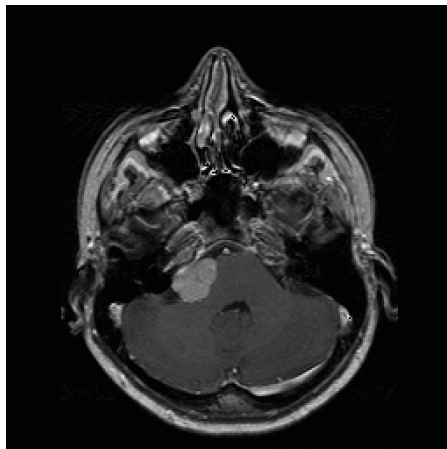
Figure 12.1 Examples of sections through three different structures that produce the same 2-D section image: (a) three discrete objects; (b) one object with simple connectivity; (c) one object with multiple connectivity.

TOMOGRAPHIC METHODS

for 3D reconstruction of internal structure of transparent body



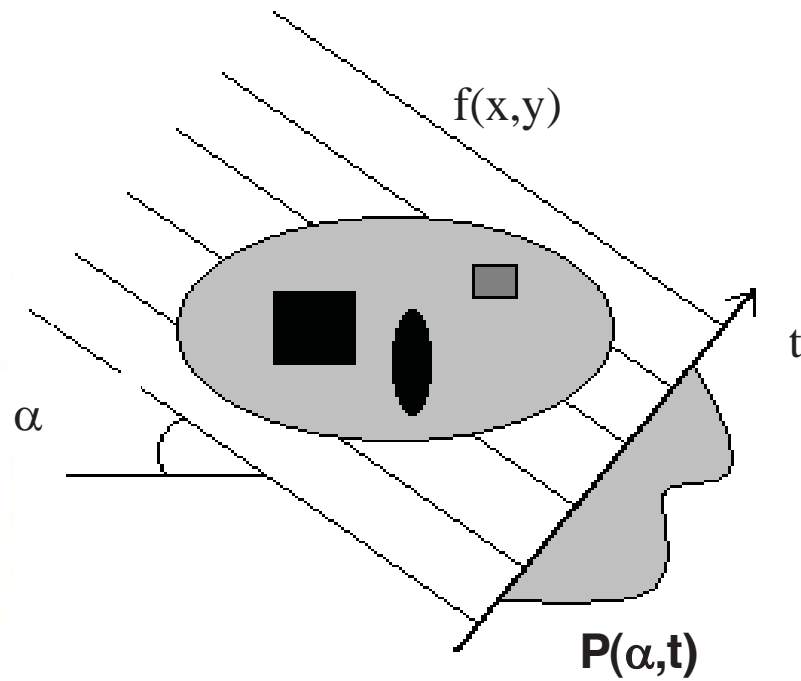
CT – computer tomography
hard tissue (bones) X rays



MRI – magnetic resonance
Imaging, soft tissue

ultrasound tomography
Terahertz tomography
Optical tomography
Diffraction tomography

Classical tomography



Single projection

Intensity in a single projection $P(\alpha, t)$

$$P(\alpha, t) = \int f(x, y) dS$$

Fourier transform of intensity

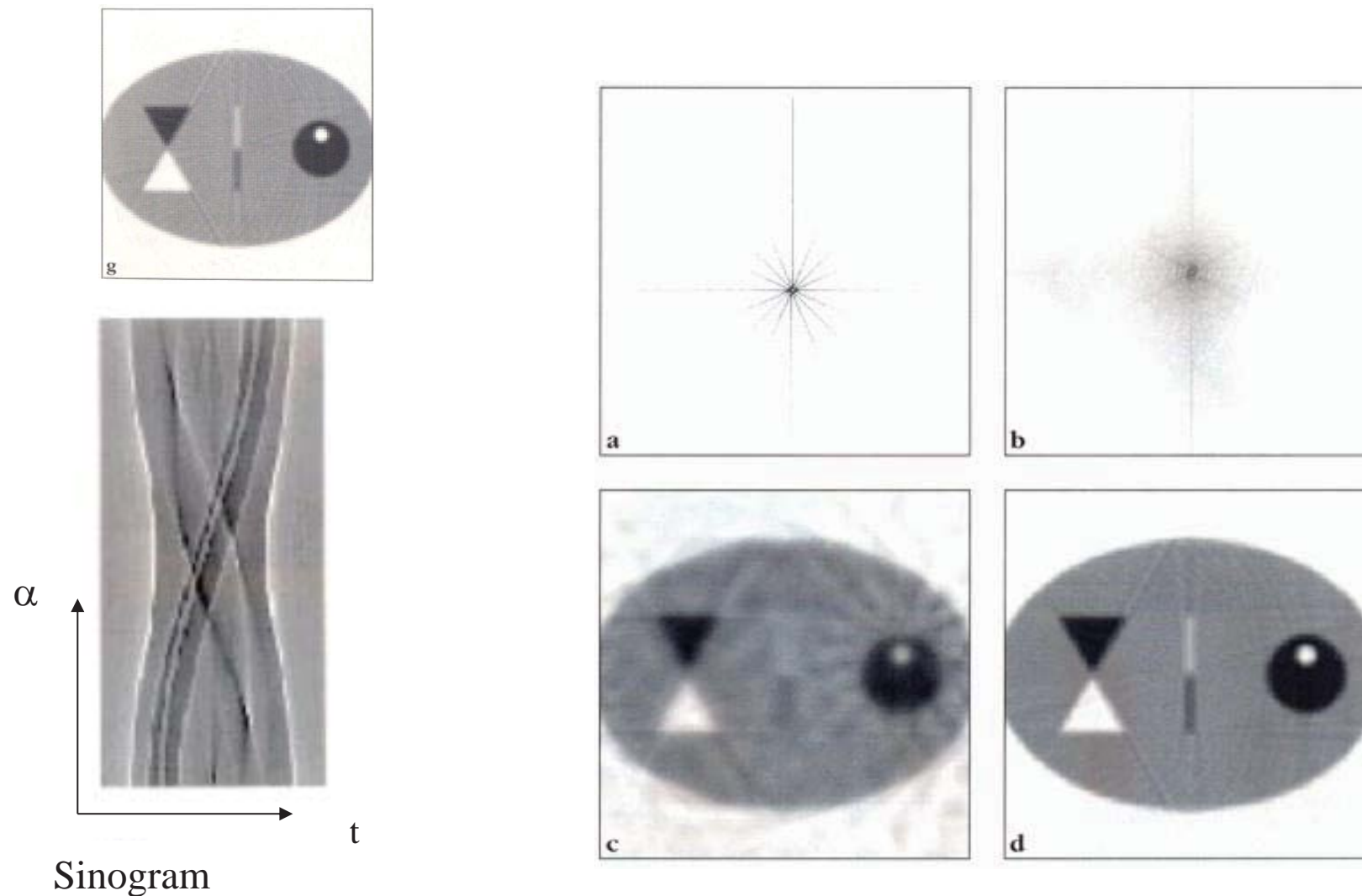
$$S(\phi, \omega) = \int P(\phi, t) \exp(-j 2\pi \omega t) dt$$

Reconstruction of object function

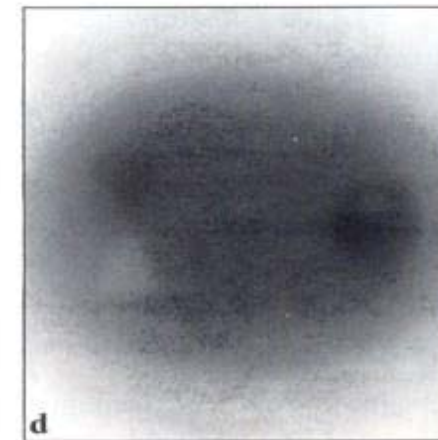
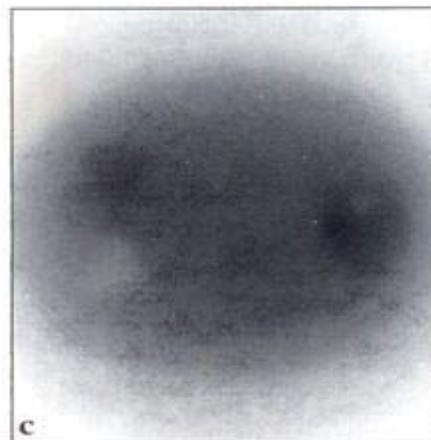
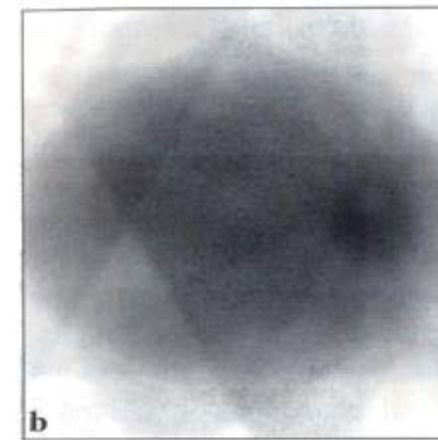
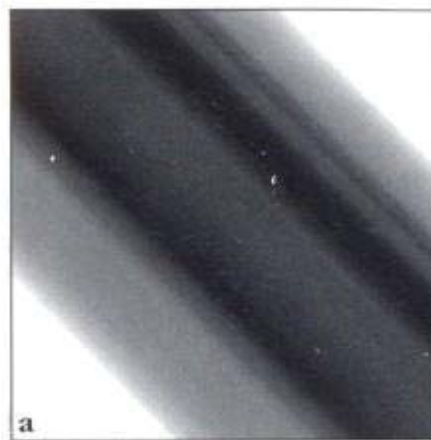
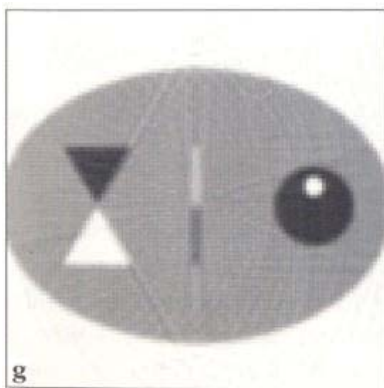
$$f(x, y) = \iint_{-\infty}^{\infty} S(\phi, \omega) |\omega| \exp(j 2\pi \omega t) d\omega d\phi$$

Tomography – the method to obtain information about internal properties in volume (x, y, z)

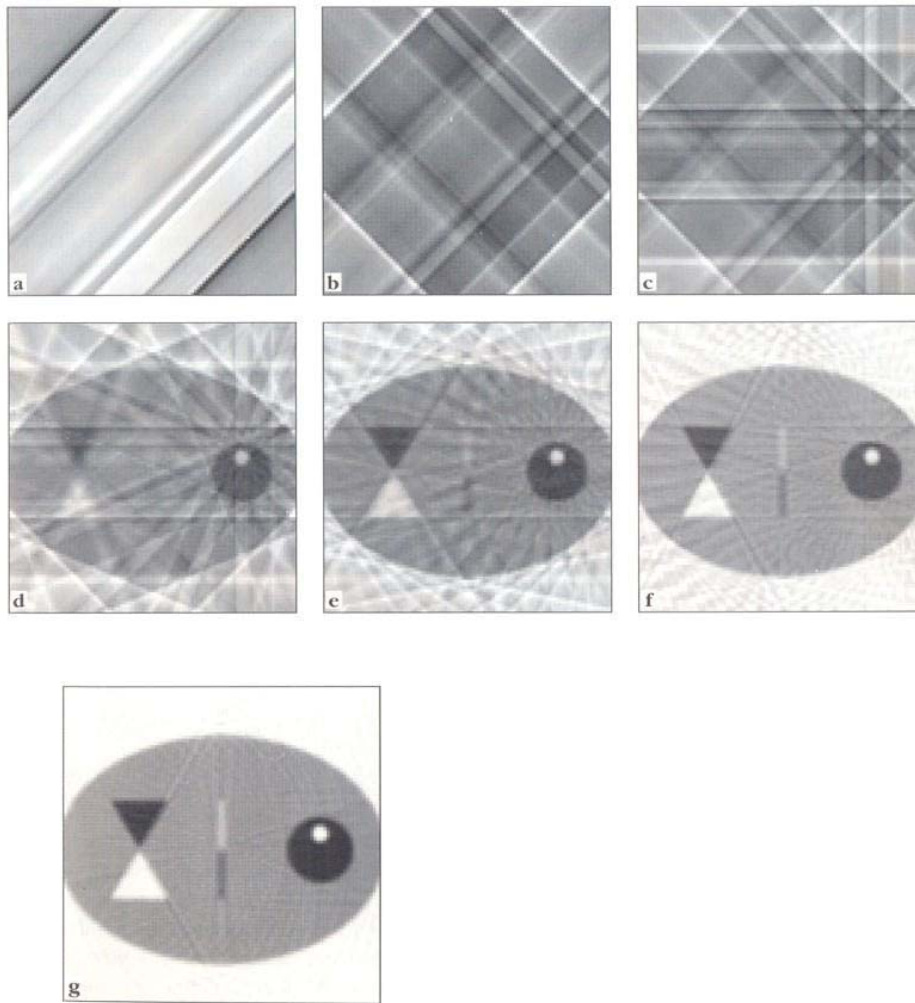
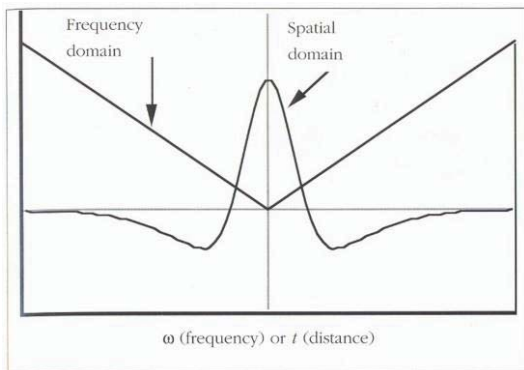
Fourier reconstruction method



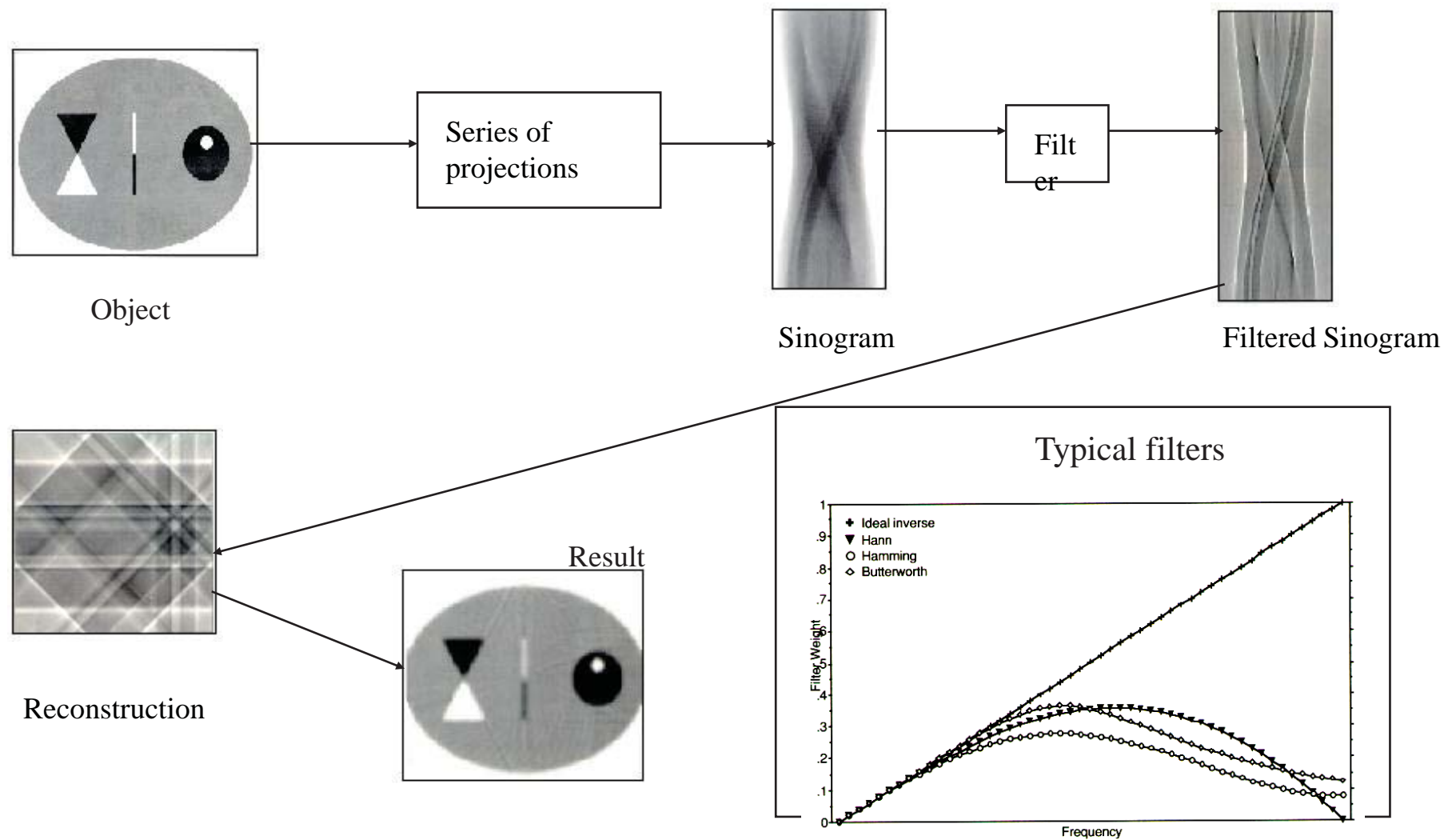
Backprojection reconstruction without filtration



Reconstruction by backprojection method with filtration

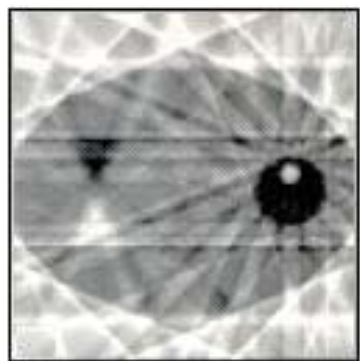


Reconstruction: Backprojection method with filtration

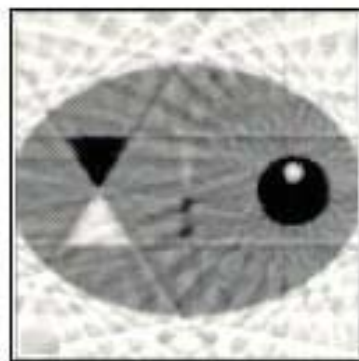


Typical sources of errors

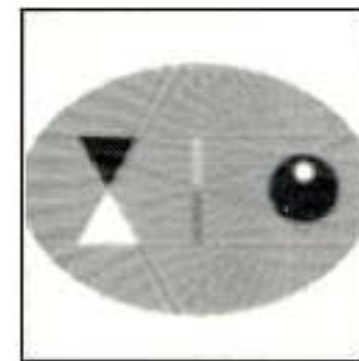
Reconstruction from small number of projections



8



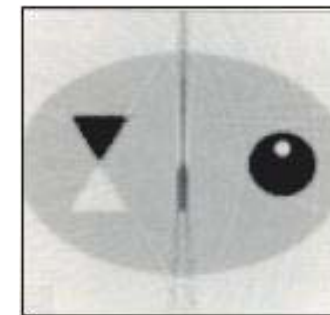
16



32

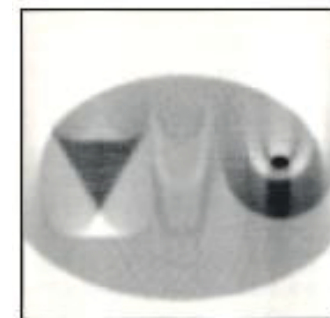
Typical errors

Presence of noises in projections



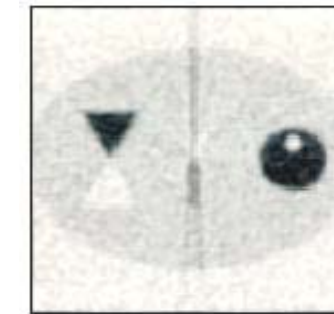
2% noise

Noncentric rotation of object



Radial run-out: 2.5%

Presence of background in projections



5% relative background

Recent challenges for Optical Tomography for photonics elements

- Provide a convenient tool for **3D material properties** determination in novel photonics materials and elements
- Provide experimental data for **optimization** of novel prototyping and production **technologies** e.g.
 - deep lithography with protons (DLP),
 - laser ablation and laser writing,
 - hot embossing,
 - injection molding.
- Provide a tool for **reliability** studies of phase photonics elements (esp. for polymer elements or elements being subjected to radiation, temperature, fatigue)
- **Quantities of interest:** refractive index, birefringence, residual stresses

Internal 3D phase objects characterization

Optical phase objects

- Isotropic (one index of refraction $n(x,y,z)$)
- fibers and preforms,
- microlenses,
- waveguides.

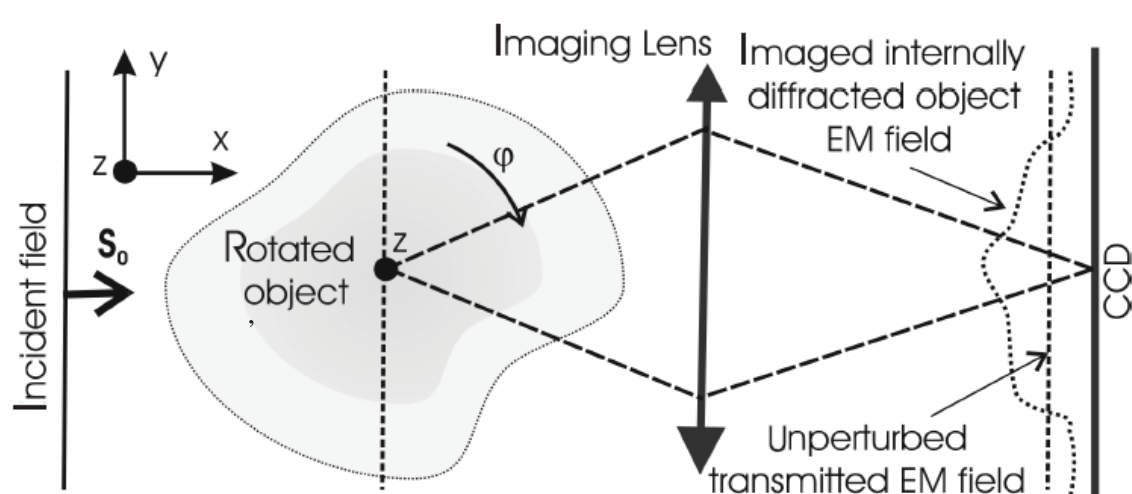
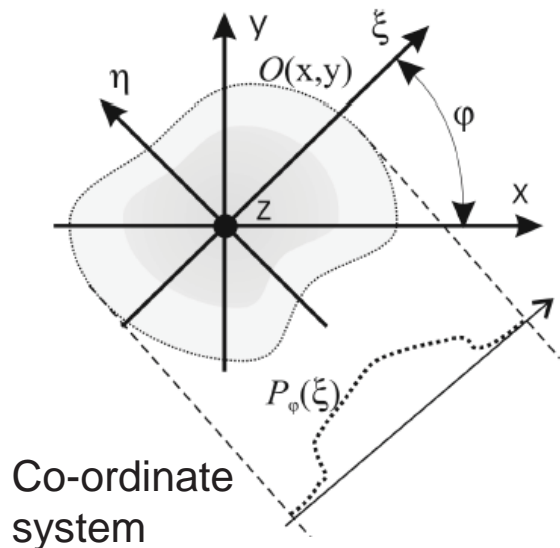
- One-axis anisotropic (two refraction indices; $n_o(x,y,z)$ $n_e(x,y,z)$)
- polarization maint. fibers,
- optical crystals
- elements with inter. stresses.

- Measurement methods:**
- microinterferometers,
 - refractive near field method,
 - optical diffract. tomography,
 - **microinterferometric tomography.**

- Measurement methods:**
- integrated photoelasticity,
 - Scattered light method,
 - **photoelastic tomography.**

Diffraction/interference tomography

The scheme of standard ODT data acquisition system



Reconstruction of internal structure by filtered back projection algorithm

$$O(x, y) = \frac{1}{(2\pi)^2} \int_0^\pi d\varphi \int_{-\infty}^{\infty} |\mathbf{k}| \tilde{P}_\varphi(\mathbf{k}) \exp \{i\mathbf{k}(x \cos \varphi + y \sin \varphi)\} d\mathbf{k}$$

where

$$\tilde{P}_\varphi(\mathbf{k}) = \int_{-\infty}^{\infty} P_\varphi(\xi) \exp \{-i\mathbf{k}\xi\} d\xi$$

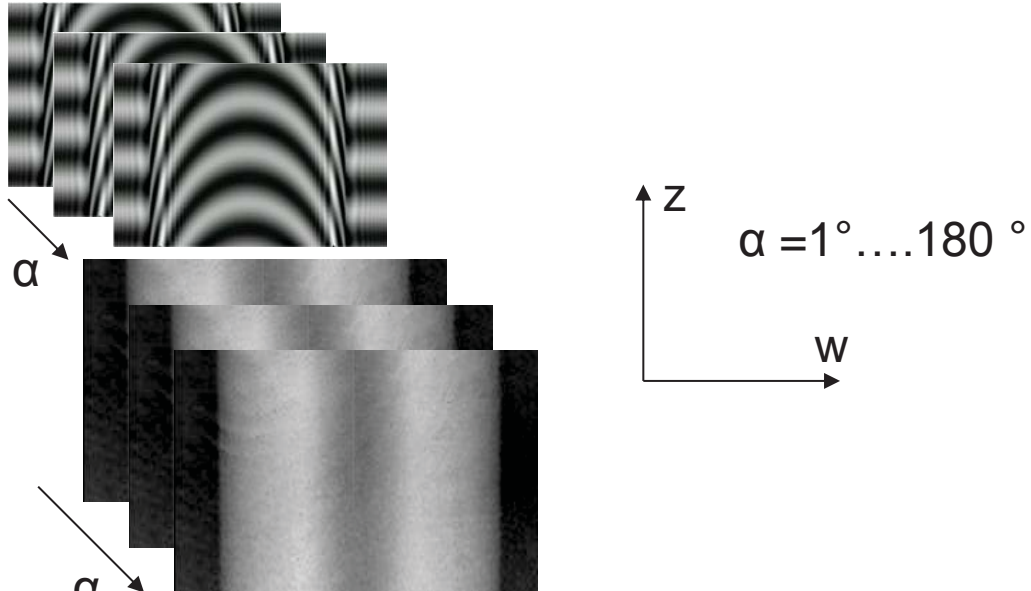
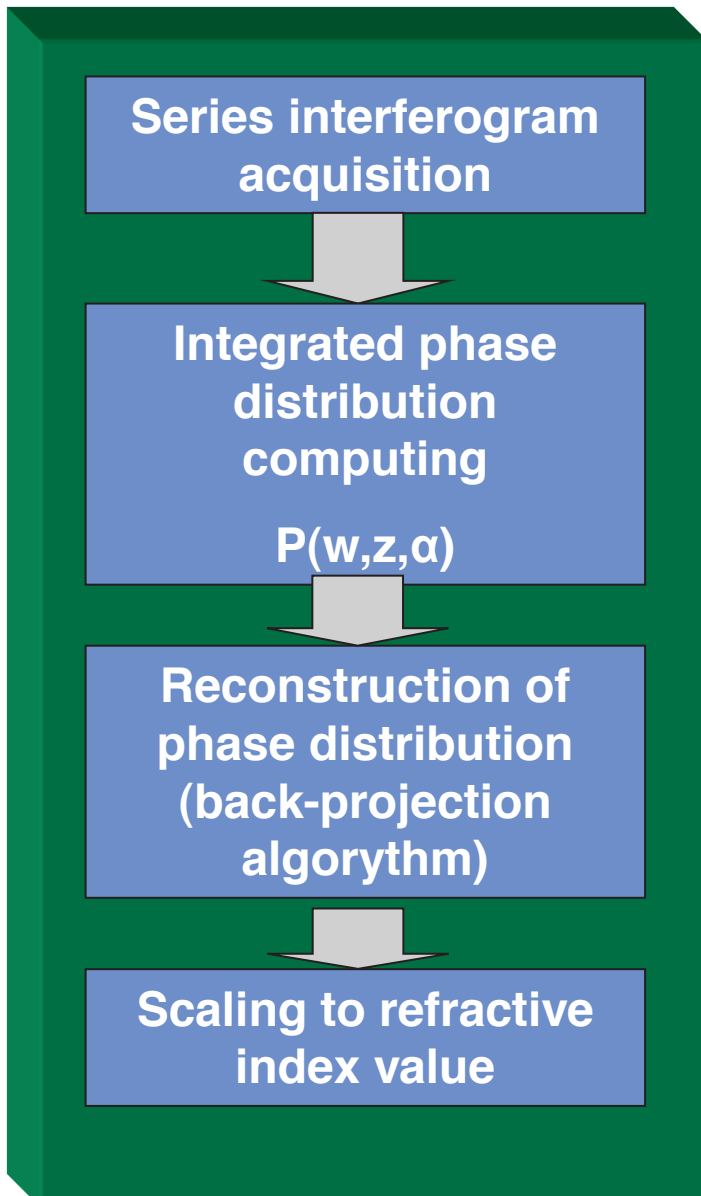
or algebraic tomographic reconstruction

Approximations in ODT

- ▶ The captured object projection P_φ must well approximate an object integrated phase and amplitude
- ▶ Tomographic reconstruction algorithms require linearization of the light interaction with an object
- ▶ Strong internal diffraction or refraction causes big errors

Major drawback of ODT applicability in measurement of micro optical elements refractive-index/birefringence structure is its **low dynamic range**,
i.e. refractive-index structures with small variations can be measured only.

Basics of refractive index measurements tomographic microinterferometry



$$\Phi(x, y, z) = \int \int S(\alpha, \varpi, z) | \varpi | \exp(j 2\pi\varpi w) d\varpi d\alpha$$

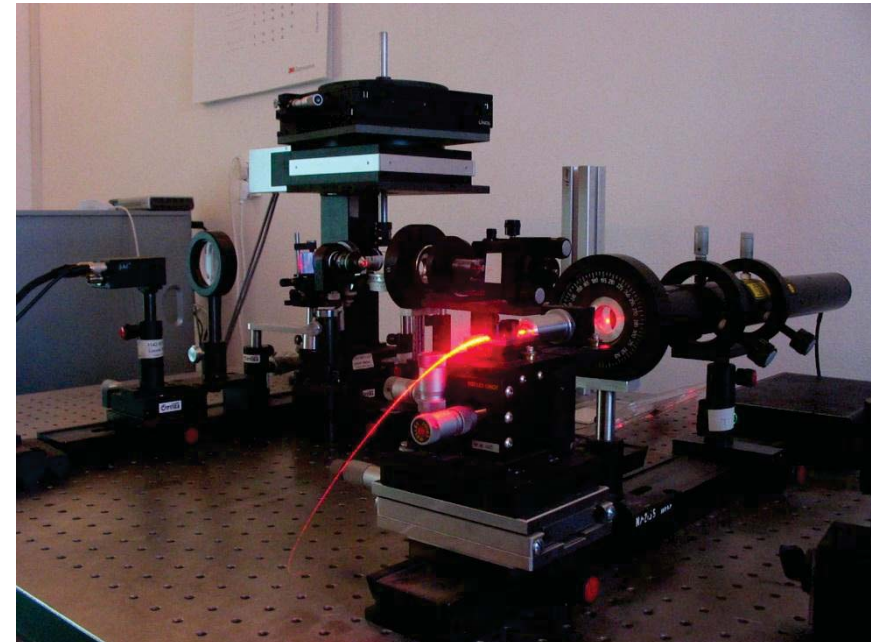
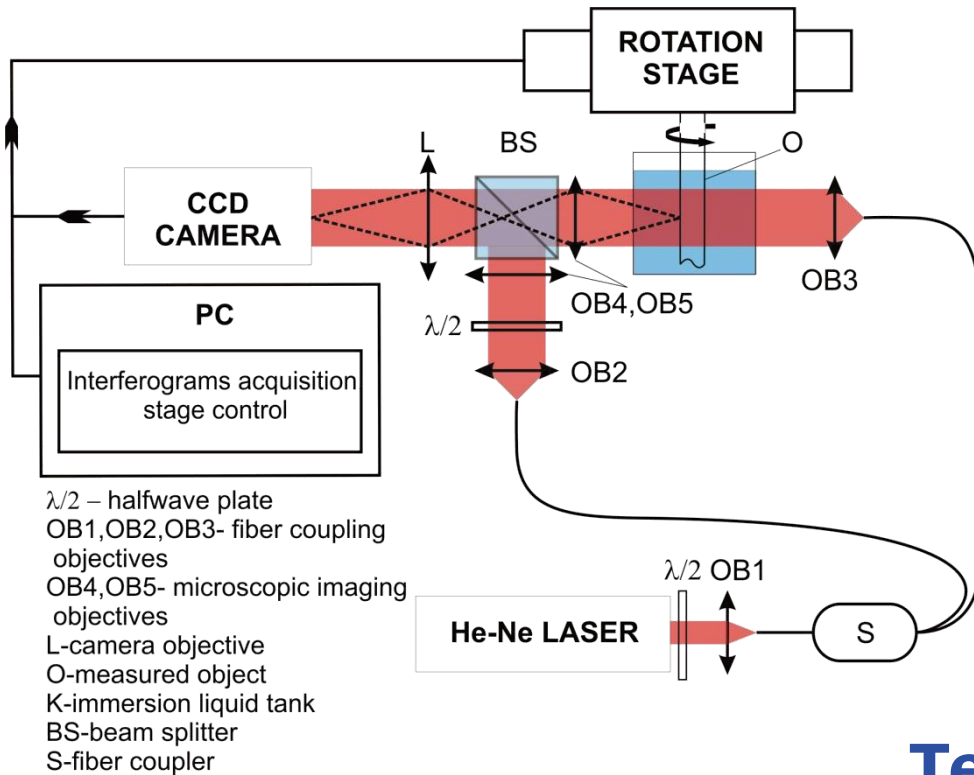
where: $S(\alpha, \varpi, z) = \int P(\alpha, w, z) \exp(-j 2\pi\varpi w) dw$,

ϖ - spatial frequency of function $P(\alpha, w, z_0)$.

$$n(x, y, z) = \frac{\Phi(x, y, z)\lambda}{2\pi d} + n_i,$$

λ -source wavelength, n_i – refractive index of immersion liquid, d -object size corresponding to pixel of camera

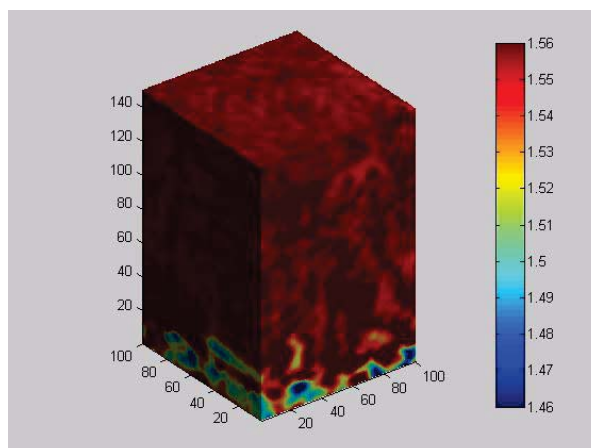
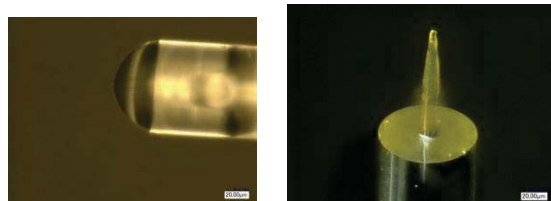
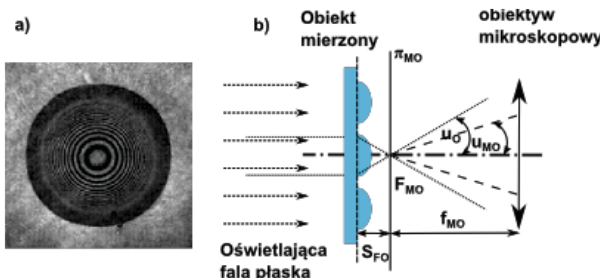
Interferometric tomograph



Technical parameters:

- detection module: high resolution CCD matrix (1376x1035pixels)
- refraction index measurement resolution: $\Delta n=0.0001$
- the smallest object dimension 2 μm (diffraction limited)

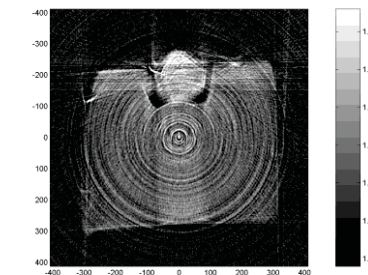
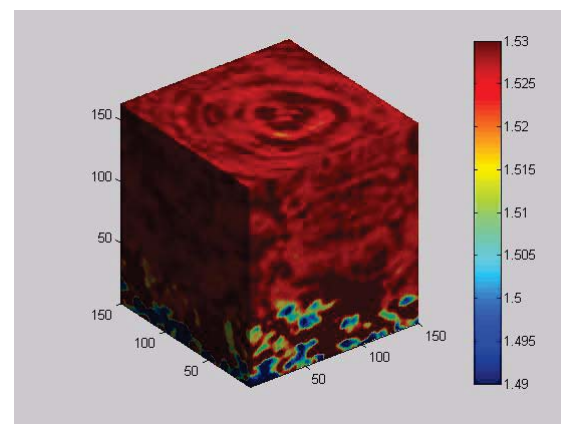
Phase microobjects: Technical



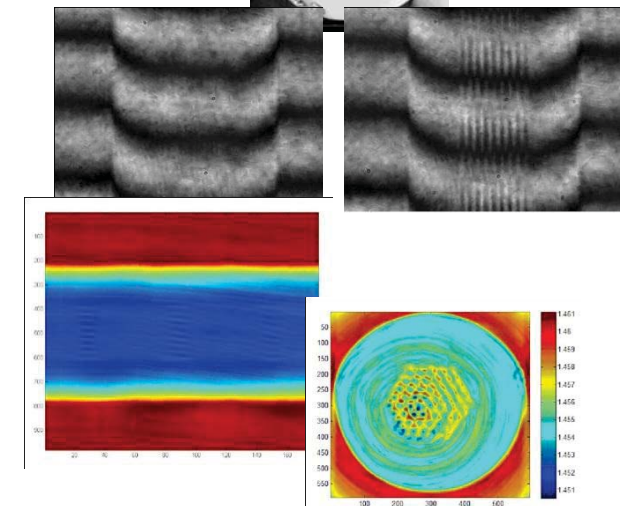
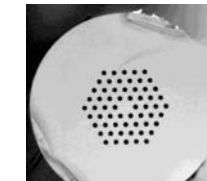
Problems:

- high-numerical aperture (microlenses)
- high-phase difference
- high-phase gradient
- high spatial resolution

Known design (theoretical model)



DPW microlenses



Microtips at an OF



INNOWACYJNA
GOSPODARKA
NARODOWA STRATEGIA SPÓŁNOŚCI

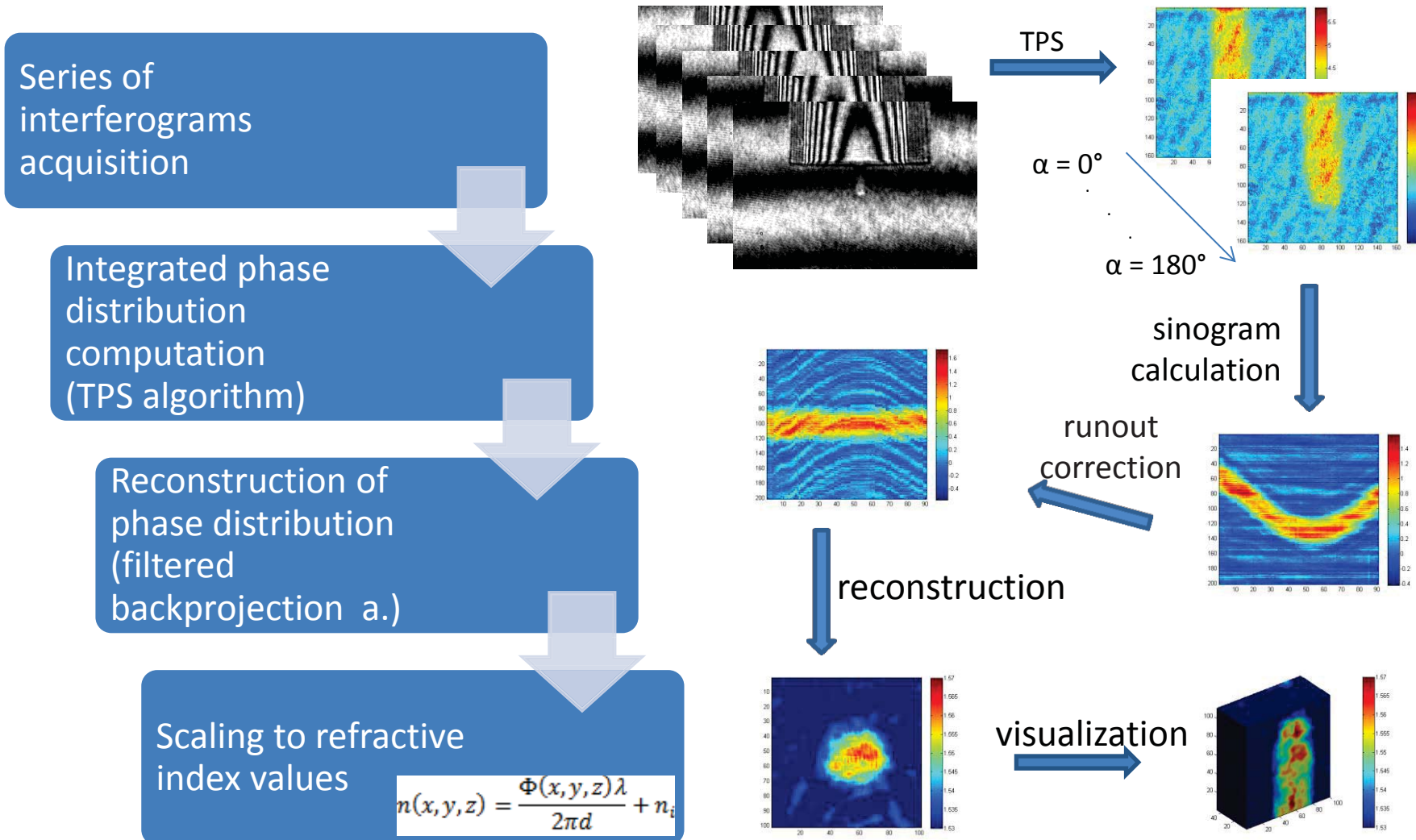
FNP
Fundacja na rzecz Nauki Polskiej

UNIA EUROPEJSKA
EUROPEJSKI FUNDUSZ
ROZWOJU REGIONALNEGO

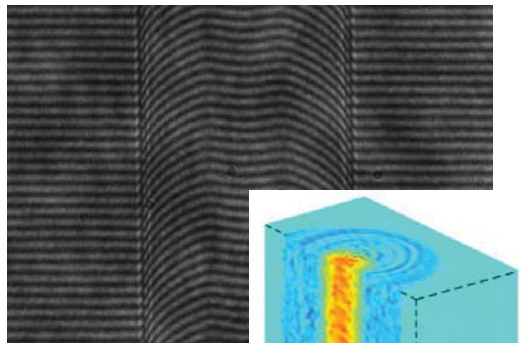


Tapered photonics OF

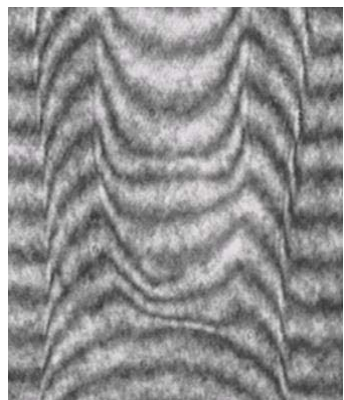
Interferometric tomography



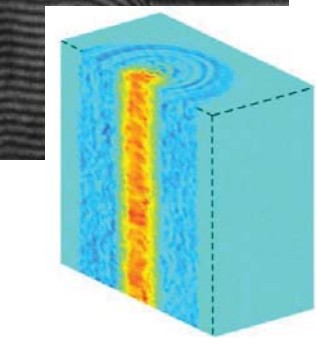
INNOVATIVE ECONOMY
NATIONAL COHESION STRATEGY



Fused optical fibre(SM
and MMF)



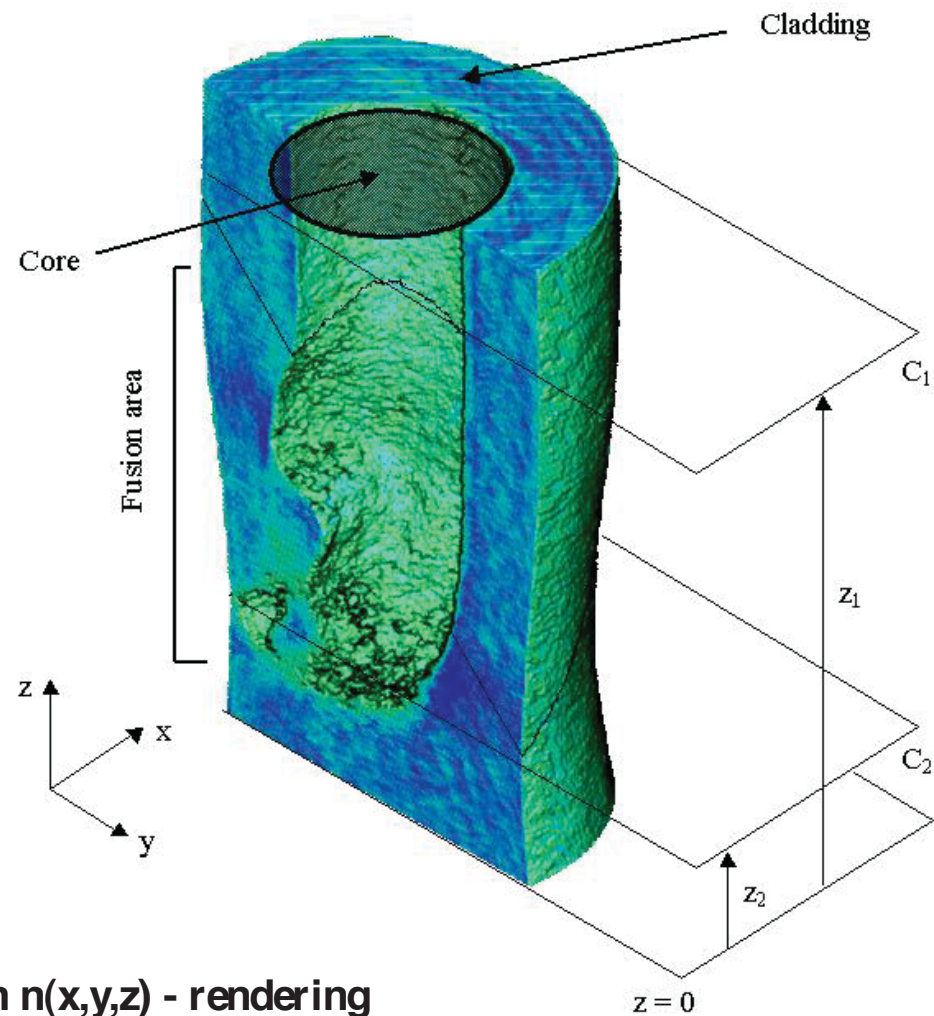
Interferogram



Multimode fibre

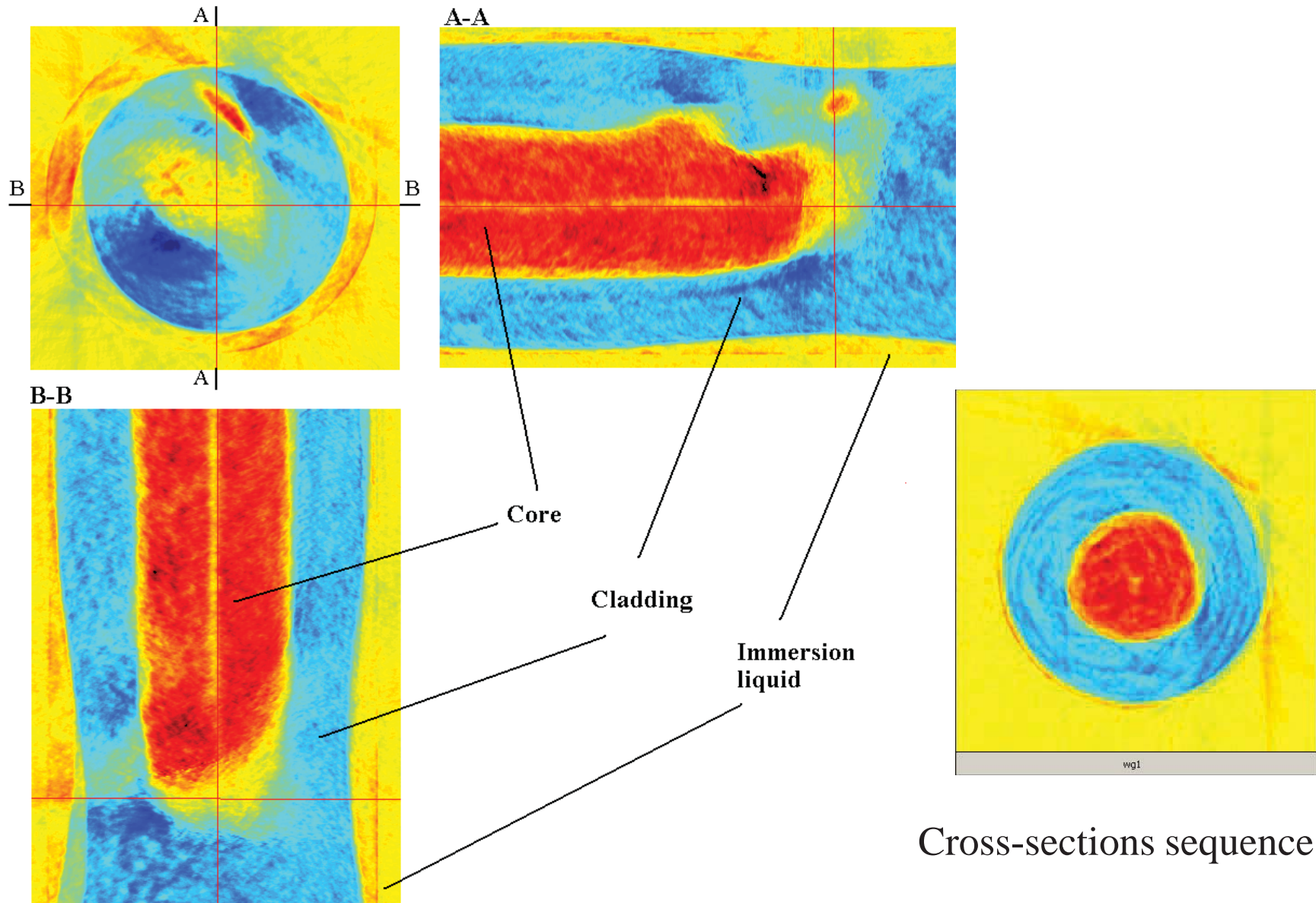
1.472
1.47
1.468
1.466
1.464
1.462
1.46
1.458
1.456

Experimental results

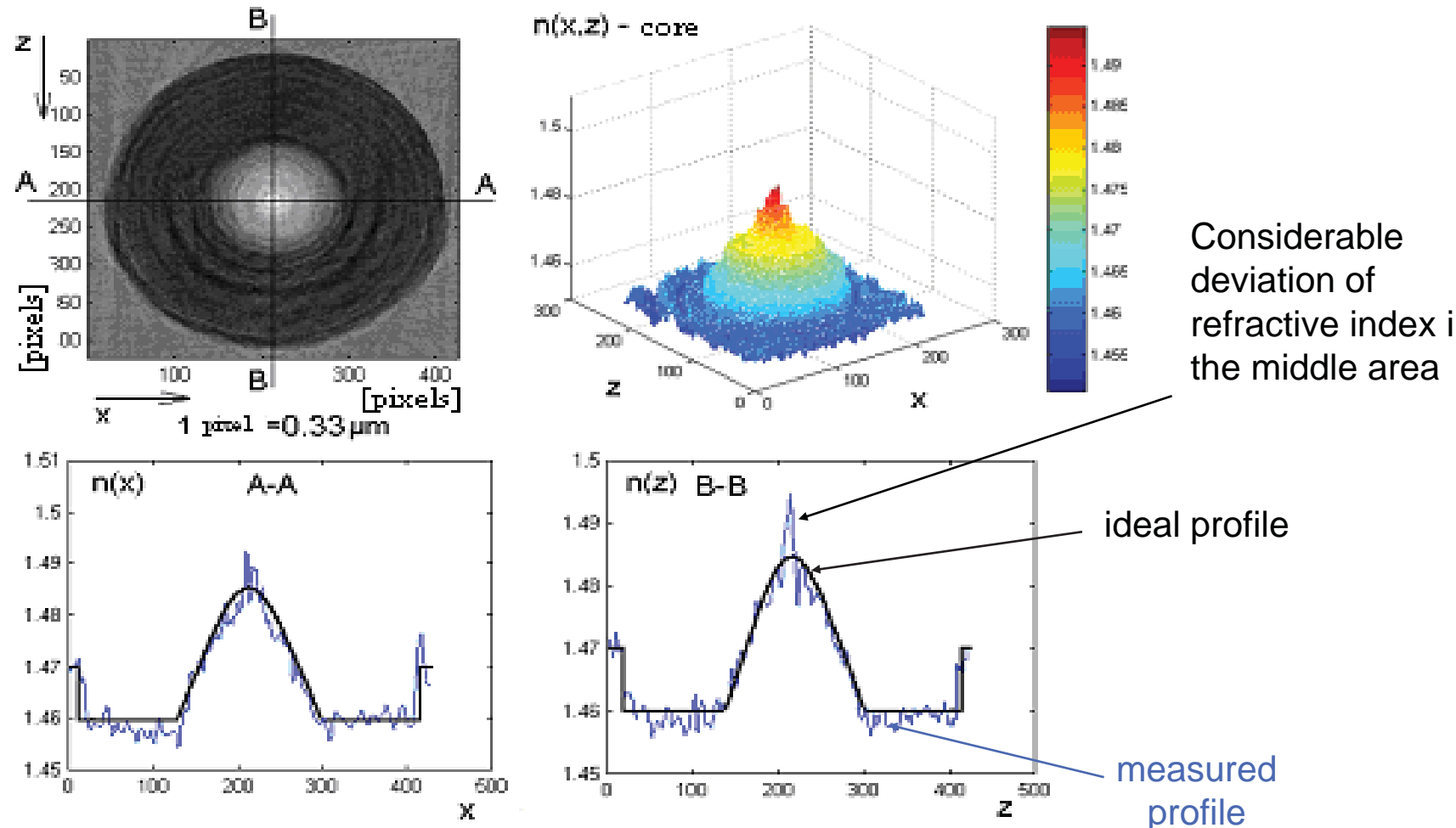


Distribution $n(x,y,z)$ - rendering

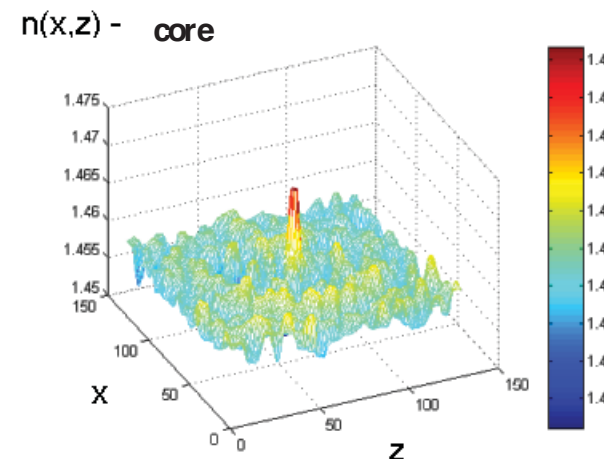
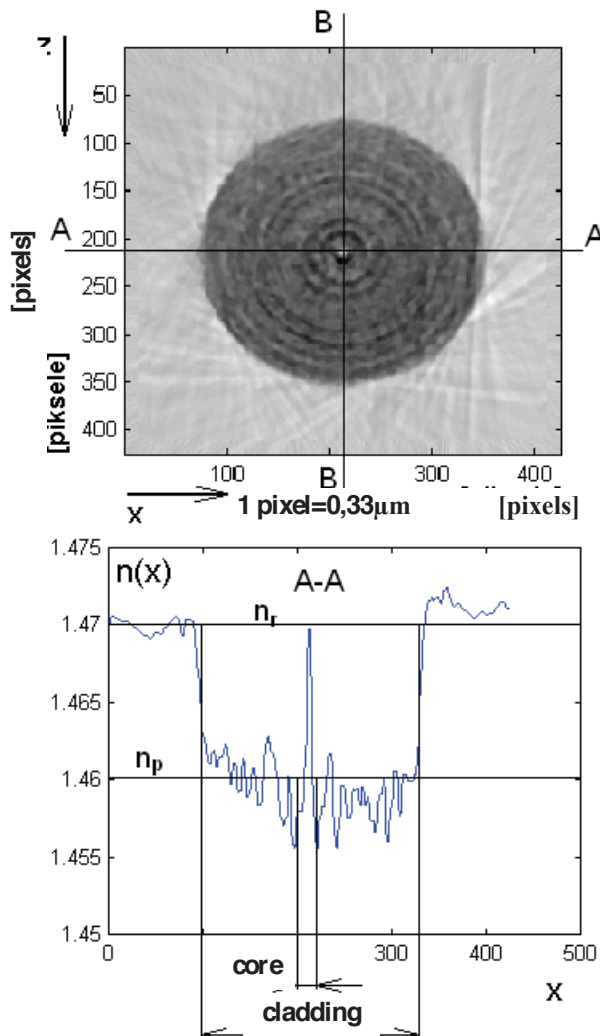
Experimental results



Multimodal Gradient Profile Fiber Inspection



Single mode fiber inspection



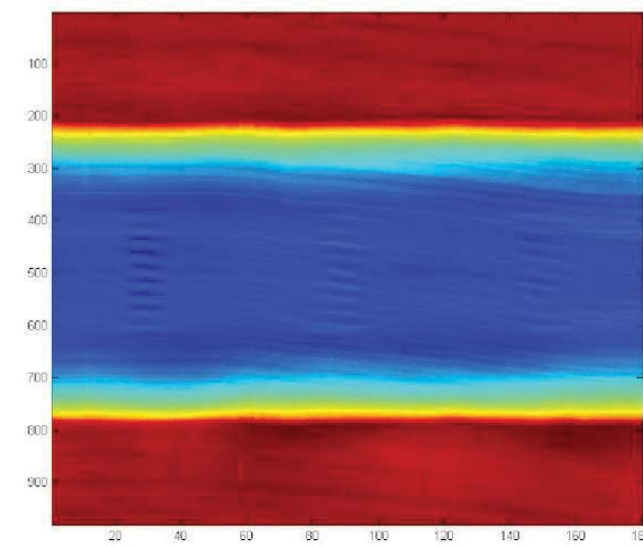
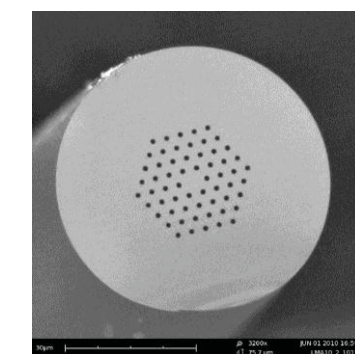
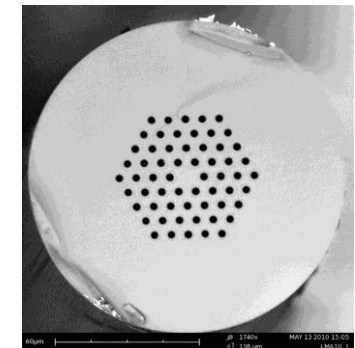
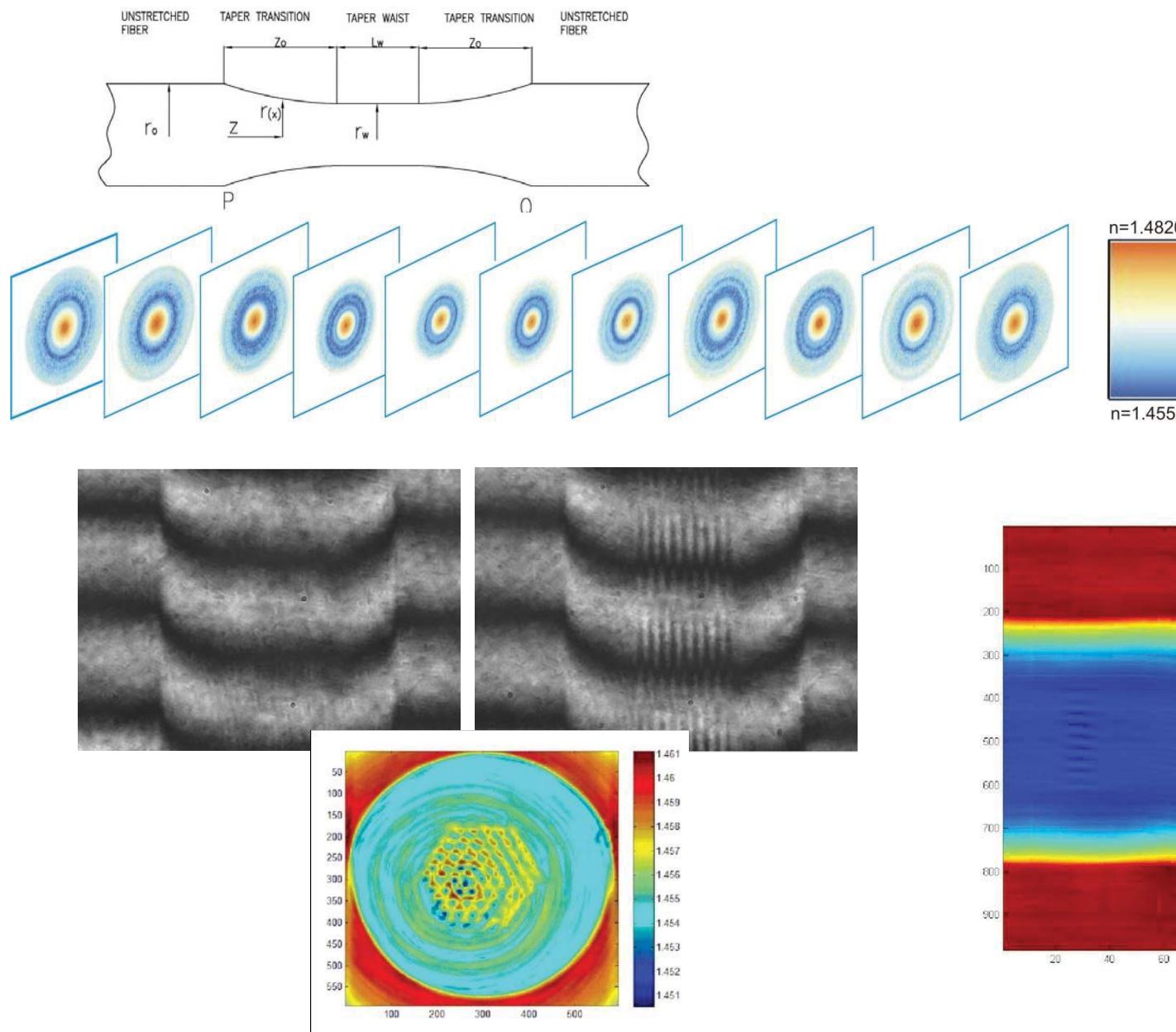
Fiber parameters:

- fiber diameter 120 μm
- core diameter 8 μm
- core refractive index 1,47
- cladding refractive index 1,46

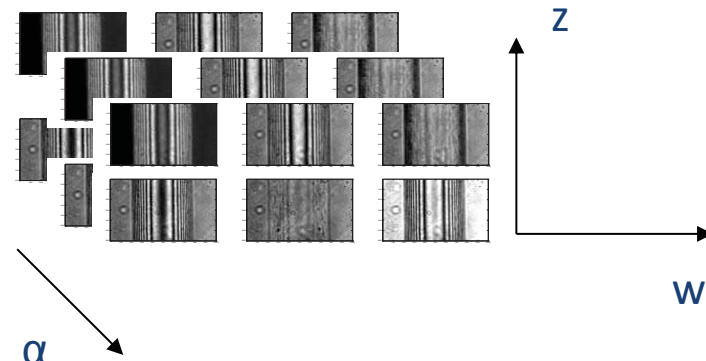
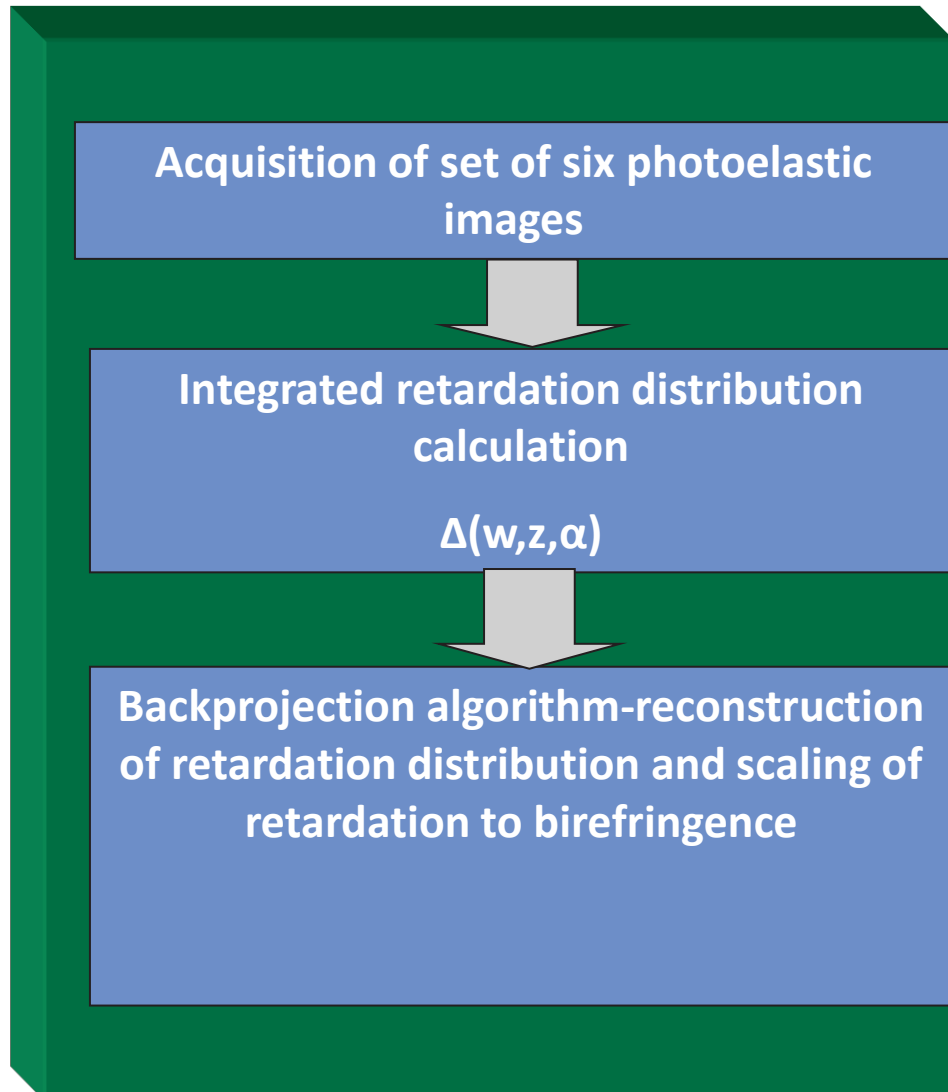
Only central core area was reconstructed properly

-refractive index determination error is considerable in core area, source of this error is difraction phenomenon on edge of core and cladding; step of refractive index is equal 0,01

Analysis of photonics fibres



Photoelastic tomography



$$\Delta_n(x, y, z_i) =$$

$$\frac{\lambda}{2\pi dx} \int_0^\pi \int_{-\infty}^{\infty} S(\alpha, \omega, z_i) |\omega| \exp(j2\pi\omega w) d\omega d\alpha$$

$$S(\alpha, \omega, z_i) = \int \Delta(\alpha, w, z_i) \exp(-j2\pi\omega w) dw,$$

ω - spatial frequency of the function $\Delta(\alpha, w, z_i)$

λ - source wavelength, dx - spatial step

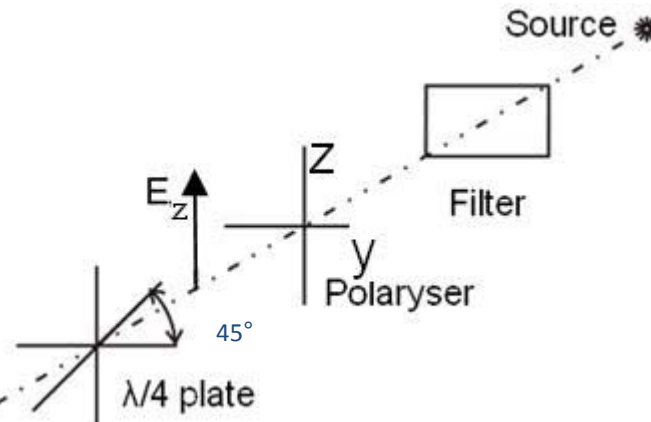
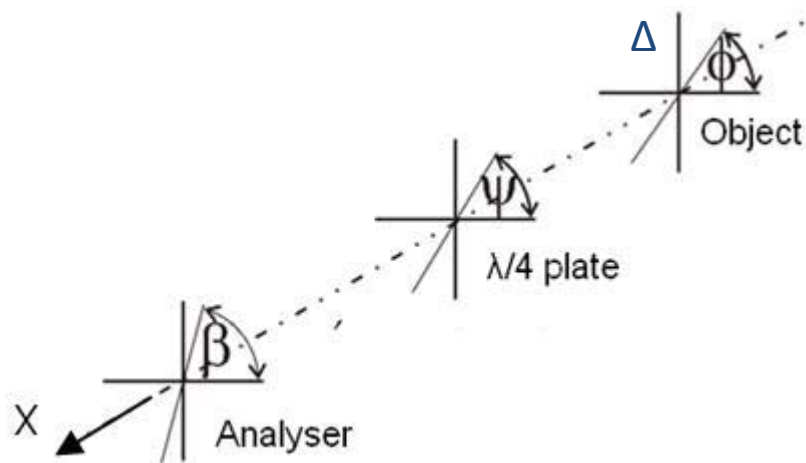
Circular polariscope and its mathematical representation

Characteristic object

parameters:

Δ - phase retardation

Φ – isoclinic angle



**Mathematical representation of system,
according to Jones calculus:**

$$\begin{aligned} \begin{Bmatrix} U \\ V \end{Bmatrix} &= \frac{1}{2} \begin{bmatrix} \cos \beta & \sin \beta \\ -\sin \beta & \cos \beta \end{bmatrix} \begin{bmatrix} 1 - i \cos 2\Psi & -i \sin 2\Psi \\ -i \sin 2\Psi & 1 + i \cos 2\Psi \end{bmatrix} \\ &\times \begin{bmatrix} \cos \Delta - i \sin \Delta \cos 2(\phi) & -i \sin \Delta \sin 2(\phi) \\ -i \sin \Delta \sin 2(\phi) & \cos \Delta + i \sin \Delta \cos 2(\phi) \end{bmatrix} \\ &\times \begin{bmatrix} 1 & i \\ i & 1 \end{bmatrix} \begin{Bmatrix} 0 \\ 1 \end{Bmatrix} k e^{i \omega t}, \end{aligned}$$

where: U - component of light vector perpendicular to polariser axis

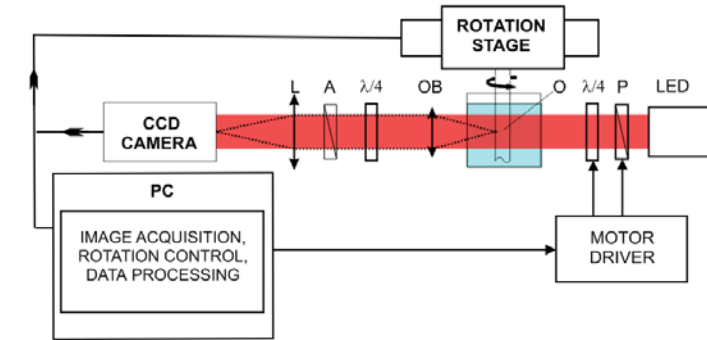
V - component of light vector parallel to polariser axis

Integrated retardation calculation by phase shift method

General output intensity equation:

$$i = i_m + i_v \sin 2(\beta - \Psi) \cos 2\Delta - i_v \sin 2(\phi - \psi) \cos 2(\beta - \Psi) \sin 2\Delta$$

| Ψ | β | Output intensity equations |
|----------|----------|---|
| 0 | $\pi/4$ | $i_1 = i_a + i_b \cos \Delta$ |
| 0 | $3\pi/4$ | $i_2 = i_a - i_b \cos \Delta$ |
| 0 | 0 | $i_3 = i_a - i_b \sin \Phi \sin \Delta$ |
| $\pi/4$ | $\pi/4$ | $i_4 = i_a + i_b \cos \Phi \sin \Delta$ |
| $\pi/2$ | $\pi/2$ | $i_5 = i_a + i_b \sin \Phi \sin \Delta$ |
| $3\pi/4$ | $3\pi/4$ | $i_6 = i_a - i_b \cos \Phi \sin \Delta$ |



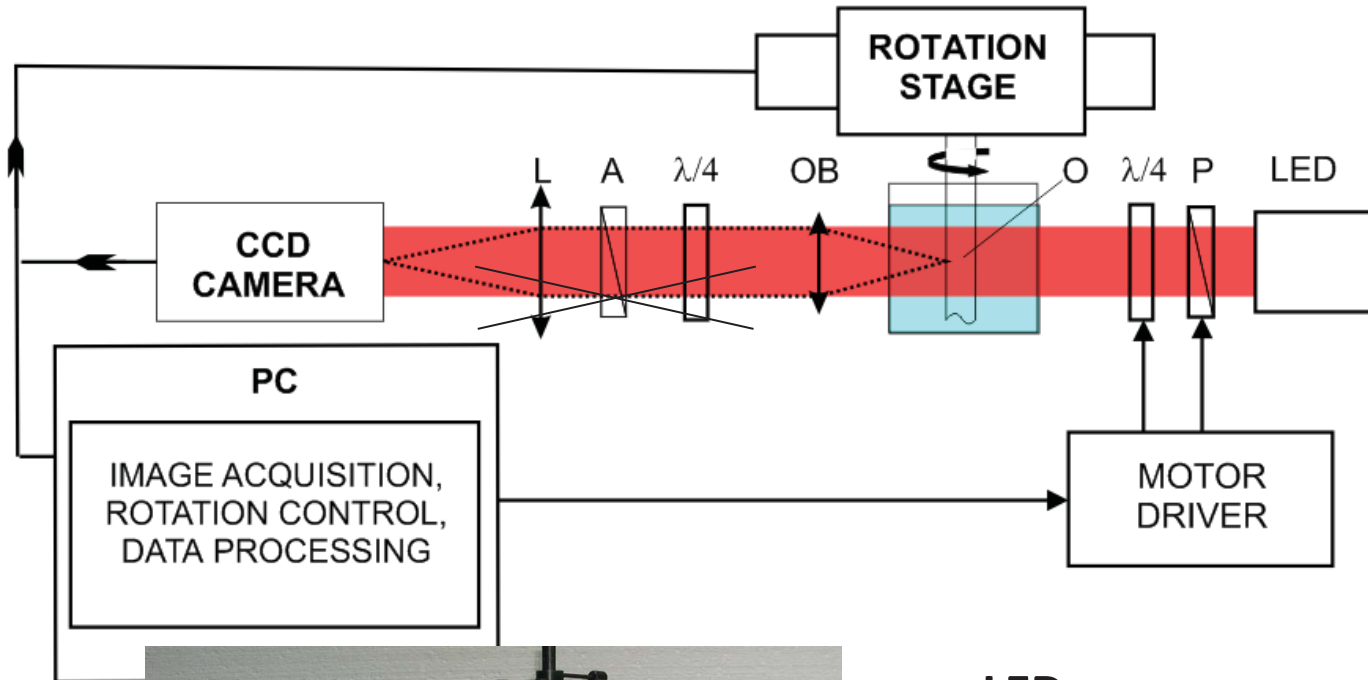
- Isoclinic angle

$$\Phi = \frac{1}{2} \arctan \left(\frac{i_5 - i_3}{i_4 - i_6} \right)$$

- Phase retardation

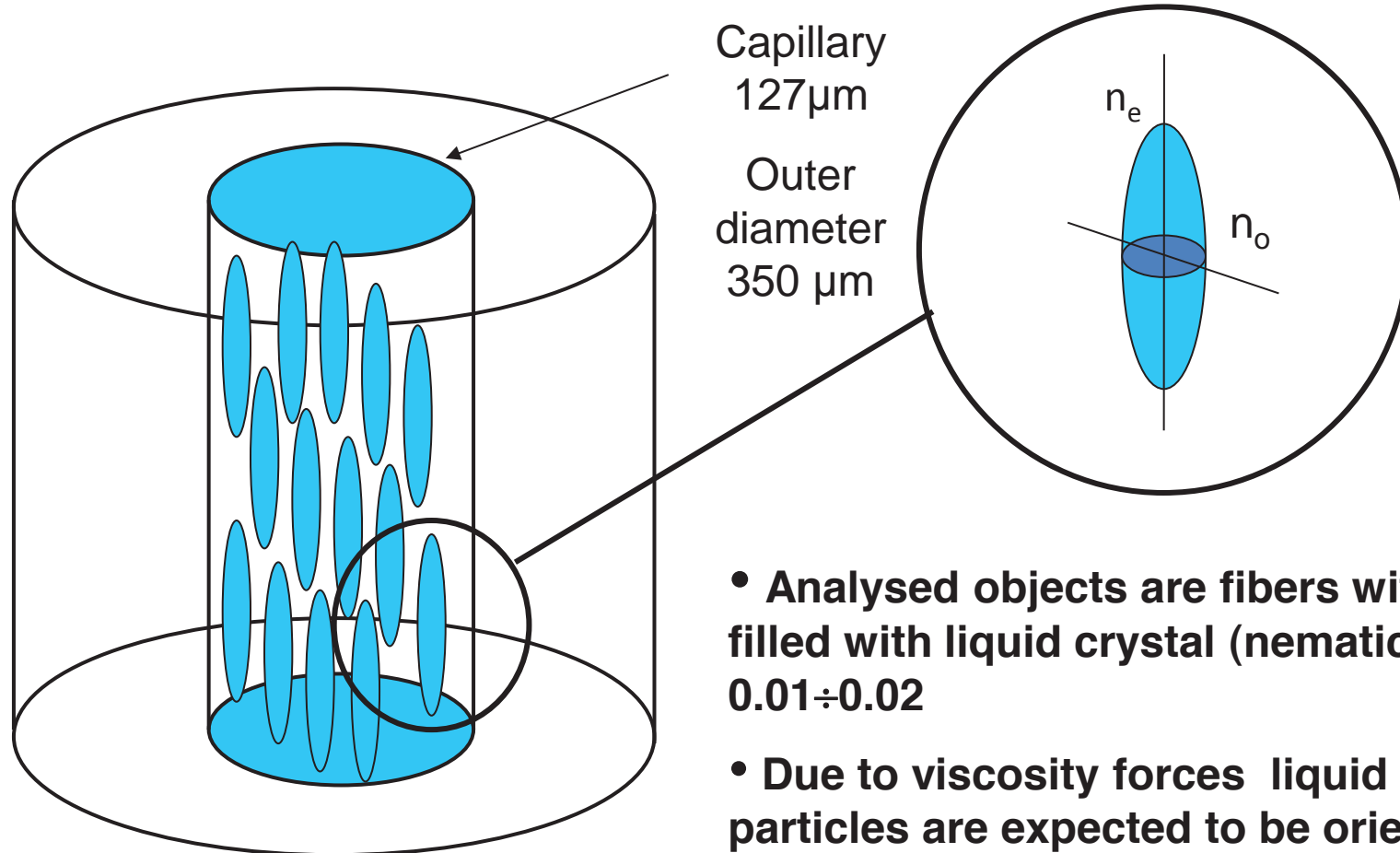
$$\Delta = -\frac{1}{2} \arctan \frac{(i_5 - i_3) \sin 2\Phi + (i_4 - i_6) \cos 2\Phi}{i_1 - i_2}$$

Elastooptics tomograph



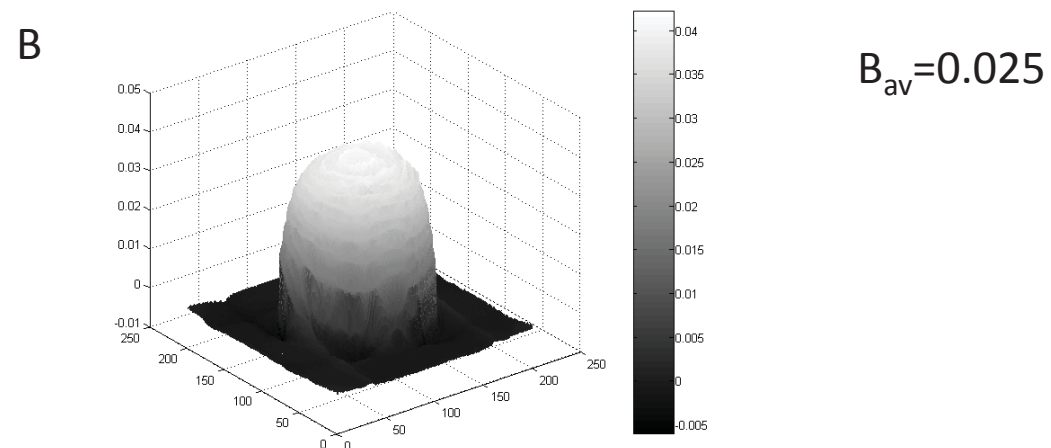
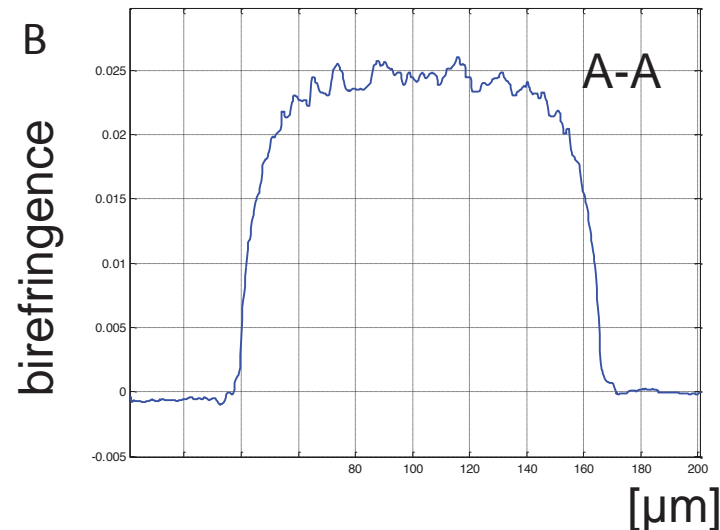
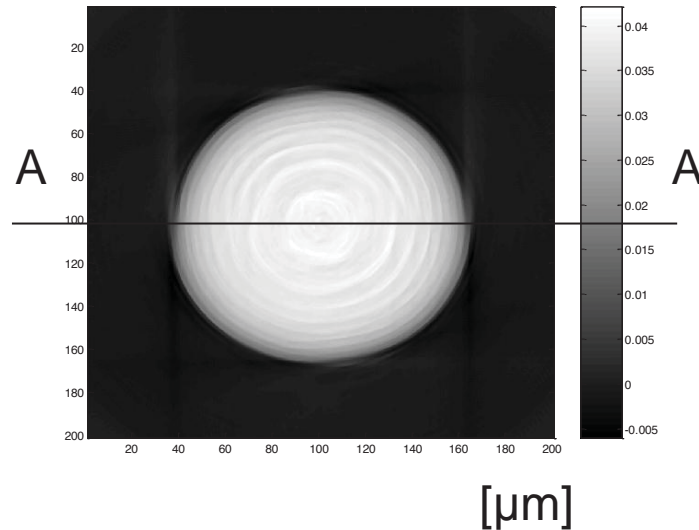
LED- source
P - polaryser
 $\lambda/4$ - quarter-wave plate,
O - measured object,
OB - microscopic objective,
A - analyzer,
L - imaging lens

Measured object – optical fiber with LC



- Analysed objects are fibers with channels filled with liquid crystal (nematic LC with $\Delta_n = 0.01 \div 0.02$)
- Due to viscosity forces liquid crystals particles are expected to be oriented paralelly to axis of capillary
- Expected birefringence B $0.02 < B < 0.06$

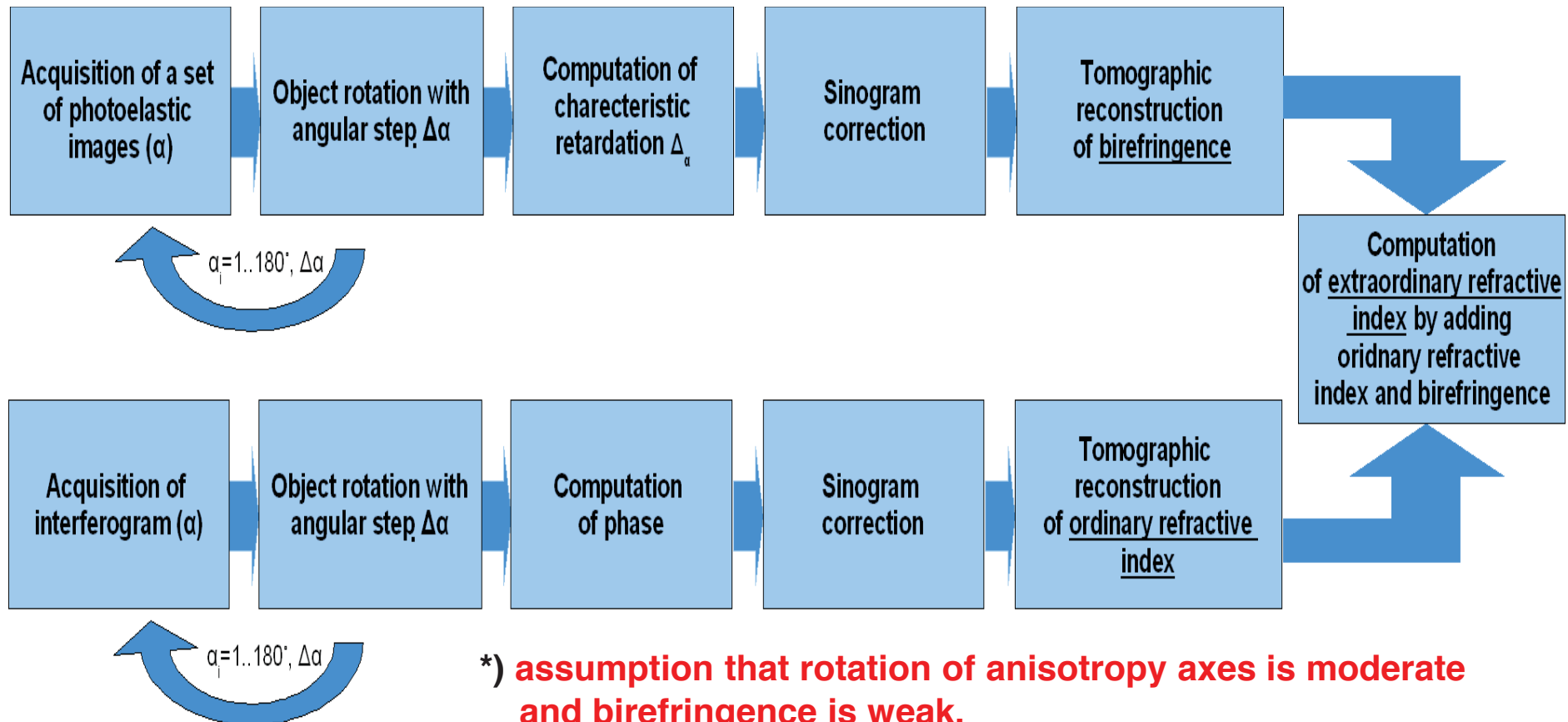
Experiment: birefringence in a single layer



3D characterization of phase photonics elements

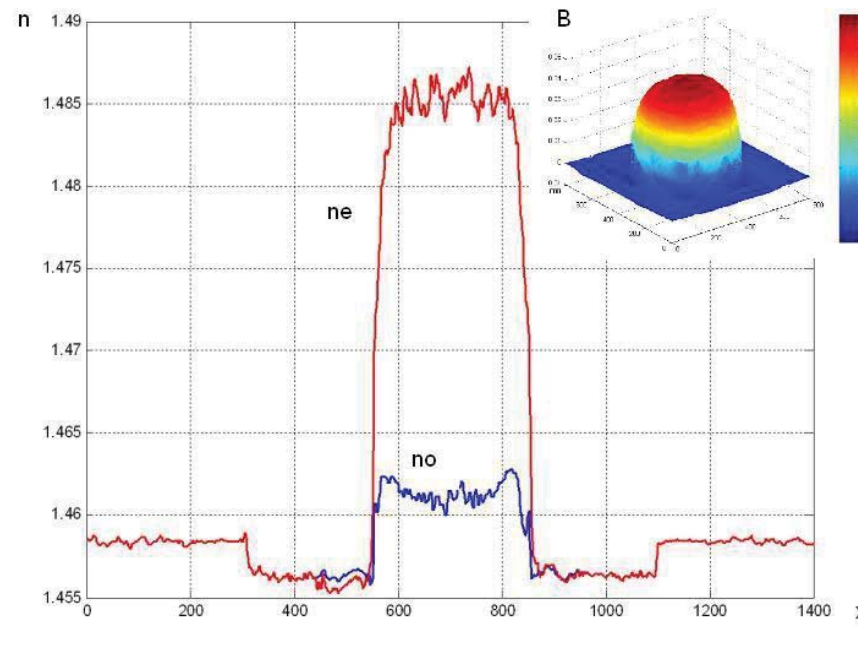
Quantities of interest:

$n(x,y,z)$ or $n_0(x,y,z)$, $n_e(x,y,z)$), and birefringence $B(x,y,z)^*$



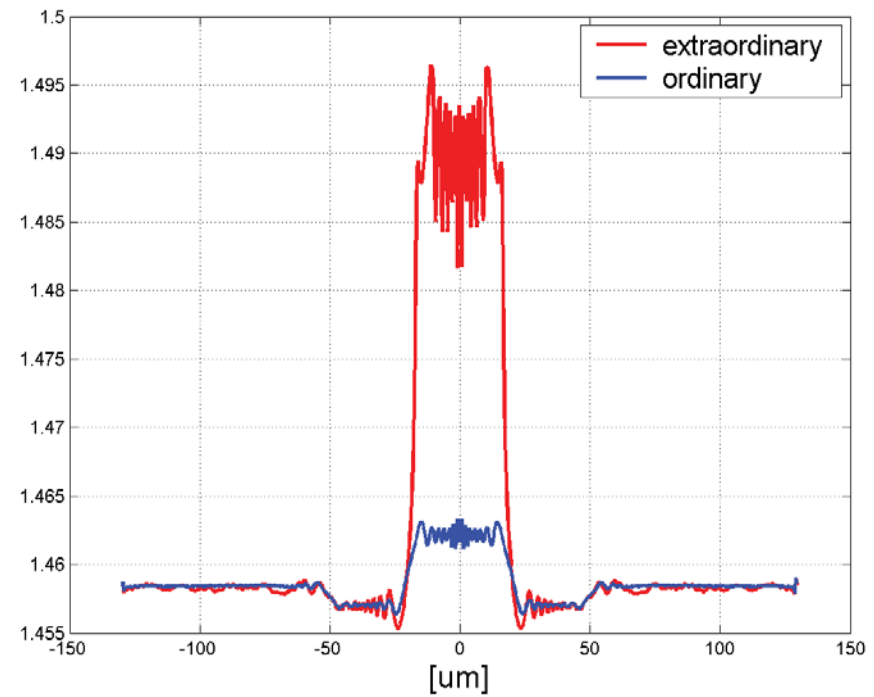
Experimental and simulation results

Experiment



Simulations

Refractive indices distribution

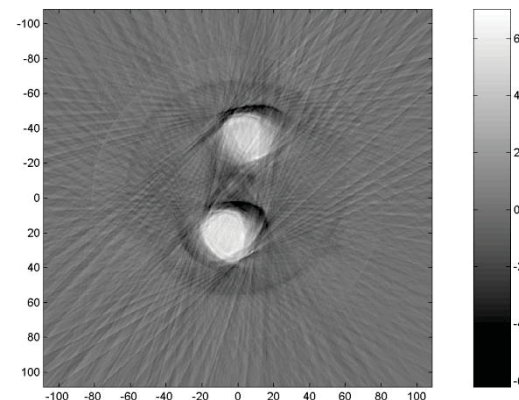


Determination of axial stress and refractive index in Panda Fiber

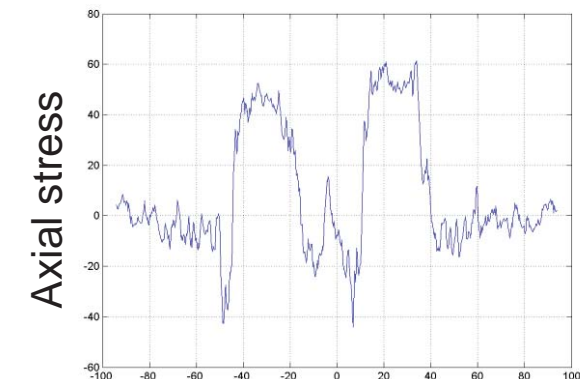
Microscopic image of sample



Determined axial stress in sample

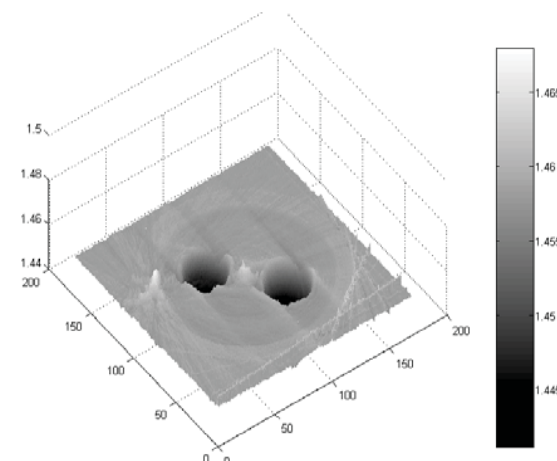


2D field of axial stress

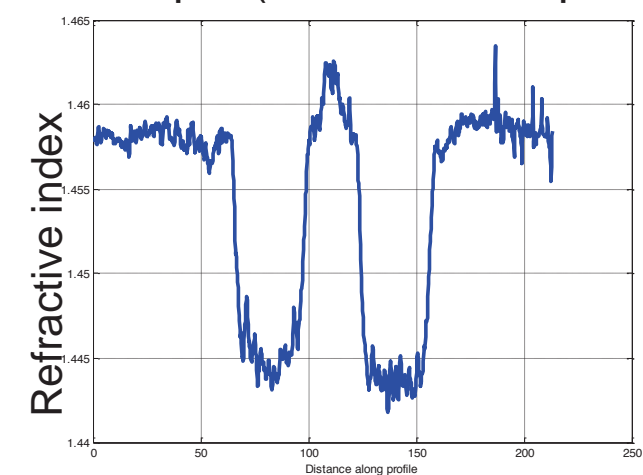


Plot of axial stress profile

Determined refractive index in sample (for horizontal plane)



2D distribution of refractive index



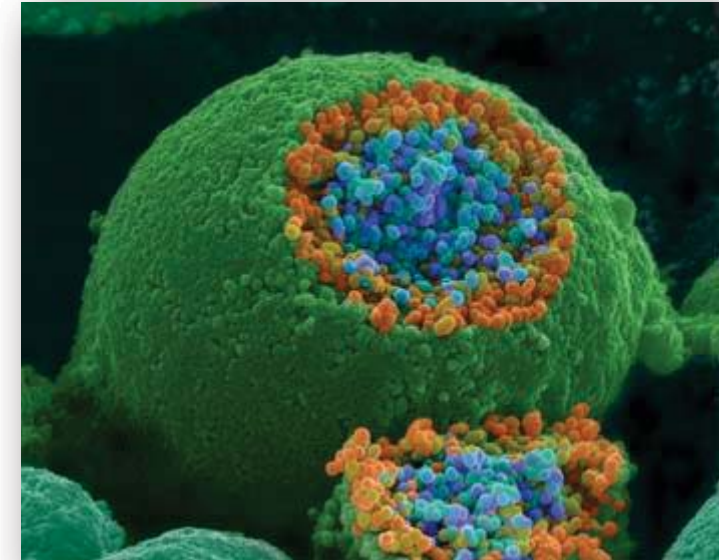
Plot of refractive index profile

- Panda type fiber
- cladding diameter 125 μm , stress members diameter 35 μm
- refractive index of cladding 1.4584 and for matching liquid 1.4582

Tomography of biological microobjects

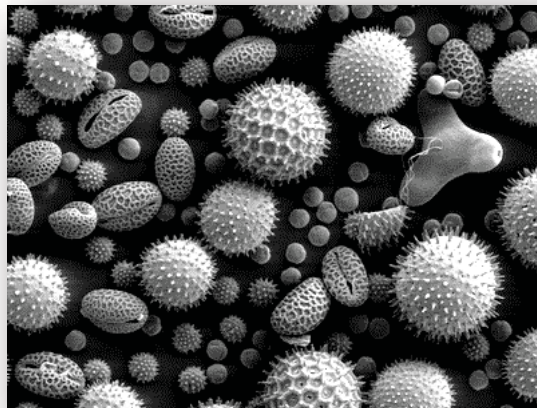
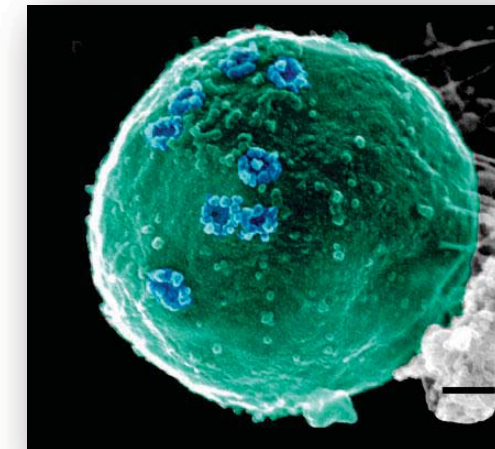
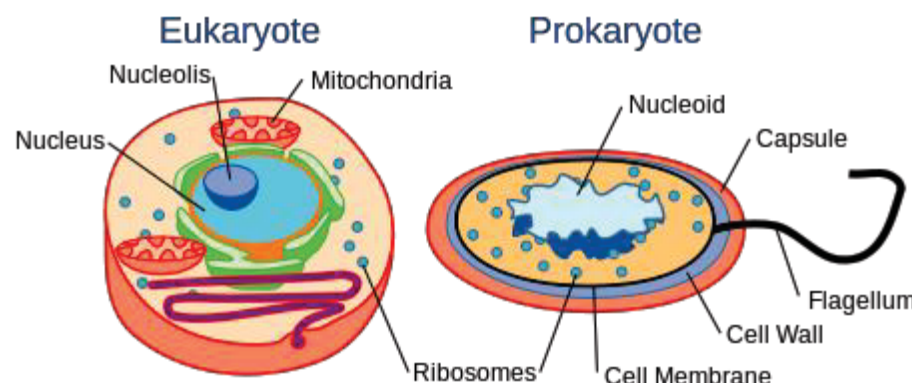
Introduction - Motivation

- Novel tools for biotechnology
- Quantitative method for cell analysis
- The need for 3D cell analysis
3D models of tumor cells
for anticancer drug testing
- Hot topics
 - label-free analysis of living cells and tissues (4D)
 - cellular biophysics, characterization of physical processes
 - vascular and tumor biology
 - recognition and monitoring of bacteria colonies

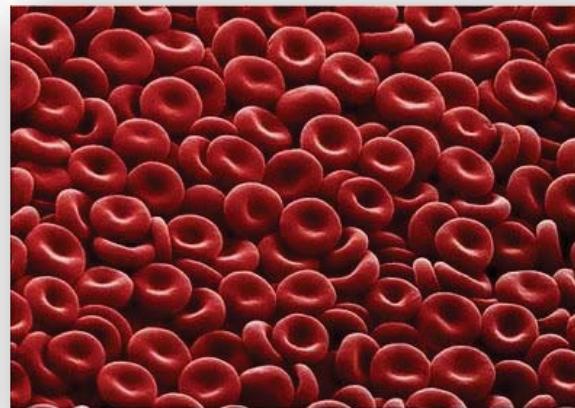


A scanning electron microscope picture of a nerve ending. Source: publications.nigms.nih.gov

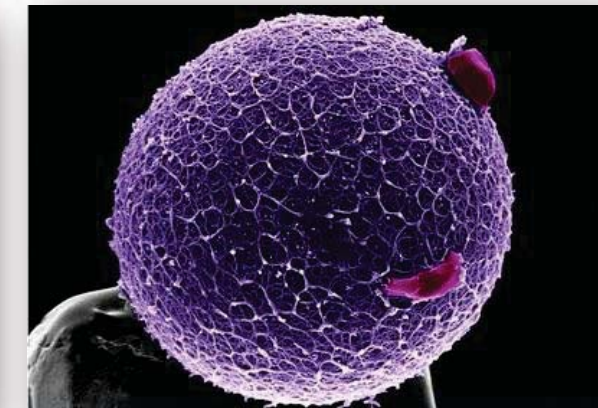
Introduction



Human egg with coronal cells



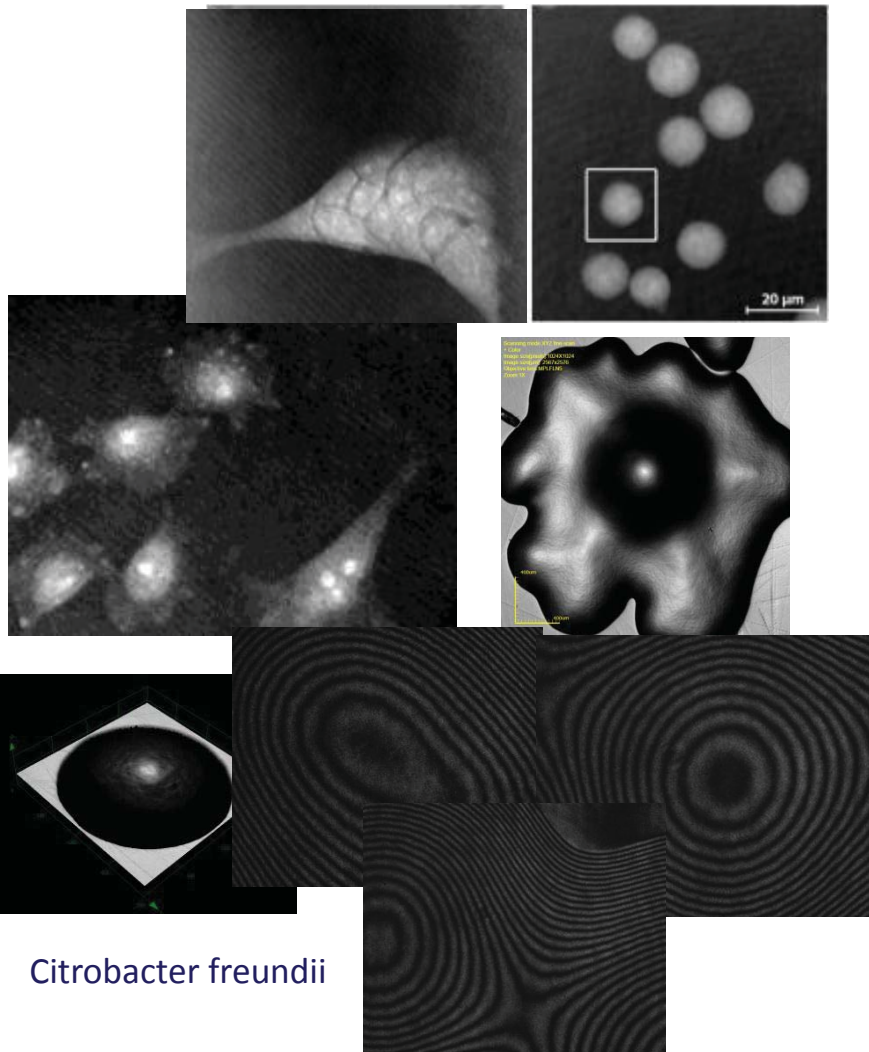
Red blood cells



Human egg with coronal cells

Nature Reviews Molecular Cell Biology 5, 427 (June 2004)

Phase microobjects: biological



Possible:

- high-numerical aperture
- high-phase difference
- high-phase gradient

High spatial resolution required

Often high temporal resolution required (for 4D reconstruction)

Most often **not known** model



INNOWACYJNA
GOSPODARKA
NARODOWA STRATEGIA SPÓŁNOŚCI

FNP
Fundacja na rzecz Nauki Polskiej

UNIA EUROPEJSKA
EUROPEJSKI FUNDUSZ
ROZWOJU REGIONALNEGO



Cells as measurement objects

| | Prokaryotes | Eukaryotes |
|-------------------------|----------------------------------|--------------------------------------|
| Typical organisms | Bacteria, archaea | protists, fungi, plants, animals |
| Type of nucleus | Nucleoid region, no real nucleus | Nucleus with double membrane |
| Typical size | ~1-10 μm | ~10-100 μm |
| Refractive index | | $n = \sim 1,05-1,55$ |
| Refractive index change | | $\Delta n < 0.1$ high-phase gradient |

Properties of bio-samples

- | | |
|-----------------------------------|---------------------------------|
| Polarization Sensitive | Birefringence Models |
| High-Phase Gradient | Depend on Choice of Wavelengths |
| Core of the Cell important | Cell boundary important |
| Use of Born / Rytov Models needed | |

Cell measurement and observation techniques

Electron
microscope

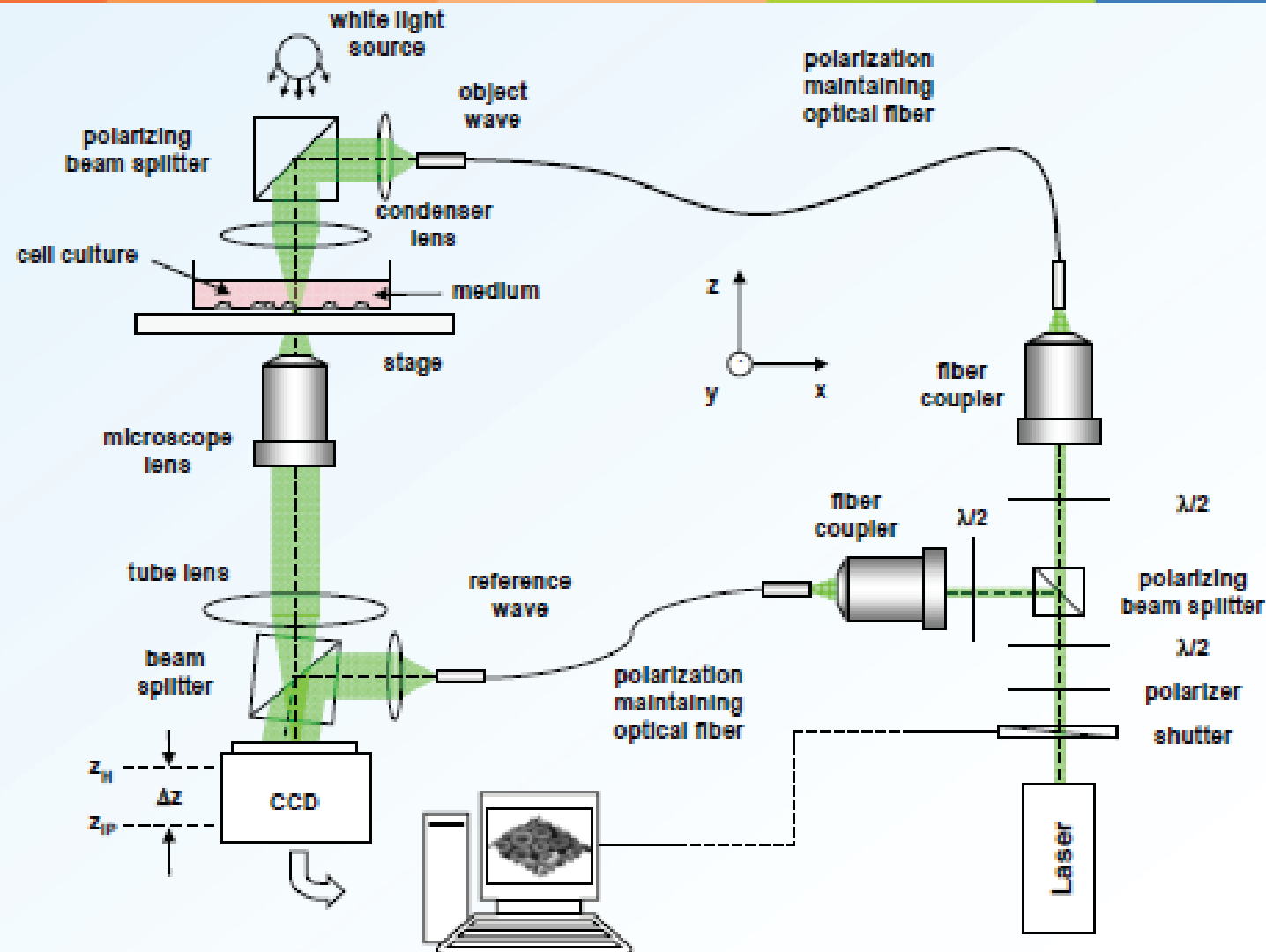
Digital holographic
microscope

Zernike/Nomarski
Phase contrasts

Fluorescence
microscopy

Confocal
microscopy

Modular DHM for Live Cell Imaging



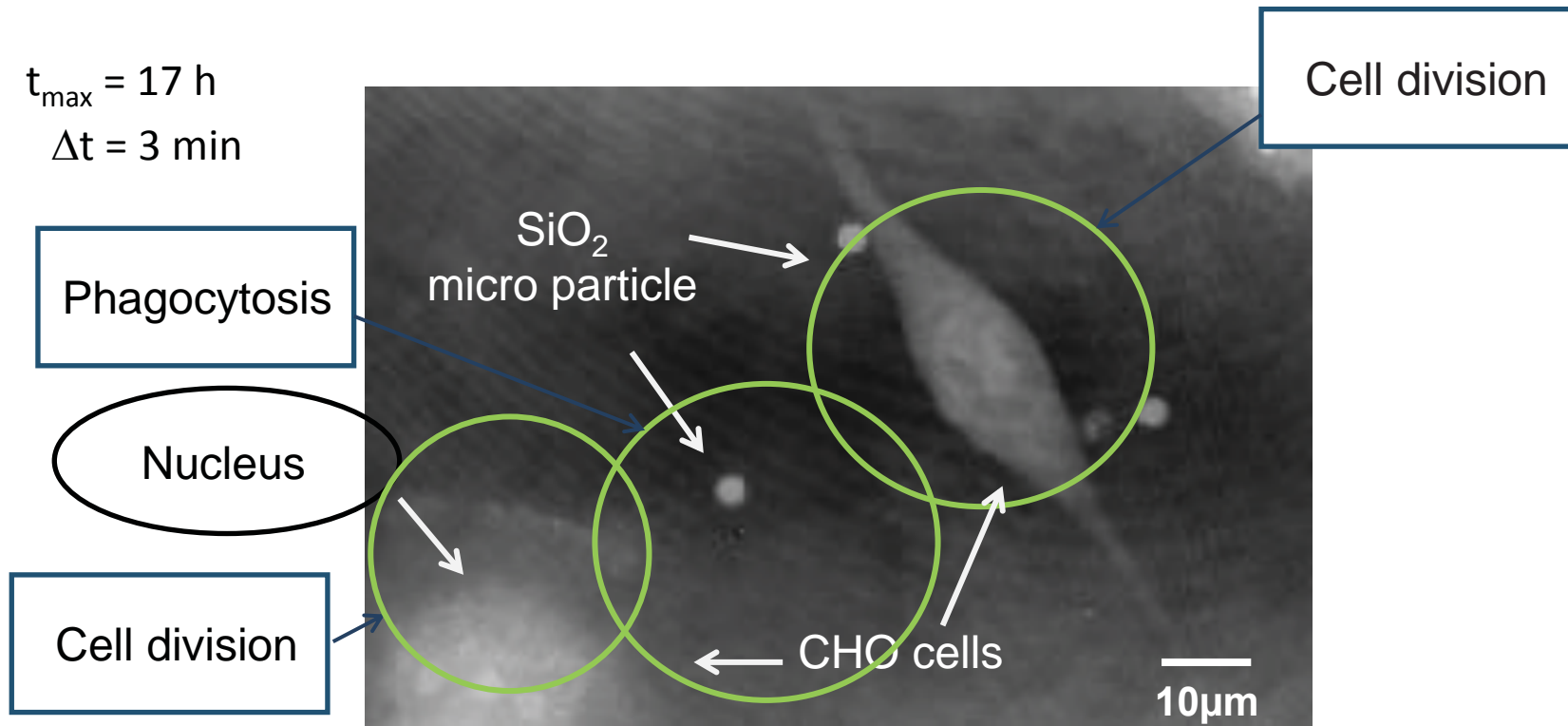
6.3.2012

B. Kemper, D. Carl, A. Hölink, G. von Bally, I. Bredebusch, J. Schnakenburger, Proc. SPIE 6191 (2006).

Internalization of particles by phagocytosis

Phagocytosis: cellular process in which the cell internalize particles

Example: DHM phase contrast video of Chinese Hamster Ovary (CHO) cells during internalization of SiO_2 micro particles ($\varnothing 3.44 \mu\text{m}$)

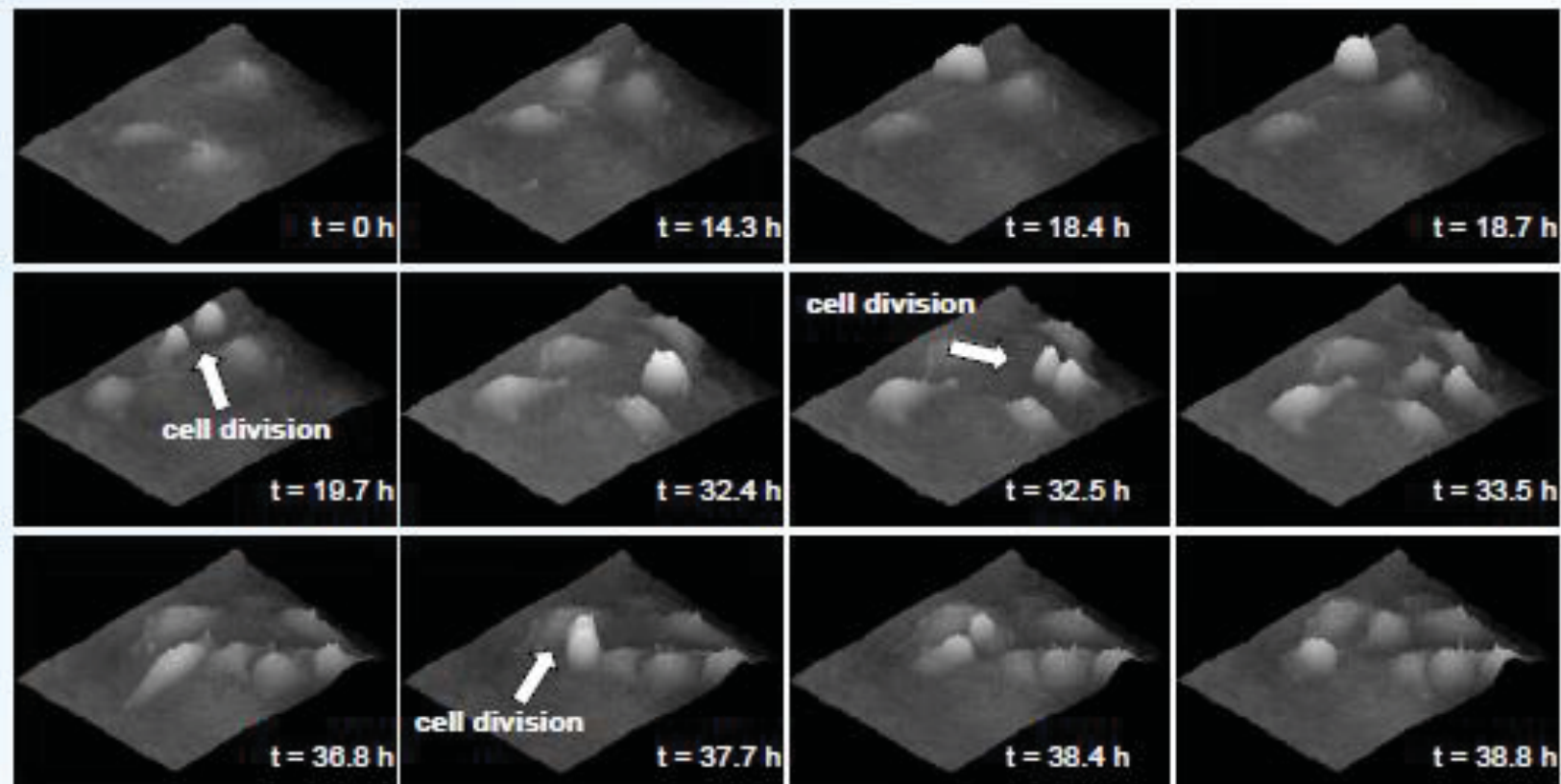


40x

ECBO, Munich 2011

Cell division monitoring

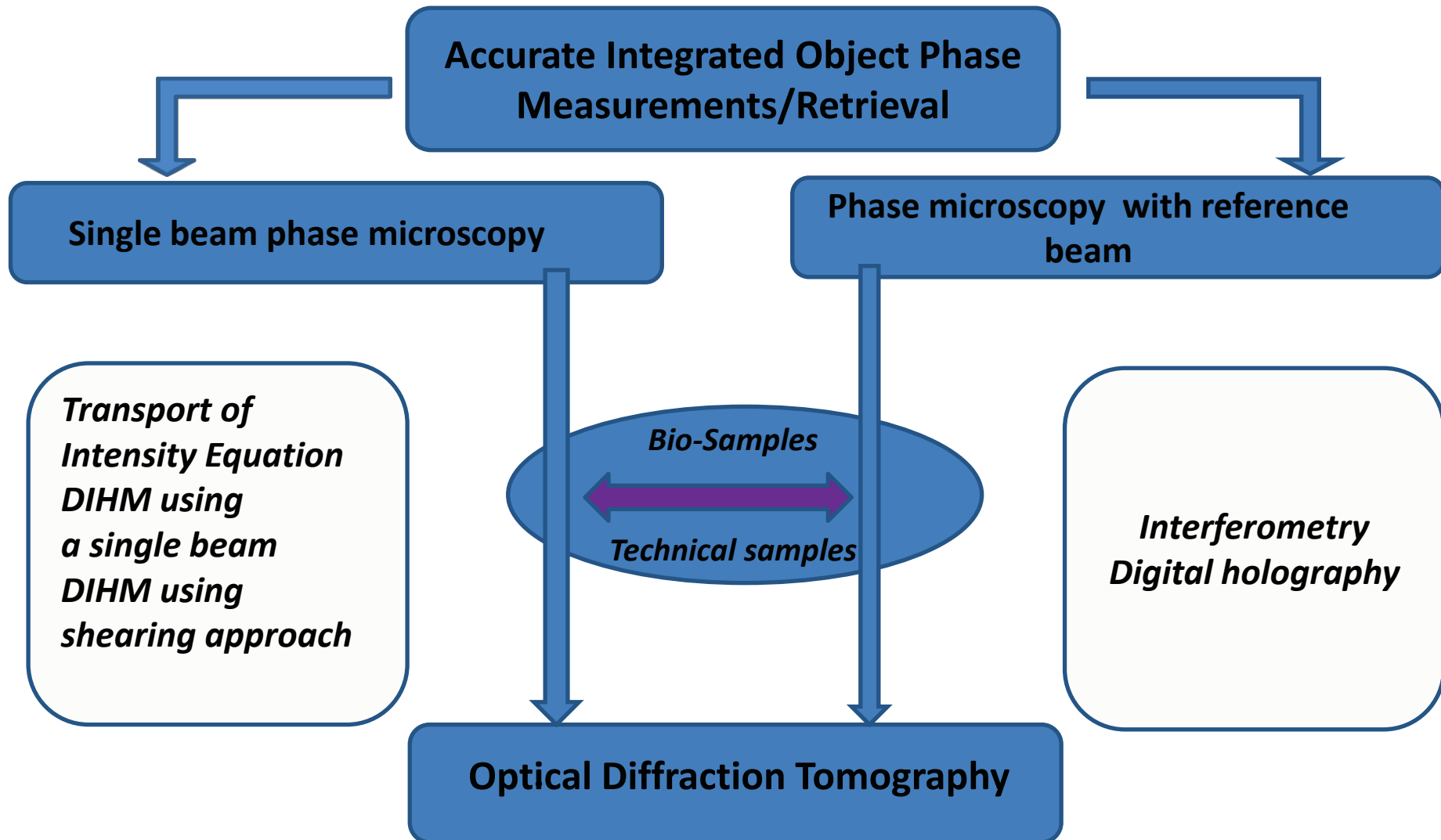
DHM phase contrast (pseudo 3D)



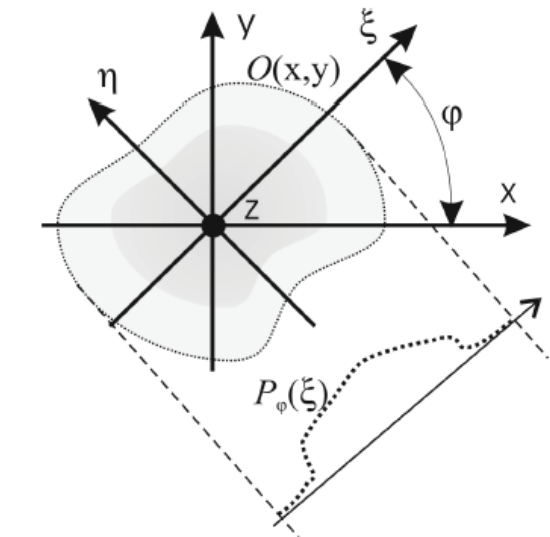
B. Kemper, A. Bauwens, A. Vollmer, S. Ketelhut, P. Langehanenberg, J. Möthing, H. Karch, G. von Bally, J. Biomed. Opt. 15, 036009 (2010)

6.3.2012

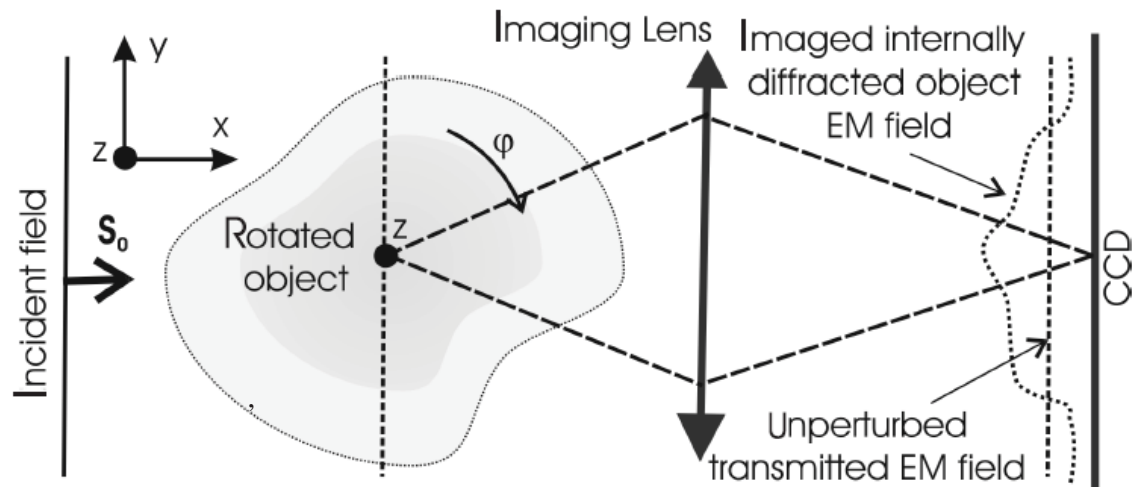
General approach to 3D phase reconstruction



Standard registration method in optical diffraction tomography



Co-ordinate system



The simplest reconstruction method : filtered back projection

$$O(x, y) = \frac{1}{(2\pi)^2} \int_0^\pi d\varphi$$

$$\int_{-\infty}^{\infty} |\mathbf{k}| \tilde{P}_\varphi(\mathbf{k}) \exp \{ i\mathbf{k}(x \cos \varphi + y \sin \varphi) \} d\mathbf{k}$$

where

$$\tilde{P}_\varphi(\mathbf{k}) = \int_{-\infty}^{\infty} P_\varphi(\xi) \exp \{ -i\mathbf{k}\xi \} d\xi$$

Approximations in ODT

- ▶ The captured object projection P_φ must well approximate an object integrated phase and amplitude
- ▶ Tomographic reconstruction algorithms require linearization of the light interaction with an object
- ▶ Strong internal diffraction or refraction causes big errors

Major drawback of ODT applicability in measurement of micro optical elements refractive-index/birefringence structure is its **low dynamic range**, i.e. refractive-index structures with small variations can be measured only.

Tomographic reconstruction algorithms

Additional requirement for biosamples
reconstruction from the limited angle of
projection



Tomographic reconstruction algorithms

Full angle FA

- Fourier slice theorem
- Filtered backprojection
- Filtered backpropagation (FBP)
- Algebraic reconstruction technique (ART + MART)

Limited angle LA

- Hybrid backpropagation
- Hybrid backprojection
- Algebraic reconstruction technique (ART + MART)
- Deconvolution-iteration
- Iterative convolution backpropagation
- Iterative constraint algorithm

Tomographic reconstruction algorithms - FA

- Fourier-slice theorem
(propagation-slice theorem)

$$F_r\{p(r, \alpha)\}(R, \alpha) = F_2\{f(x, y)\}(R \cos \alpha, R \sin \alpha)$$

- $f(x, y)$ – two-dimmensional object function
- $p(r, \alpha)$ – projection of $f(x, y)$

$$F_r\{p(r, \alpha)\} = \int_{-\infty}^{\infty} p(r, \alpha) e^{-2\pi r R} dr$$

$$F_2\{f(x, y)\} = \int_{-\infty}^{\infty} f(x, y) e^{-2\pi i(xX + yY)} dx dy$$

Tomographic reconstruction algorithms - FA

- Filtered backprojection
 - weak scattering
 - no diffraction
 - straight-line propagation
 - $\Delta n < 0.1$ (gradient index)
 - $\Delta n < 0.03$ (step index)

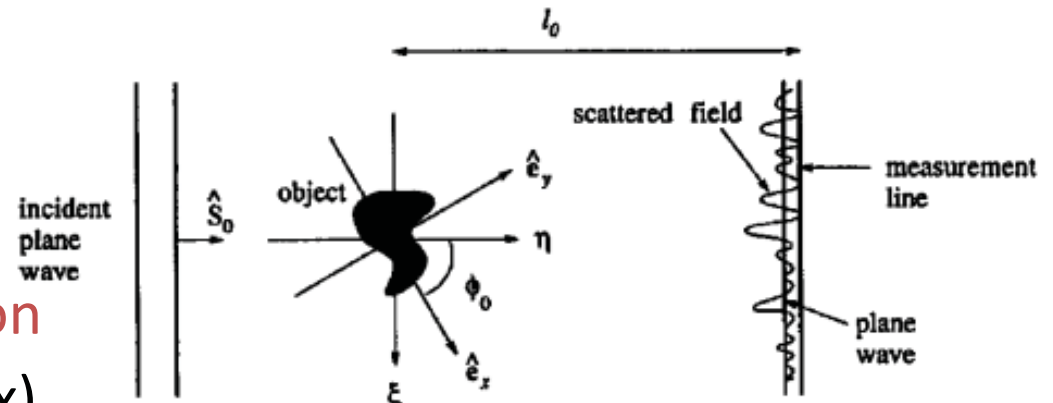


Fig. 1. Classical scan configuration.

$$f_S = -\frac{s_0^2}{\pi a_S} \int d\hat{\mathbf{u}} \cos^2 \alpha \frac{1}{a_R} \mathcal{H} p_s(\mathbf{r}_R, t = \tau_S + \tau_R),$$

- Hybrid algorithm
 - numerically backpropagation of total field to the center of the reconstruction area using inverse diffraction before the filtered backprojection algorithm is used

T. C. Wedberg, J. J. Stammes, and W. Singer, Appl. Opt. 34 6575-6581 (1995)
 C. Esmersoy and D. Miller, Geophysics 54 921-926 (1989)

Tomographic reconstruction algorithms - FA

- Filtered backpropagation (FBP)

- weak scattering
- **diffraction**
- Rytov or Born approximation

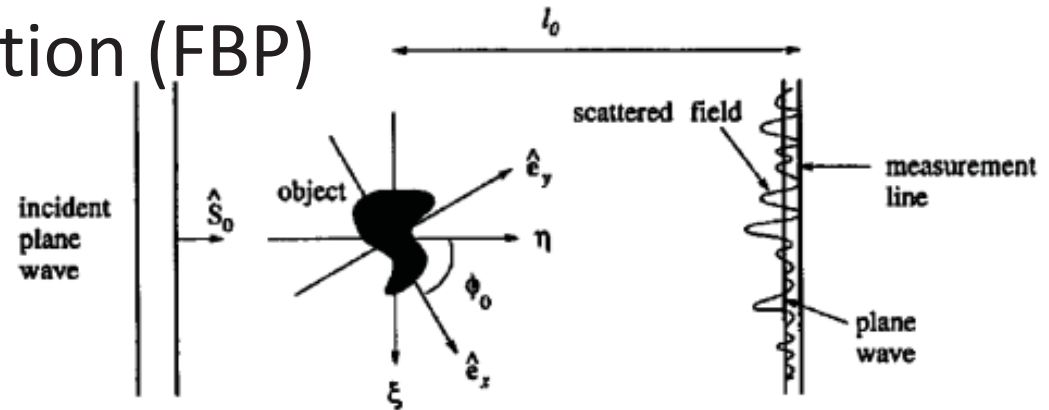


Fig. 1. Classical scan configuration.

$$f_R(\mathbf{r}) = -\frac{s_0^2}{\pi a_S} \int d\hat{\mathbf{u}} \cos^2 \alpha \mathcal{H}q(\hat{\mathbf{u}}, t = \tau_S - s_0 \hat{\mathbf{u}} \cdot \mathbf{r})$$

- Hybrid algorithm

- numerically backpropagation of total field to the centre of the reconstruction area using inverse diffraction before the FBP algorithm is used

T. C. Wedberg, J. J. Stammes, and W. Singer, Appl. Opt. 34 6575-6581 (1995)
 C. Esmersoy and D. Miller, Geophysics 54 921-926 (1989)

Tomographic reconstruction algorithms - FA

- Filtered backpropagation (FBP)

$$O_{lp}(\mathbf{r}) = \frac{1}{2\pi} \int_{-\pi}^{\pi} \Pi_{\phi_0}(x \sin \phi_0 - y \cos \phi_0, x \cos \phi_0 + y \sin \phi_0) d\phi_0$$

$$\Pi_{\phi_0}(\xi, \eta) = \frac{1}{2\pi} \exp[ik(l_0 - \eta)] \int_{-k}^{\infty} \tilde{\Gamma}_{\phi_0}(\kappa) |\kappa| \times \exp[i\gamma(\eta - l_0)] \exp(i\kappa\xi) d\kappa$$

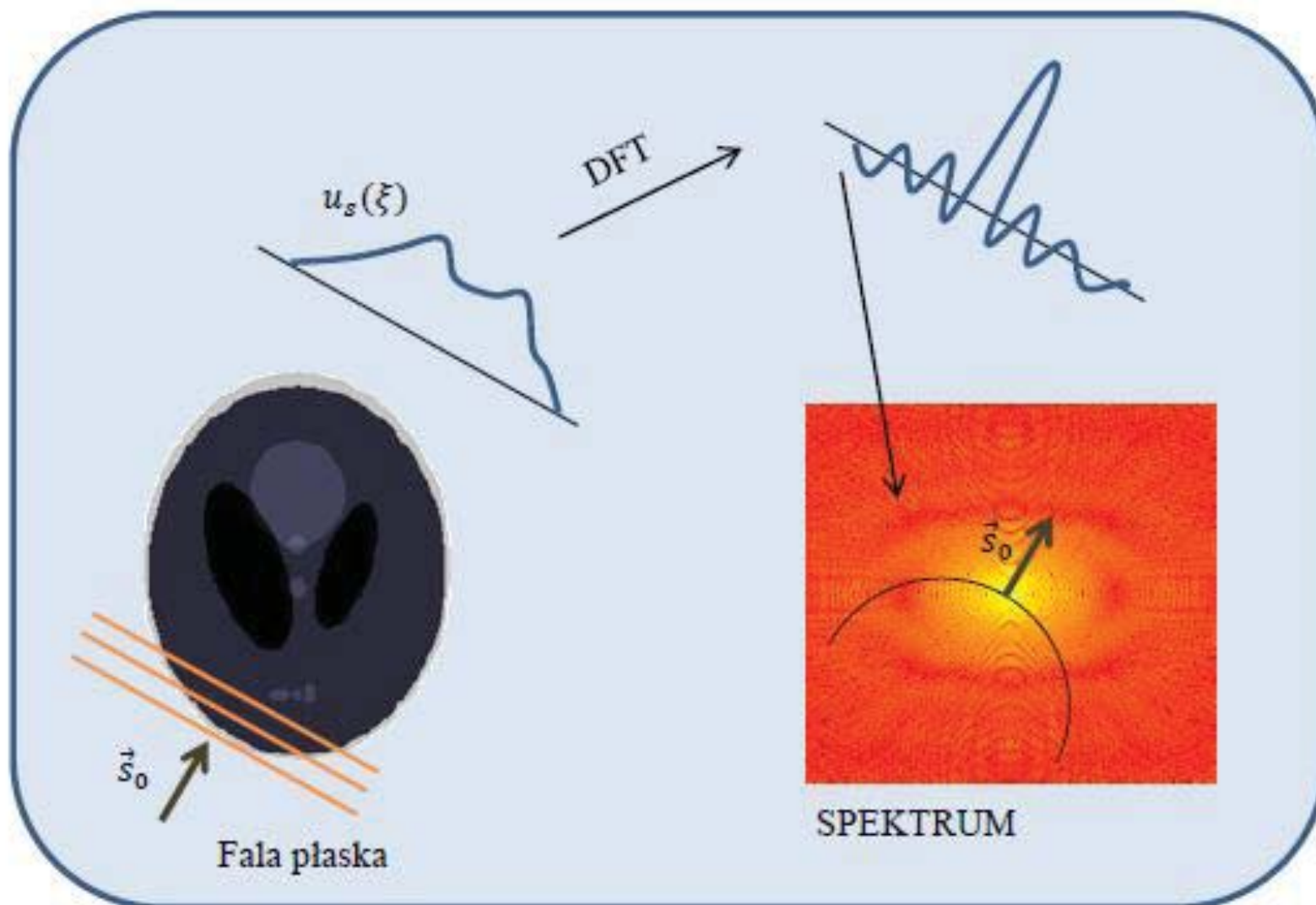
- Born approximation: _____
 - total phase delay must be less than $\pi/2$ **scattering field neglected**
 - not suitable for live cell measurement
- Rytov approximation: _____
 - not sensitive to the size of the sample or the total phase delay
 - sensitive to the gradient of refractive index **scattering field considered**

$$n_\delta \gg \left(\nabla \varphi^{(s)} \frac{\lambda}{2\pi} \right)^2, \text{ with } \varphi^{(s)} = \ln \left(\frac{U(\vec{R})}{U^{(I)}(\vec{R})} \right)$$

$$\Gamma_{\phi_0}(\xi) = \begin{cases} \frac{i}{k} \ln \left[\frac{U(\xi)}{U_0(\xi)} \right] & \downarrow \\ \frac{i}{k} \frac{U(\xi) - U_0(\xi)}{U_0(\xi)} & \uparrow \end{cases}$$

Y. Sung, W. Choi, C. Fang-Yen, K. Badizadegan, R. R. Dasari,
and M. S. Feld, Opt. Express 17 266-277 (2009)

Illustration of backpropagation algorithm



Tomographic reconstruction algorithms FA

- Algebraic reconstruction technique (ART)

$$\Psi = W\mathbf{O} \quad \xleftarrow{\hspace{1cm}} \quad \mathbf{O}^{q+1} = \mathbf{O}^q + \frac{\psi_i - \langle \mathbf{w}_i, \mathbf{O}^q \rangle}{\left(\sum_{j=1}^{MN} w_{i,j} \right)^2} \mathbf{w}_i, \quad \sum_{j=1}^{MN} w_{i,j} \neq 0$$

– $\langle \mathbf{w}_i, \mathbf{O}^q \rangle$ indicates the inner product of vectors \mathbf{w}_i and \mathbf{O}^q , q indicates the iteration number, \mathbf{w}_i is the i -th row of the projection matrix, and ψ_i is the corresponding measured *ray sum*. If $\sum_{j=1}^{MN} w_{i,j} = 0$, \mathbf{O} is left unchanged.

- Multiplicative algebraic reconstruction technique (MART)

$$O_j^{q+1} = R_j^q O_j^q \quad \text{for } j = 1, \dots, MN$$

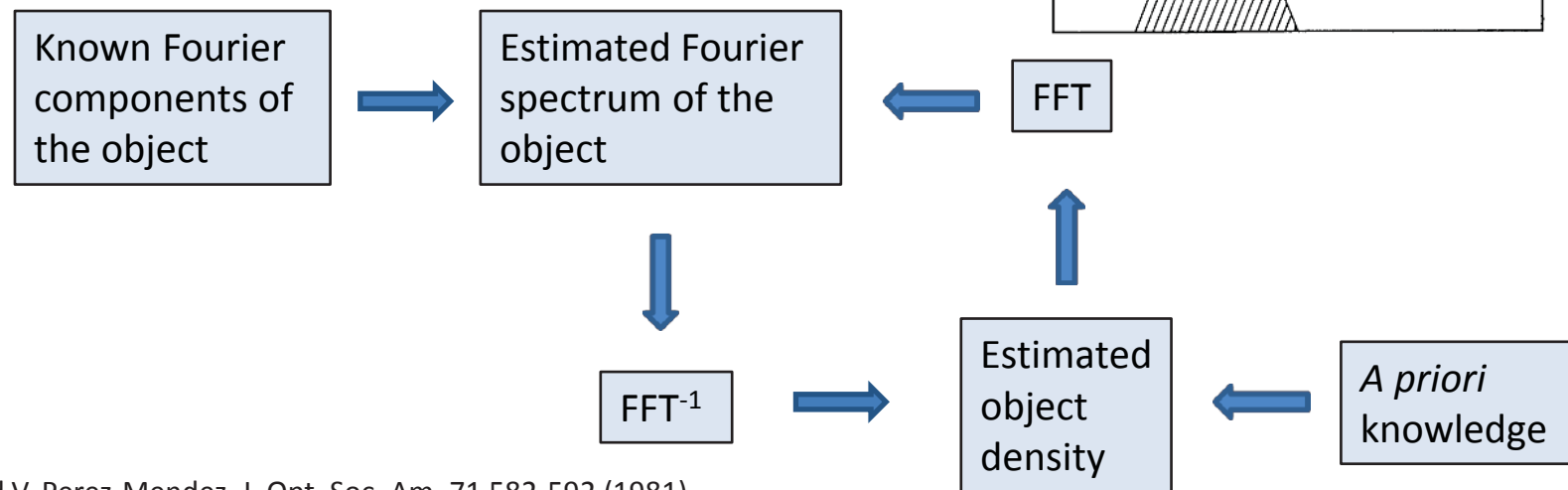
↓

$$\begin{cases} R_j^q = 1 - \lambda w_{i,j}^* \left(1 - \frac{\psi_i}{\langle \mathbf{w}_i, \mathbf{O}^q \rangle} \right), & \langle \mathbf{w}_i, \mathbf{O}^q \rangle \neq 0 \\ R_j^q = 1, & \text{otherwise.} \end{cases}$$

– The normalized weight w_{ij}^* is equal to w_{ij}/w_{max} , where w_{max} is the largest element of the projection matrix W and λ is a relaxation parameter. The ray sum number i is given by $(q \bmod P) + 1$.

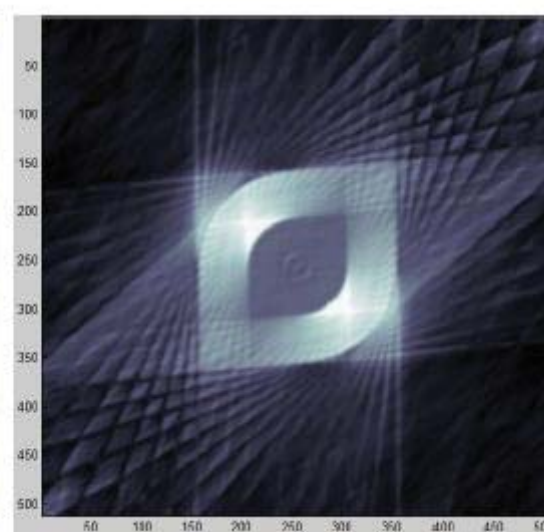
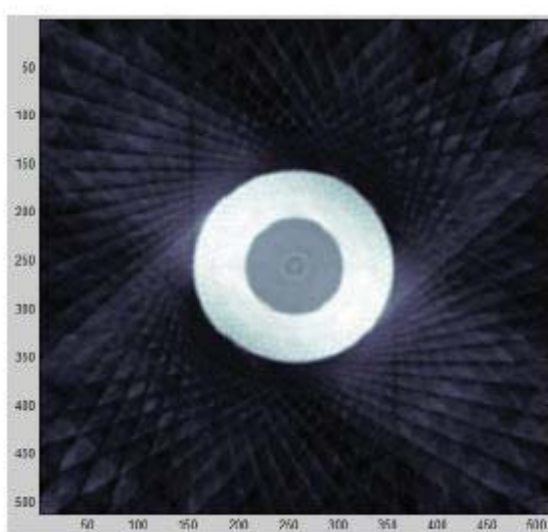
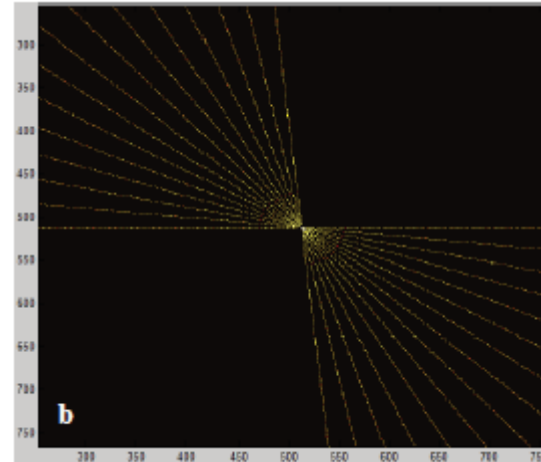
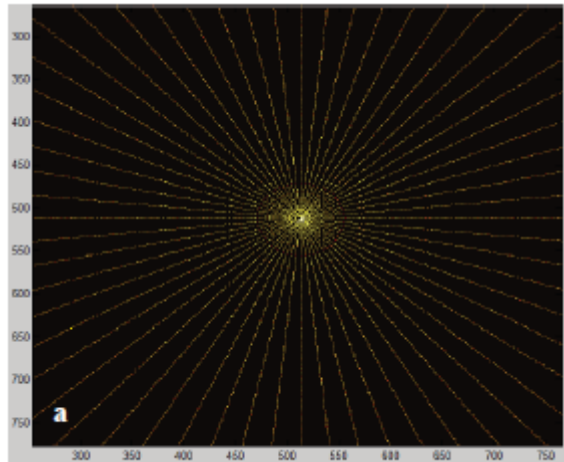
Tomographic reconstruction algorithms - LA

- Deconvolution-iteration
 - Fourier-transform-iteration scheme for filling in missing Fourier components



K. C. Tam and V. Perez-Mendez, J. Opt. Soc. Am. 71 582-592 (1981)

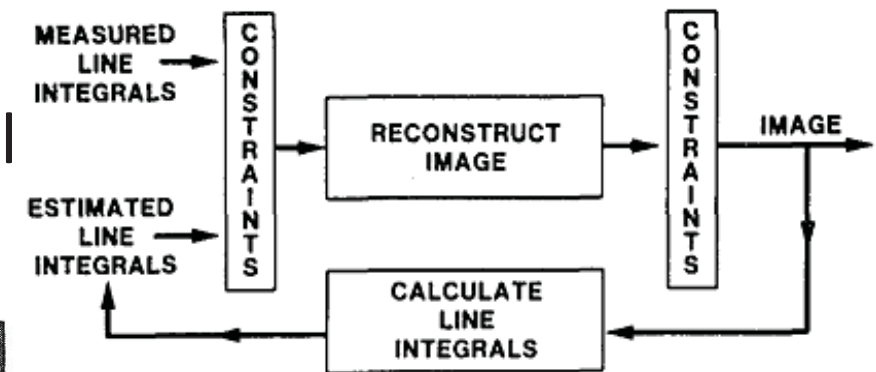
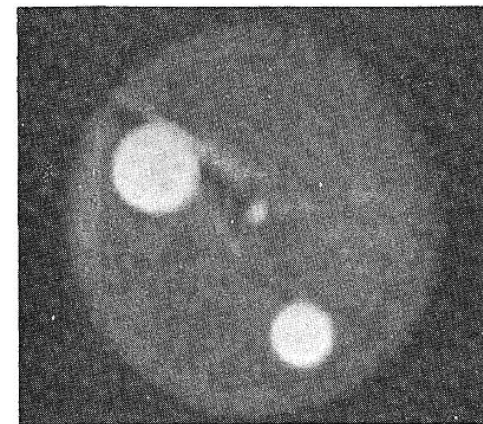
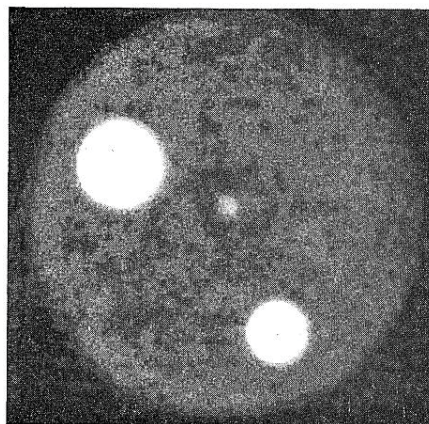
Reconstruction from limited AP



Tomographic reconstruction algorithms

- Iterative convolution backprojection

– *a priori* knowledge about the image and line-integral data – constraints



$$\hat{x}_{i+1} = \mathbf{T}(\hat{x}_i) = \mathbf{S}^x \mathbf{C}^I \mathbf{R} \begin{bmatrix} \mathbf{C}^x \hat{x}_i \\ y \end{bmatrix}$$

B. P. Medoff, W. R. Brody, M. Nassi, and A. Macovski, J. Opt. Soc. Am. 73 1493-1500 (1983)

Tomographic reconstruction algorithms

- Iterative constraint algorithm
 - based on iterative convolution backpropagation and deconvolution-Fourier iteration
 - used modified Fourier diffraction theorem

$$\hat{F}(K_x, K_y, K_z) = \frac{ik_z}{\pi} \hat{U}^{(S)}(k_x, k_y; z^+ = 0)$$

$$\hat{F}(K_x, K_y, K_z) = \frac{i(K_z + k_{z0})}{\pi} \hat{U}^{(S)}(K_x + k_{x0}, K_y + k_{y0}; z^+ = 0)$$

- Born approximation

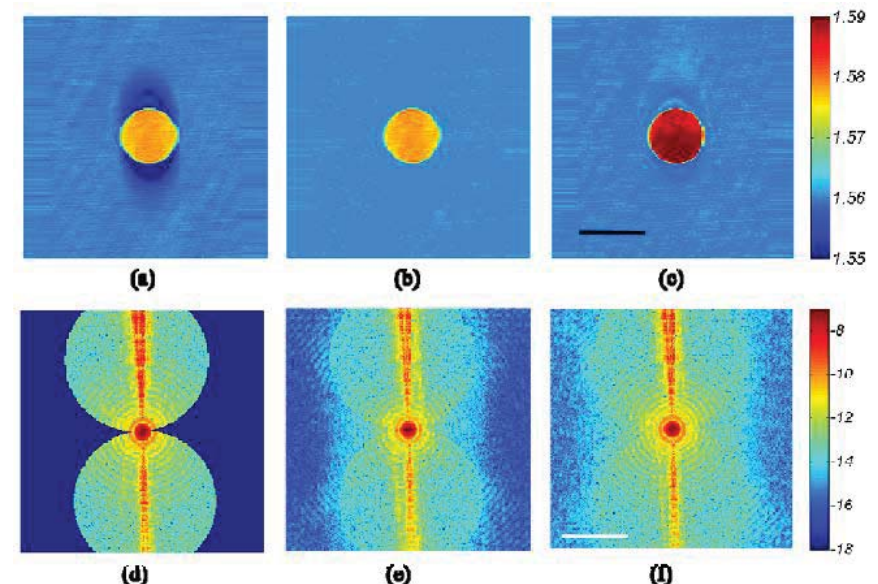
$$\hat{U}^{(S)}(K_x + k_{x0}, K_y + k_{y0}; \theta) = \iint (U(x, y; \theta) - U_{bg}(x, y; \theta)) / U_{bg}(x, y; \theta) e^{-iK_x x - iK_y y} dx dy$$

- Rytov approximation

$$\hat{U}_{Rytov}^{(S)}(K_x + k_{x0}, K_y + k_{y0}; \theta) = \iint \ln(U(x, y; \theta) / U_{bg}(x, y; \theta)) e^{-iK_x x - iK_y y} dx dy$$

Tomographic reconstruction algorithms

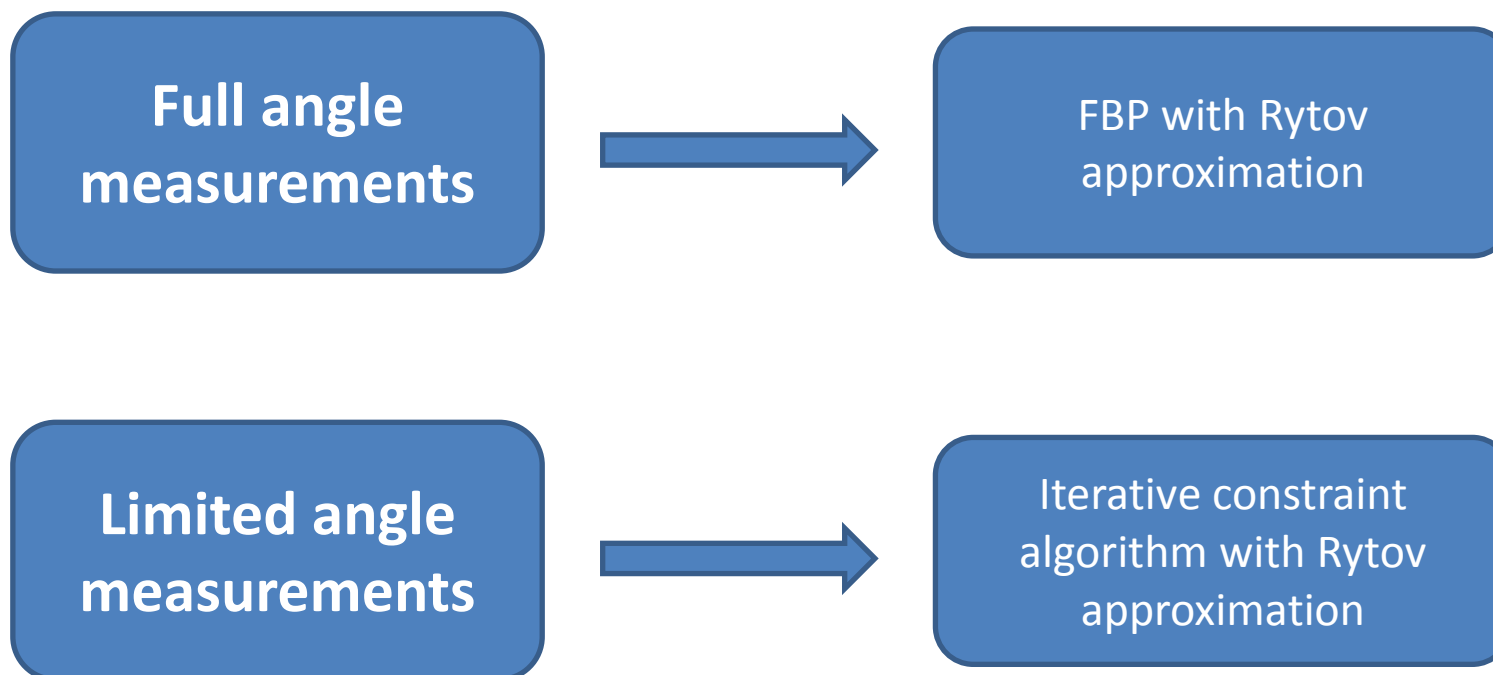
- Iterative constraint algorithm
 - slice image before application of the constraint algorithm
 - same slice image as in (a) after application of the non-negative constraint
 - same slice image as in (b) after 100 iterations
 - amplitude distribution in K_x - K_y plane before application of the constraint algorithm
 - 3D Fourier transform of tomogram after non-negative constraint
 - 3D Fourier transform of tomogram after 100 iterations



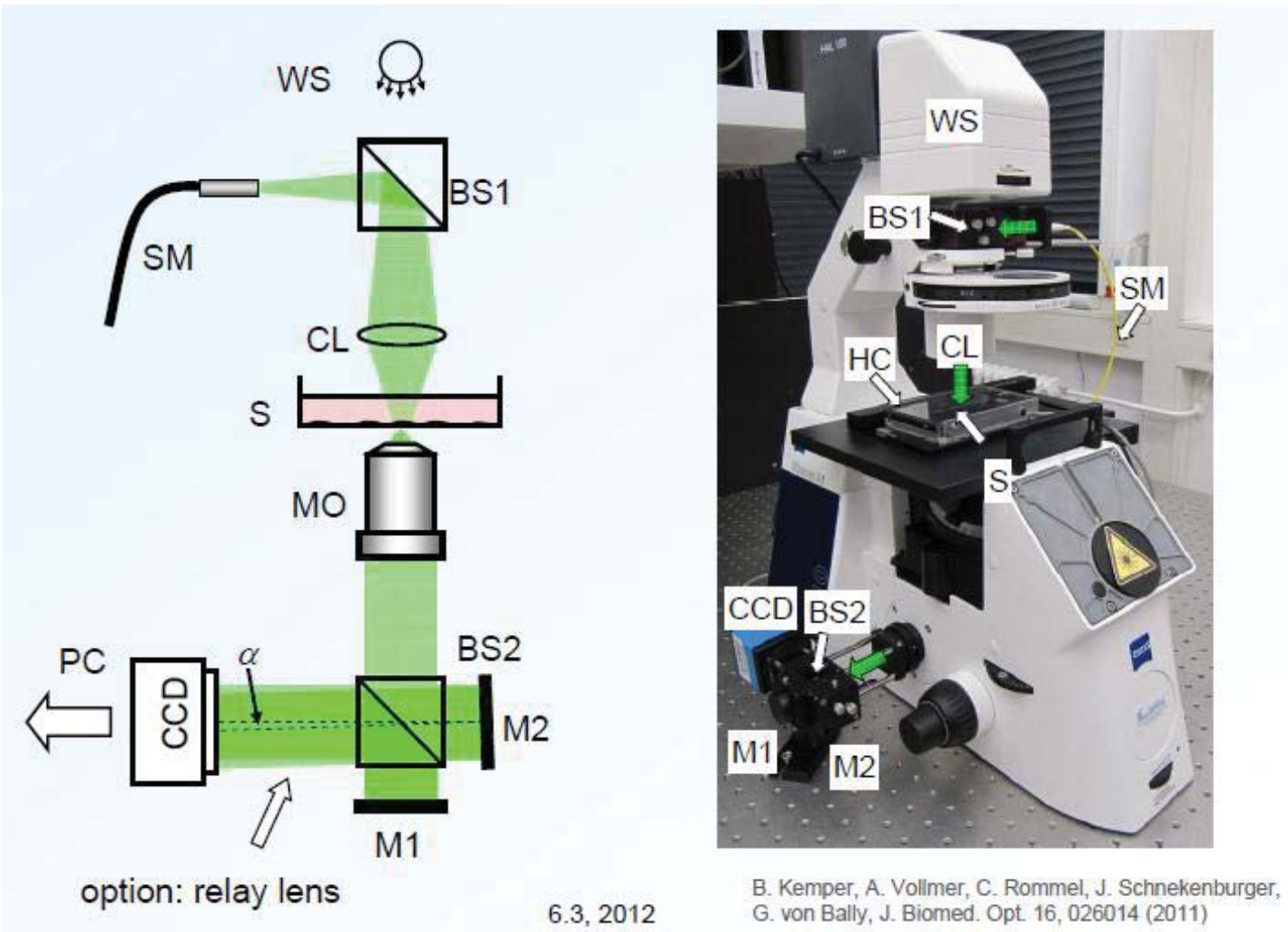
Y. Sung, W. Choi, C. Fang-Yen, K. Badizadegan, R. R. Dasari,
and M. S. Feld, Opt. Express 17 266-277 (2009)

Tomographic reconstruction algorithms

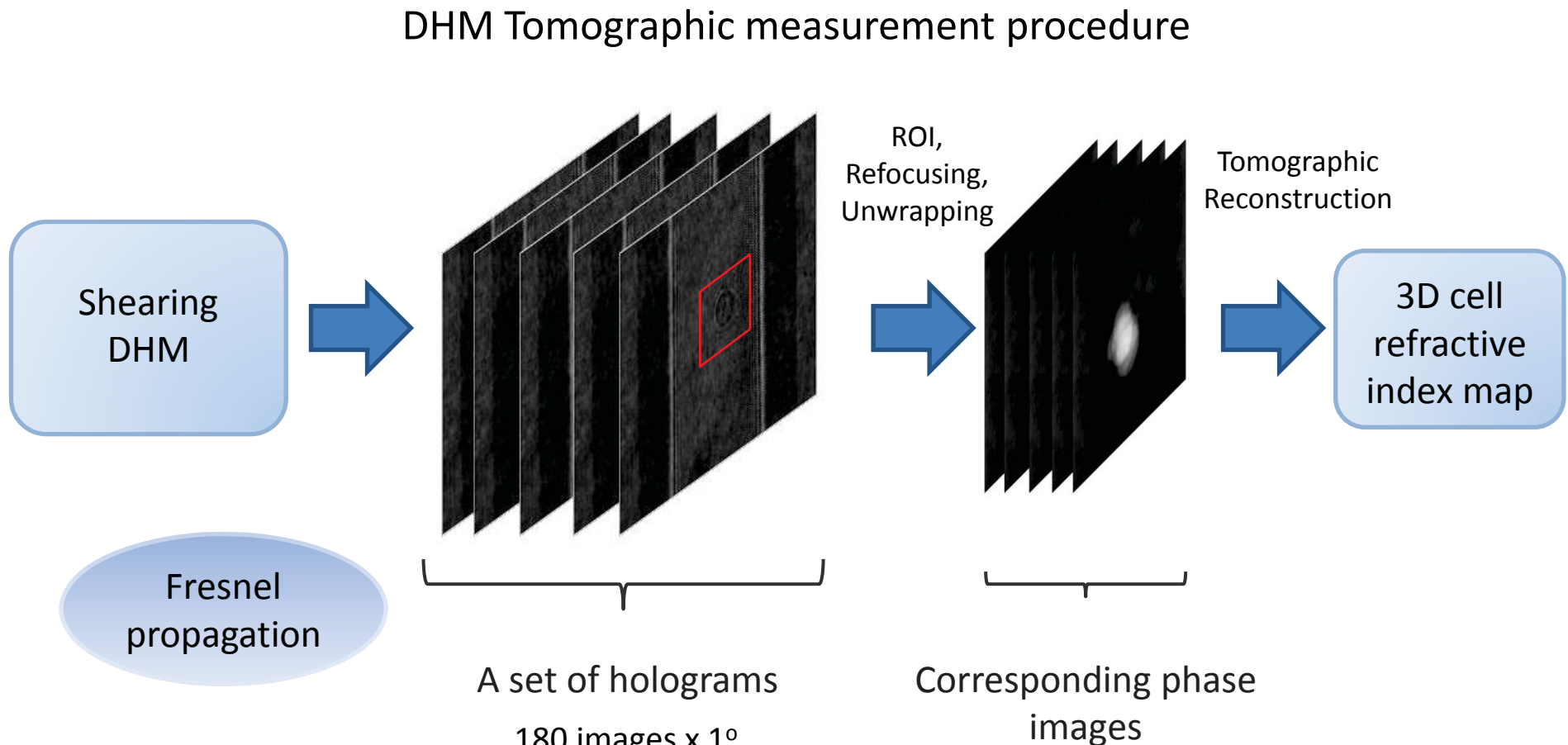
- Biological objects measurements:



Digital Holographic Shearing Microscope



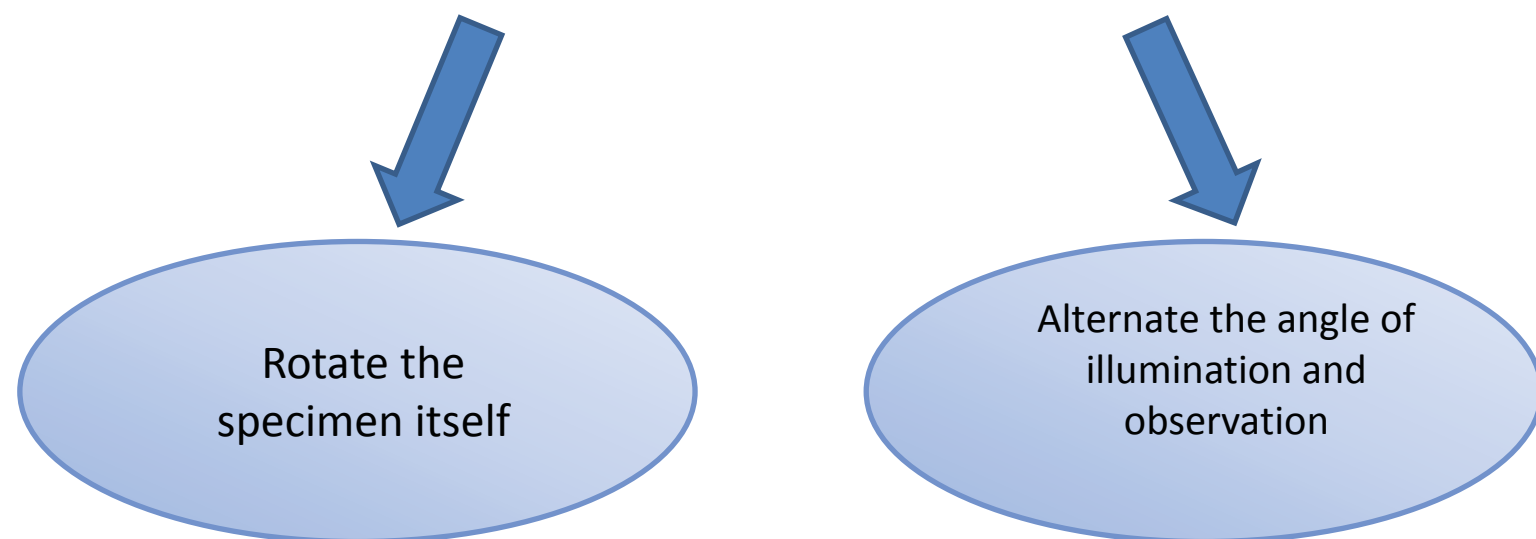
Holographic Microscope



Kemper B. and von Bally G., Appl. Opt. 47 A52-A61 (2008)

To convert DHM into tomograph we need to add specimen rotation to capture several projections

Specimen rotation



Specimen rotation

- Cell cultivation tools (Petri dishes) limit the angle of observation

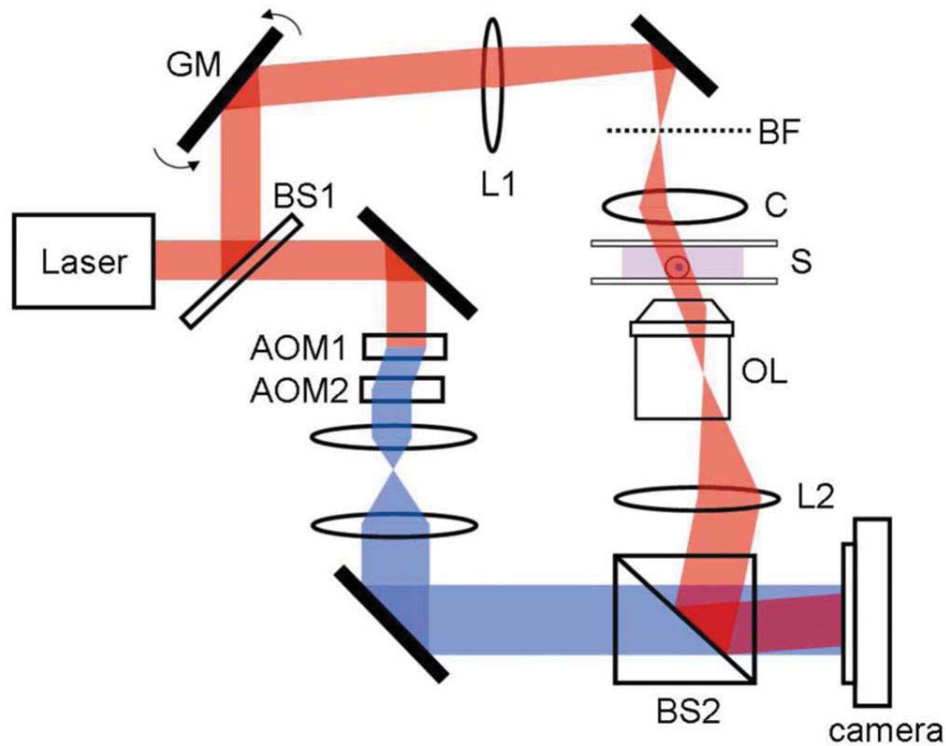


- Manipulate the specimen without optical system modifications

Specimen rotation -requirements

- Fast and accurate living cells rotation
- Rotation - perpendicular to optical axis
- Versatile concept
- Module-based built
- Integration with a microscope system
- Applicable to tomographic setup

Alternate illumination angle

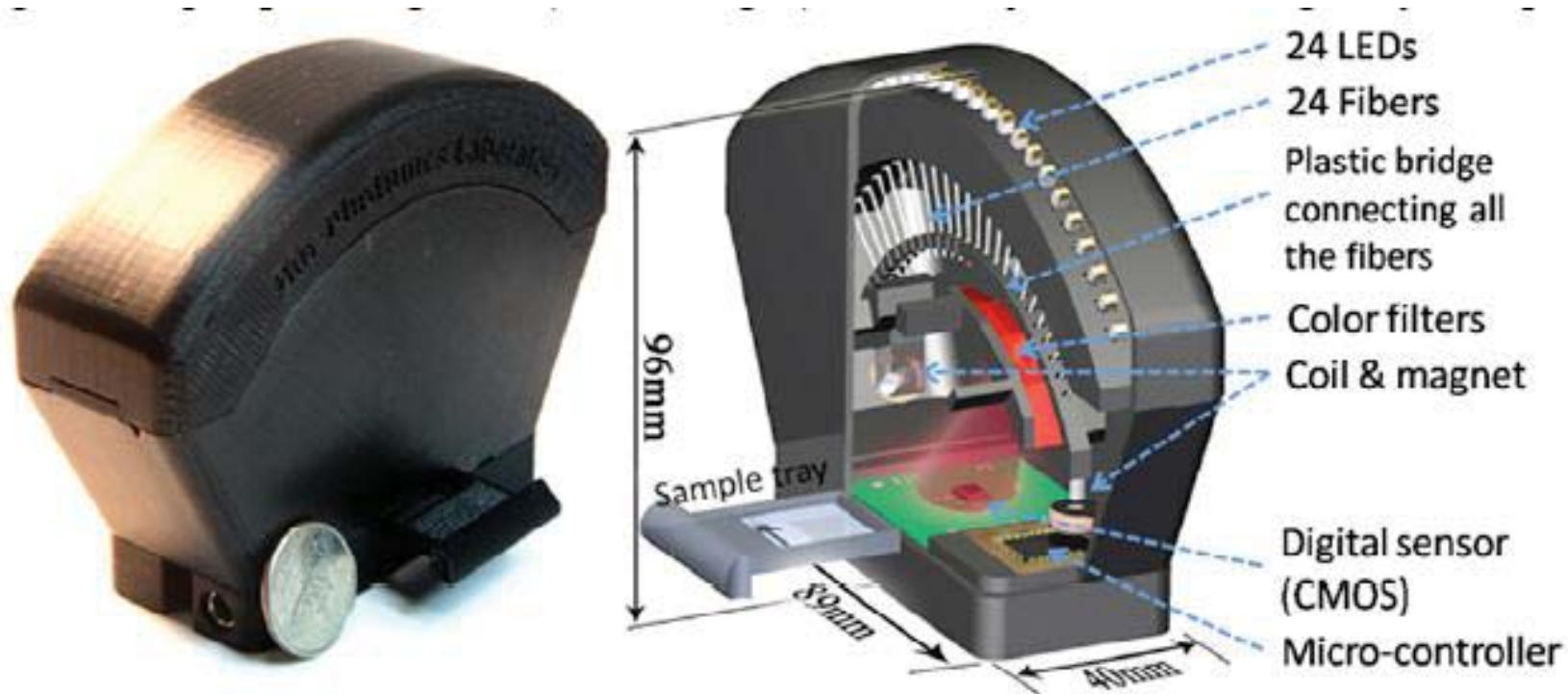


Tomographic phase microscope with varying illumination angle

GM, galvanometer scanning mirror; L1, focal length $f=250$ mm lens; BF, backfocal plane of the condenser lens; C, condenser lens; S, sample; OL, objective lens; L2, $f=200$ mm lens; AOM1 and 2, acousto-optic modulators; BS1 and BS2, beam splitters. The frequency-shifted reference laser beam is shown as darkned after AOM

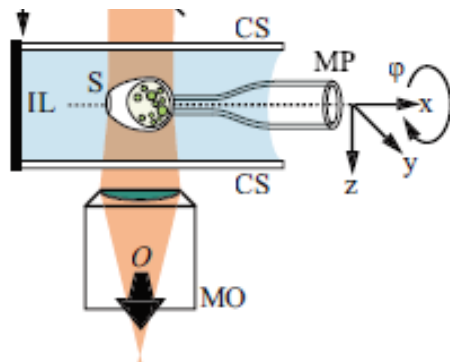
Choi W, Yu CC, Fang-Yen C, Badizadegan K, Dasari RR, Feld MS. Field-based angle-resolved light-scattering study of single live cells. Opt. Lett. 2008;33:1596–1598

Illumination angle



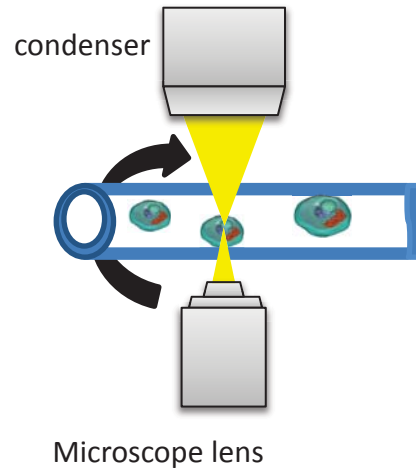
Isikman, S.O. et al., 2011. Lens-free optical tomographic microscope with a large imaging volume on a chip. *Proceedings of the National Academy of Sciences of the United States of America*, 108(18), pp.7296-301.

Specimen rotation



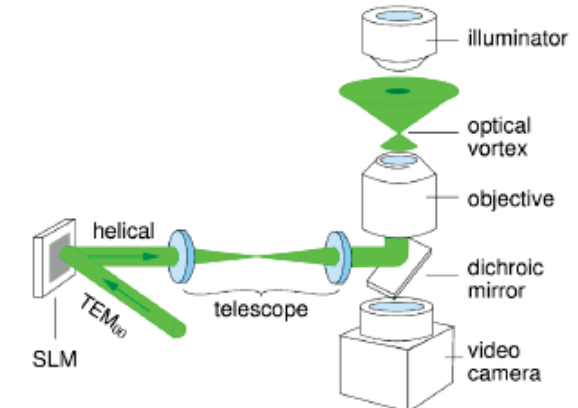
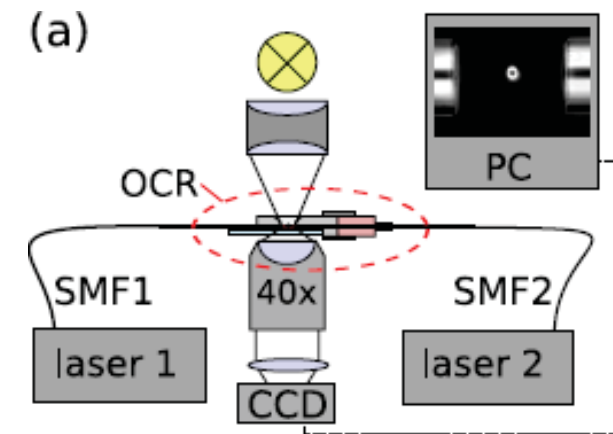
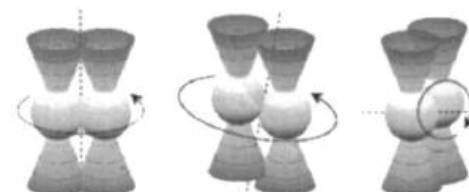
Mechanical

- Single cell mounted on a rotating micropipette
- Cells inside a rotating hollow fibre



Optical

- Double trap Optical Cell Rotator
- Two independent optical traps – rotation about any desired axis.



Specimen rotation: comparison

Mechanical rotation (fiber)

- No additional optical components required
- Fast and uncomplicated software
- Living cells observation



Optical tweezers

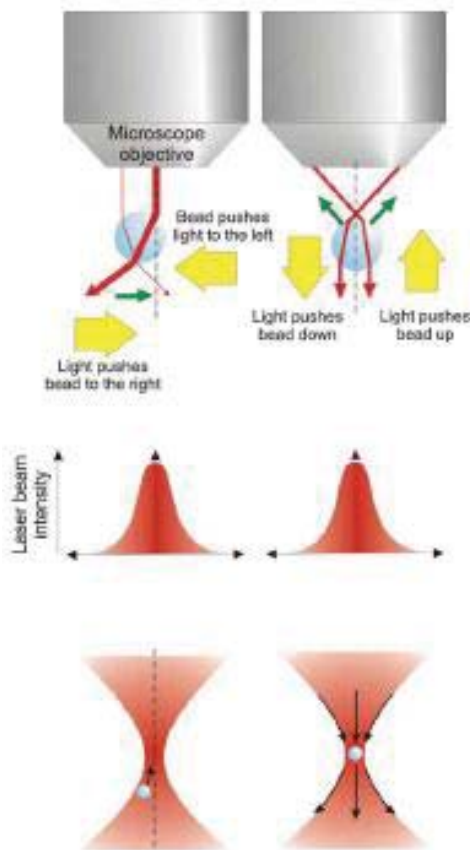
- Only one immersion liquid
- Rotation about any desired axis
- Large number of traps – rotating many cells simultaneously
- High precision

- Refractive indices matching (fluids)
- Cells tend to attach to fiber's walls
- Axial runout – mechanical adjustment
- Particles can move inside the fiber – fluid density related



- High power coherent light source required (100 mW per trap in specimen plane)
- Expensive components
- Risk of cell destruction

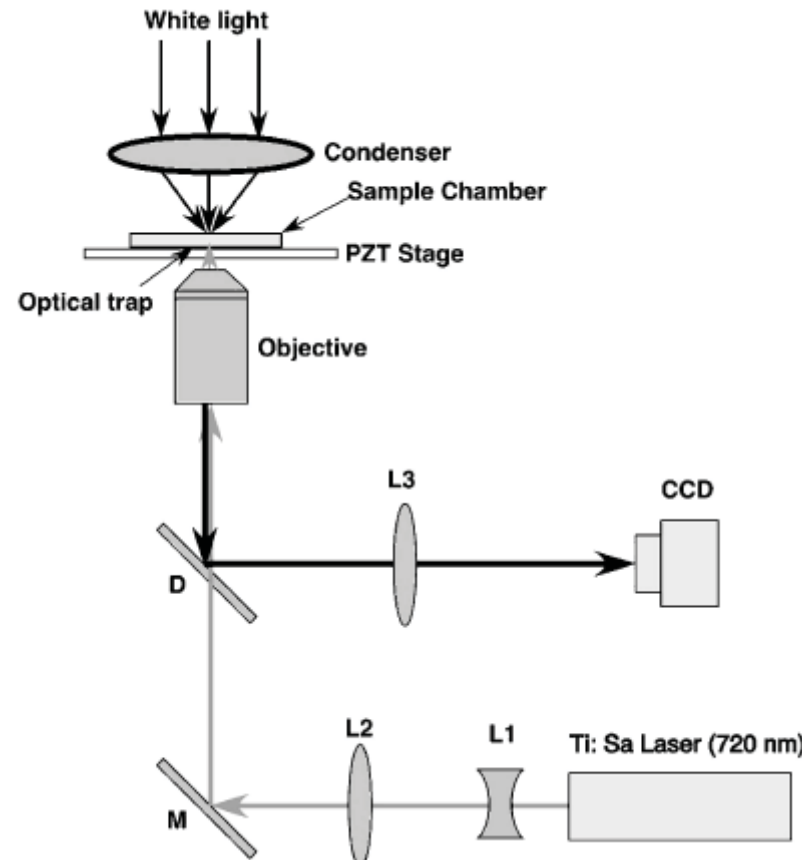
Optical tweezers



- Light refracted through a transparent object imparts momentum to the object to balance its change in direction.
- At Rayleigh size scale, the electromagnetic field (E) of the light causes an object to act as an induced dipole (p), which is drawn into the brightest part of the beam (the focus) where its energy is minimized.

Dholakia, K. & Reece, P., 2006. Optical micromanipulation takes hold Light can influence the motion of particles , from the size of a single cell forefront of many studies in the natural sciences . , 1(1), pp.18-27.

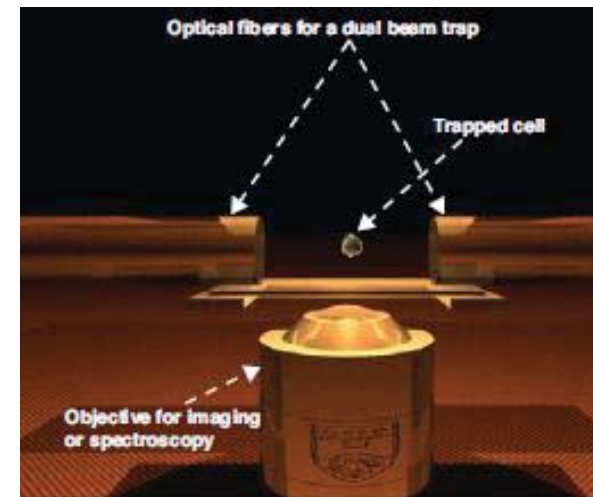
Optical trapping systems



Ã, X.-cheng Y.A.O. & Hang, D.-zhong Z., 2004. Micro-Rotation by Flow-Induced Torque in an Optical Trap . , 11(1), pp.4-6.

Basic optical trapping systems

- High NA objectives (100x NA 1.3)
- Optical fiber trapping systems

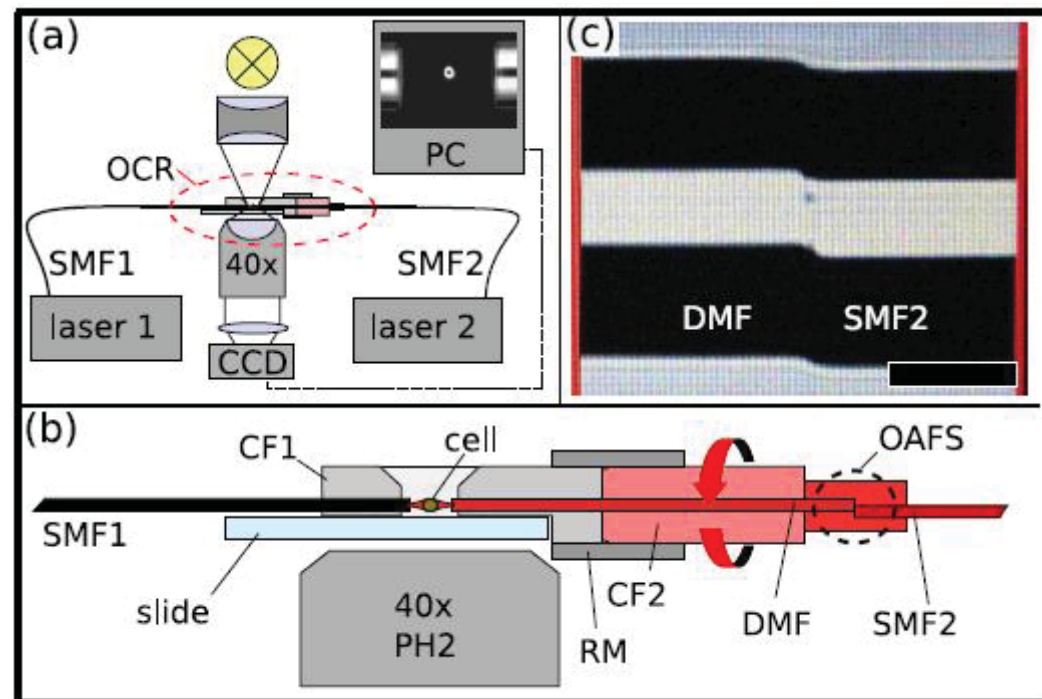


Ashok, P.C. & Dholakia, K., 2012. Optical trapping for analytical biotechnology. *Current opinion in biotechnology*, 23(1), pp.16-21.

Optical cell rotator

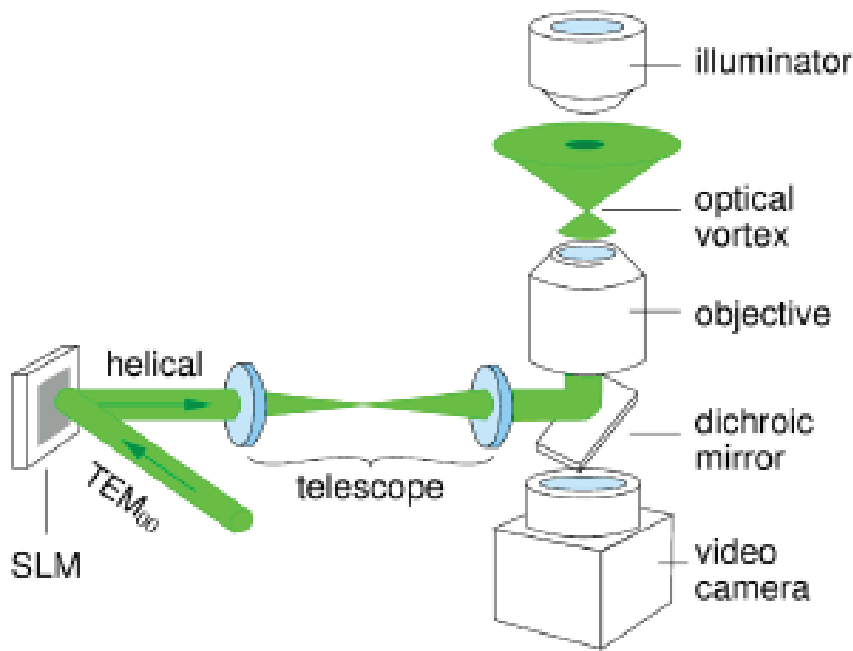
Optical particle rotation

- Dual beam 1064 nm trap
- Beam shaping using single and dual mode fiber
- Mechanical fiber rotation
- Intermediary solution – both mechanical and optical components



Kreysing, M.K. et al., 2008. The optical cell rotator, Optics express, 16(21), pp.912-914

Optical trapping systems



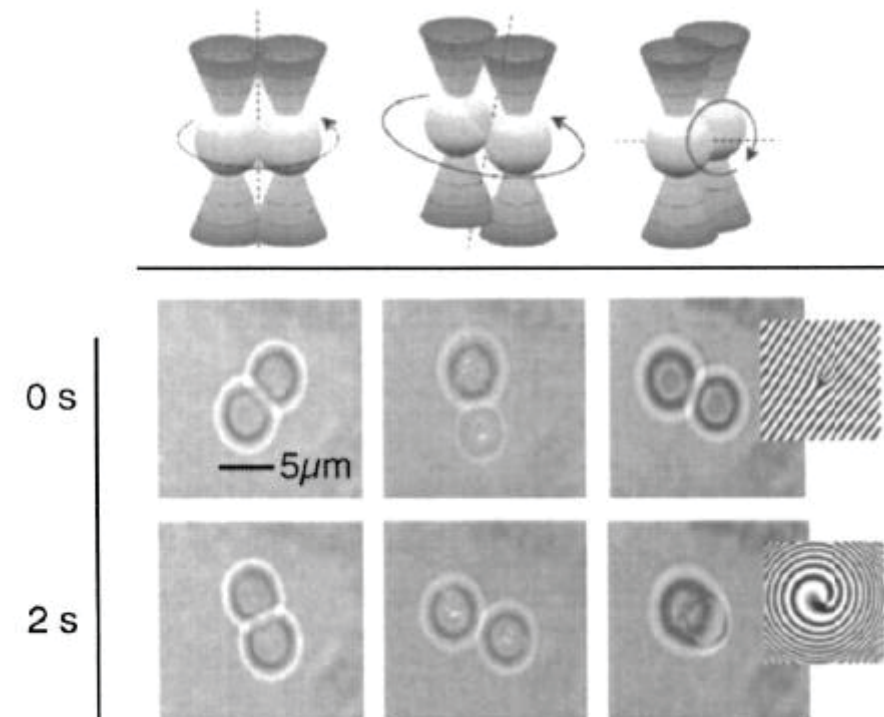
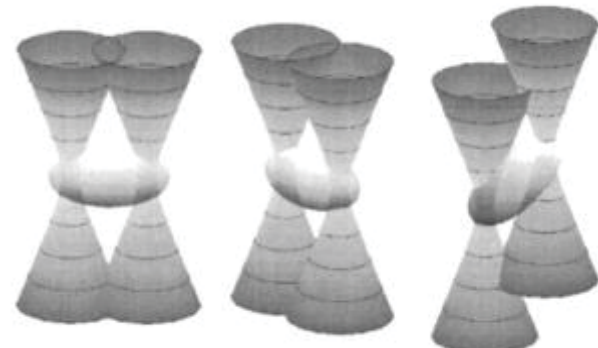
- Holographic Optical Tweezers (HOT) concept
- Large number of traps
- Versatile use
- Beam profile modification
- SLM required

Curtis, J. & Grier, D., 2003. Structure of Optical Vortices.
Physical Review Letters, 90(13), pp.13-16.

Optical trapping systems

Particle rotation in HOT

- Two traps for one object
- 3-D rotation
- 3-D translation



Bingelyte, V. et al., 2003. Optically controlled three-dimensional rotation of microscopic objects. *Applied Physics Letters*, 82(5), p.829.

Mechanical rotation

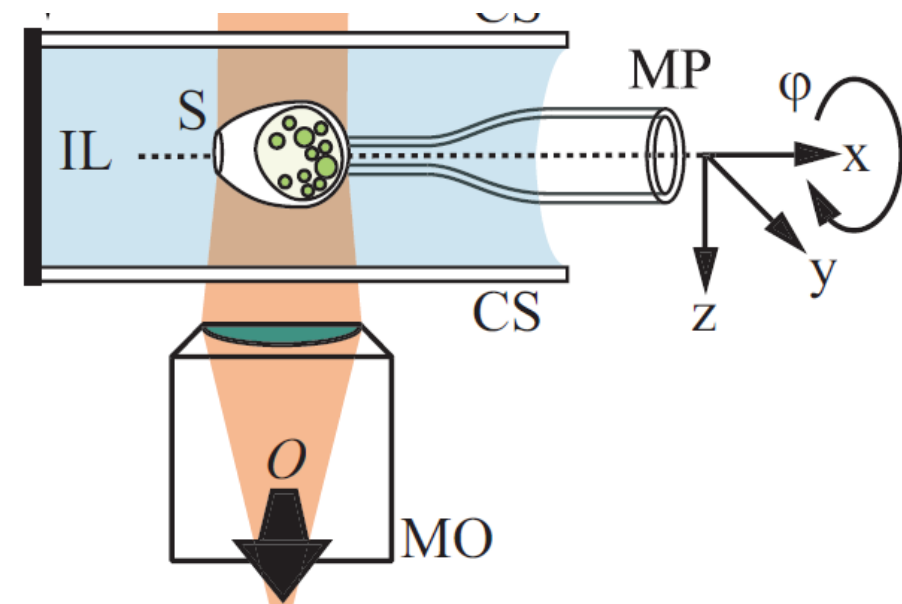
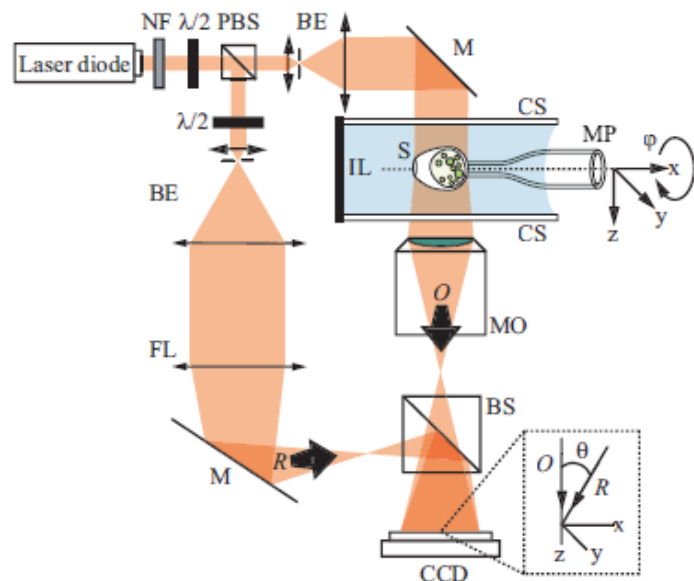


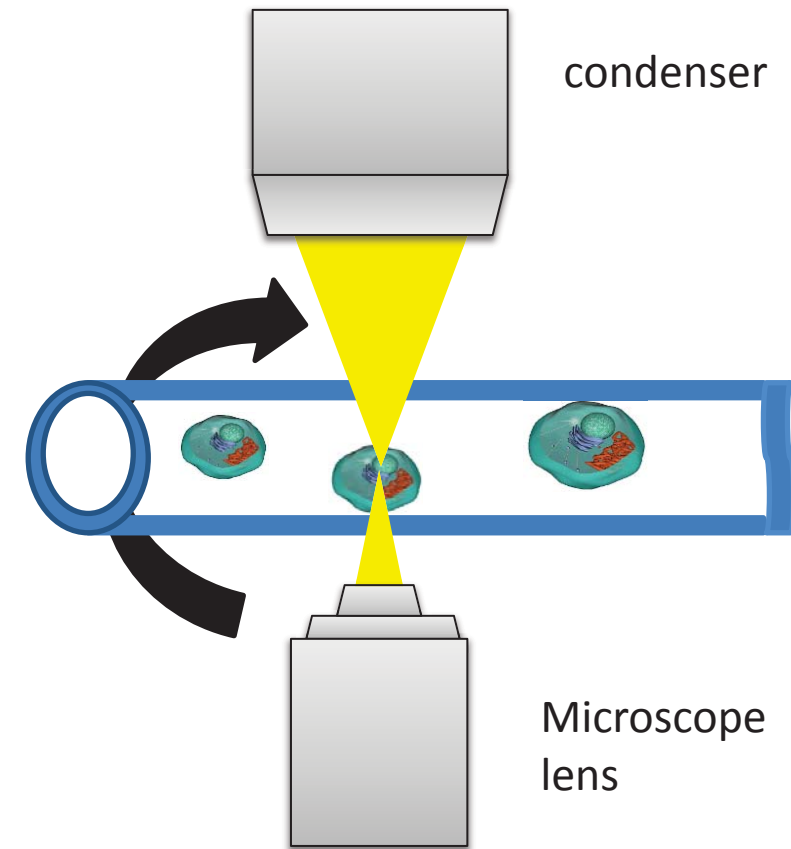
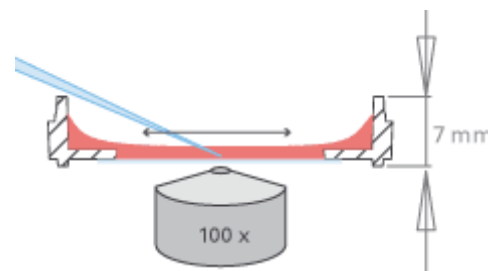
Fig. 2. Holographic microscope for transmission imaging: NF neutral density filter; PBS polarizing beam splitter; BE beam expander with spatial filter; $\lambda/2$ half-wave plate; MO microscope objective; FL field lens; M mirror; BS beam splitter; O object wave; R reference wave; MP micropipette; CS coverslip; S specimen; IL immersion liquid. Inset: a detail showing the off-axis geometry at the incidence on the CCD.

Charrière, F. et al., 2006. Living specimen tomography by digital holographic microscopy: morphometry of testate amoeba. *Optics express*, 14(16), pp.7005-13.

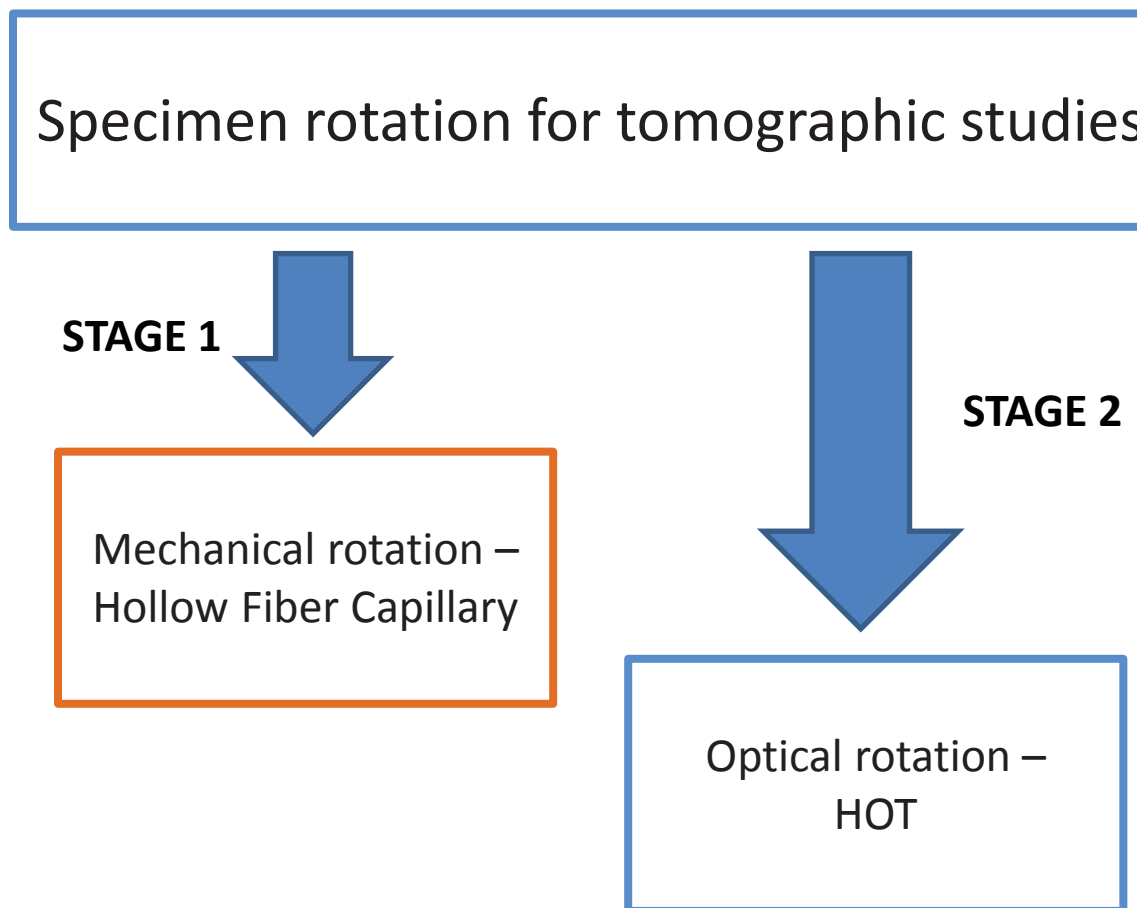
Mechanical rotation

Mechanical particle rotation

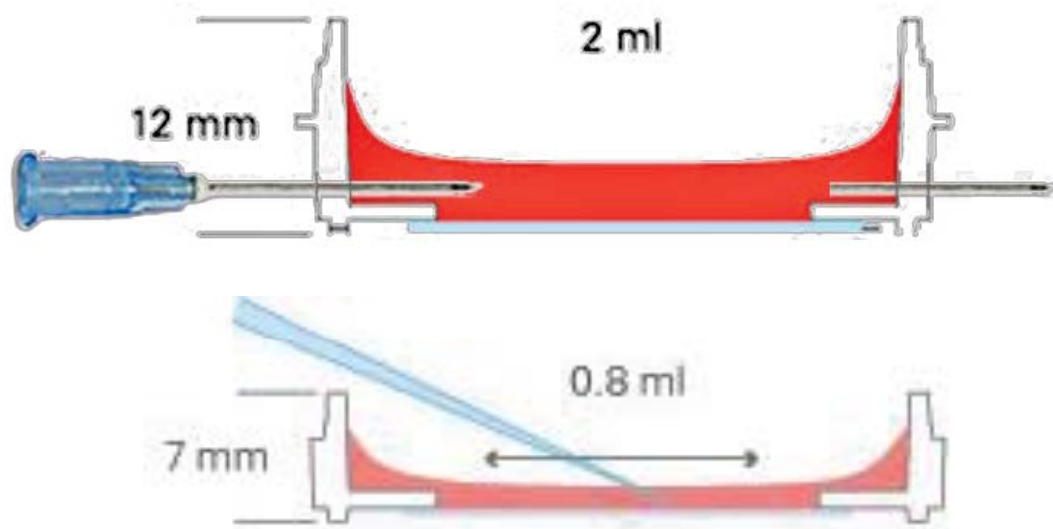
- Hollow core fiber - capillary
- Rotational fiber holder
- Inverted microscope
- Immersion liquid dish that would allow a fibre rotation



Specimen rotation - conclusion

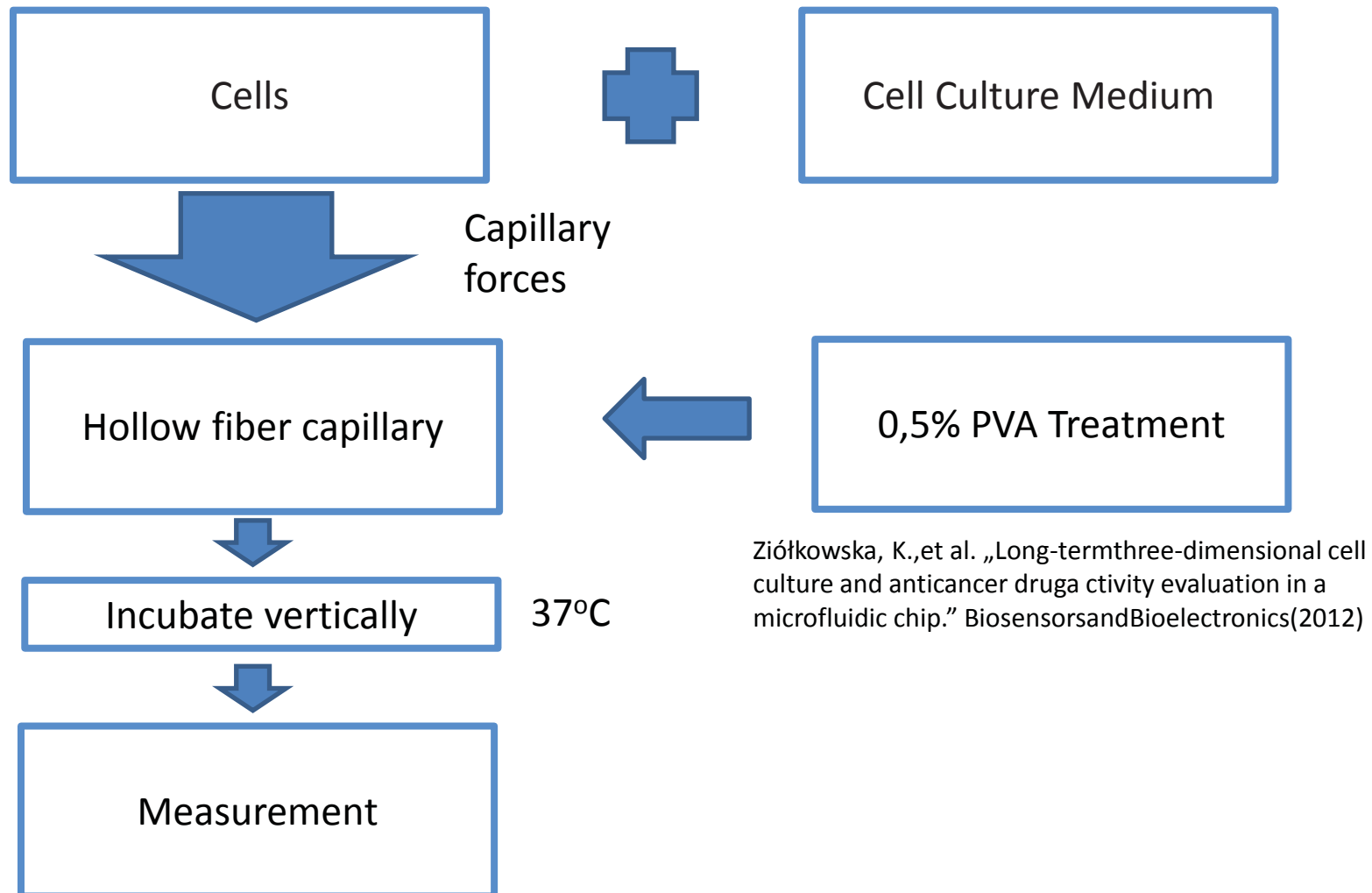


Mechanical specimen rotation



| Gauge | Needle ID [μm] | Capillary OD[μm] | Capillary ID [μm] |
|-------|----------------|------------------|-------------------|
| 25 | 260 | 250 | 140 |
| 24 | 311 | 300 | 111/212 |
| 23 | 337 | 340 | 128 |

Cell culture preparation



Cell culture preparation

| object | PVA coated | inside collagen 0,08% | inside collagen 0,16% | inside Agar 0,15% | inside Glycerin | outside immersion oil | Outside Phosphat Buffered Saline | Inner diameter [μm] | Incubation time | result |
|--------------------------------|------------|-----------------------|-----------------------|-------------------|-----------------|-----------------------|----------------------------------|----------------------------------|-----------------|--|
| HT1080 fibroblasts | + | + | | | | + | | 128 | 1h | most cells stick to the wall |
| HT1080 fibroblasts | + | | | | + | + | | 128 | 0h | cells stick to the wall and shrink |
| Agarose beads 30 μm | | | | | + | + | | 111 | 0h | good results, less diffraction |
| U937 Human Leukemia | + | | | + | | | + | 212 | 0h | good results, some cells are in the middle of the fiber, diffraction not important |
| HT1080 fibroblasts | + | | + | | | | + | 212 | 24h vertical | good results, most cells stick to the wall but some are in the middle of the fiber |
| HT1080 fibroblasts | | + | | + | | + | | 111 | 24h vertical | good results, strong cells, centered |

Cells under study

Fibrosarcoma

HT1080

- Fibroblastic sarcoma – malignant mesenchymal tumor derived from fibroblasts
- Fibroblasts are the most common cells of connective tissue



Pancreatic Tumor

PaTu-8988T

- Human pancreas tumor
- A suitable model for Adenocarcinoma Pancreas Tumor studies
- The most common pancreatic cancer



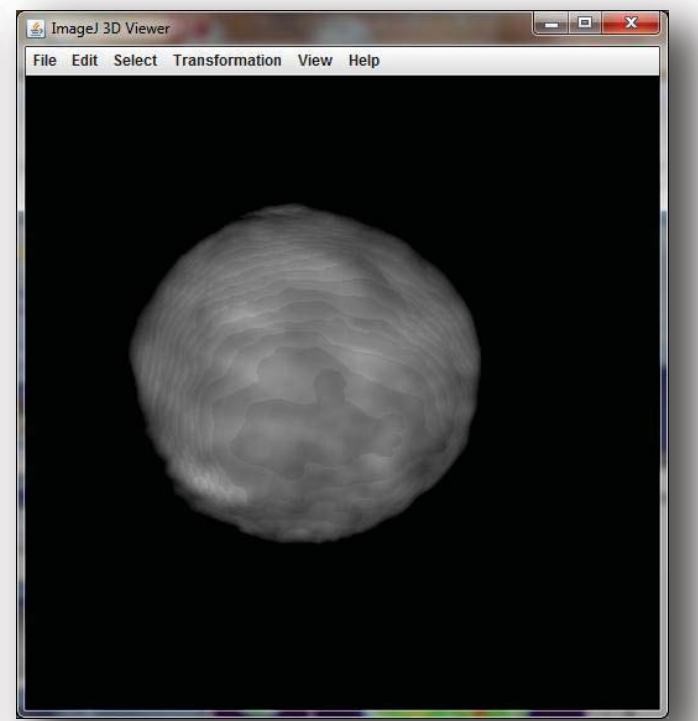
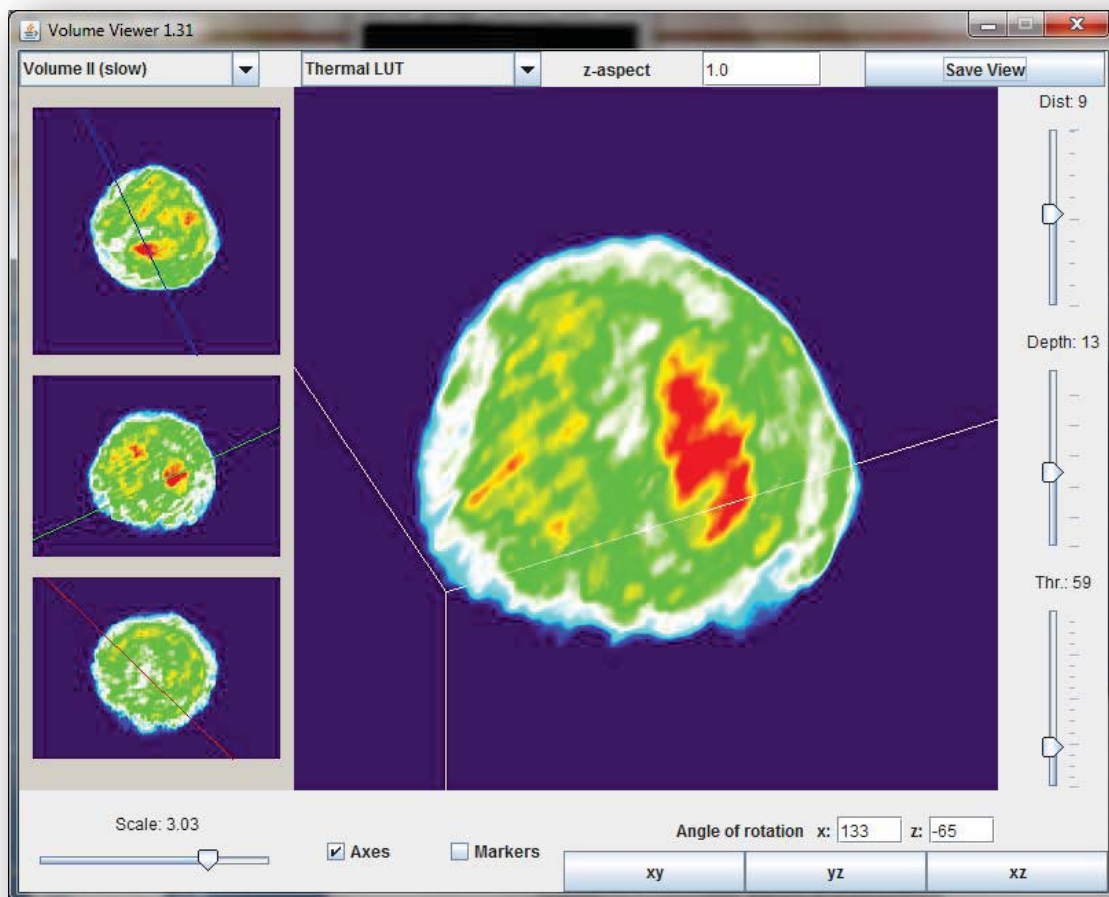
Human Leukemia

U937

- Lymphoma – cancer of the lymphocytes
- Are used to study the behaviour and differentiation of monocytes



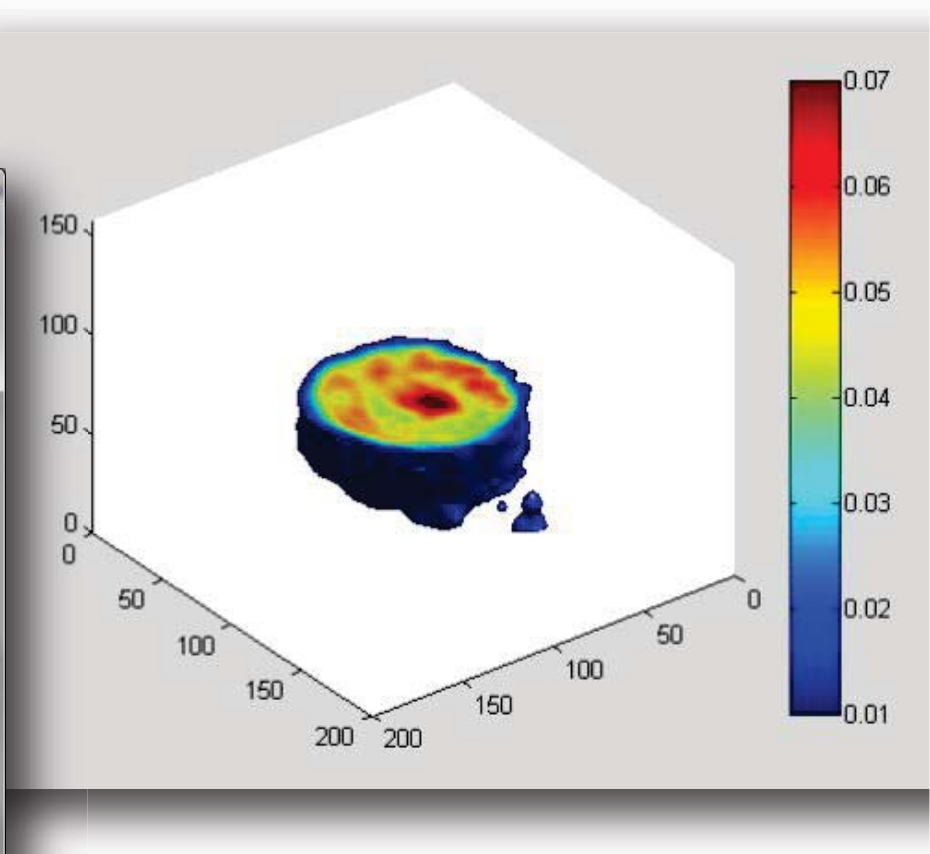
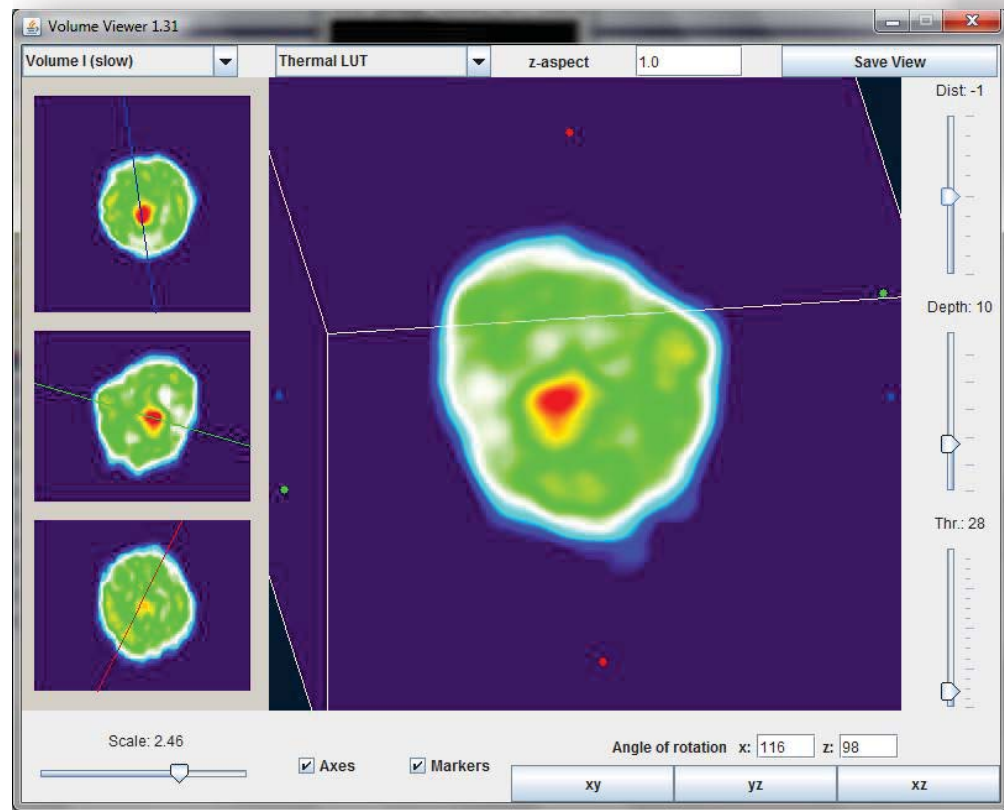
Results



U937 Human Leukemia cells
212/300 μm capillary

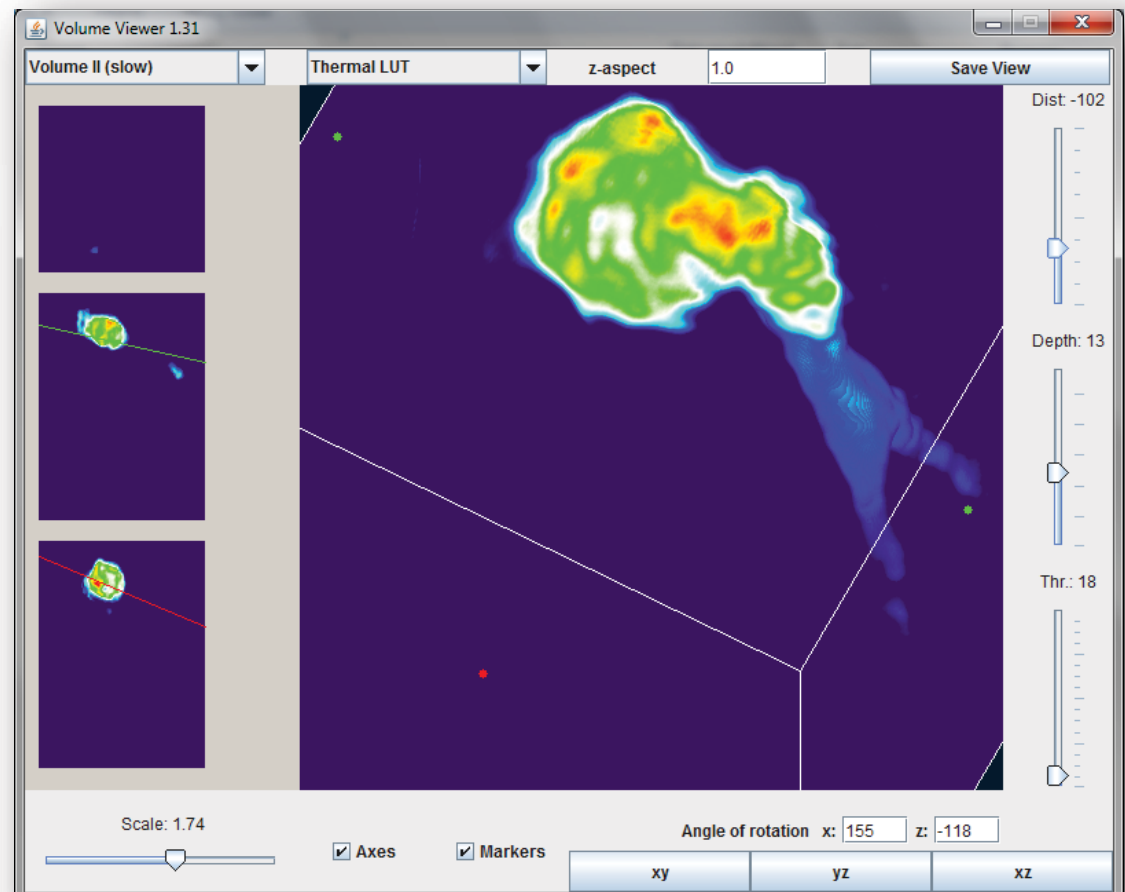
Results

PaTu8988-T cells
212/300 μm capillary

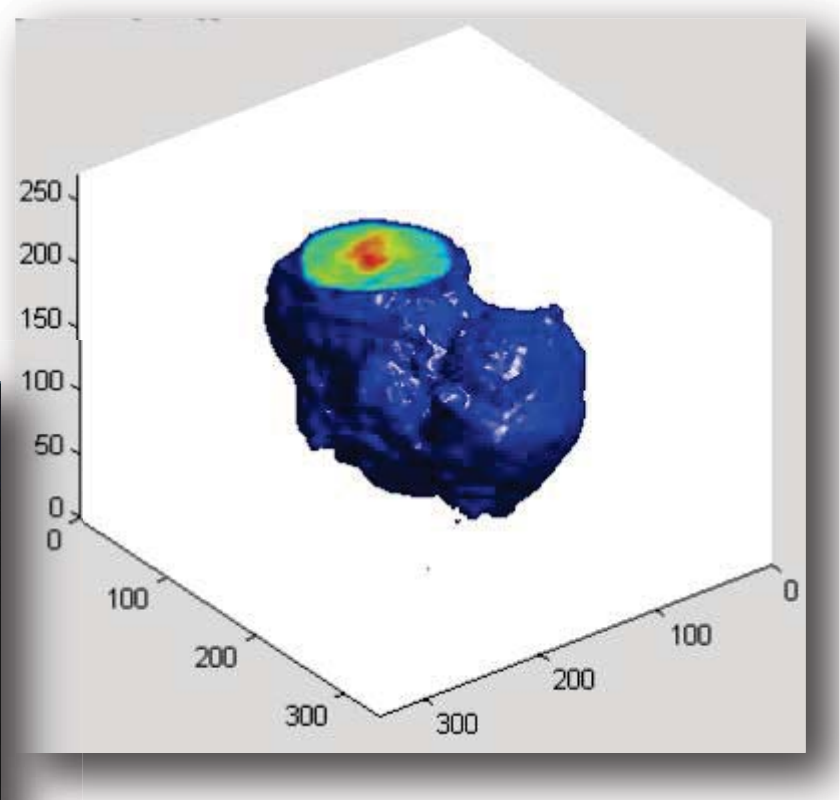
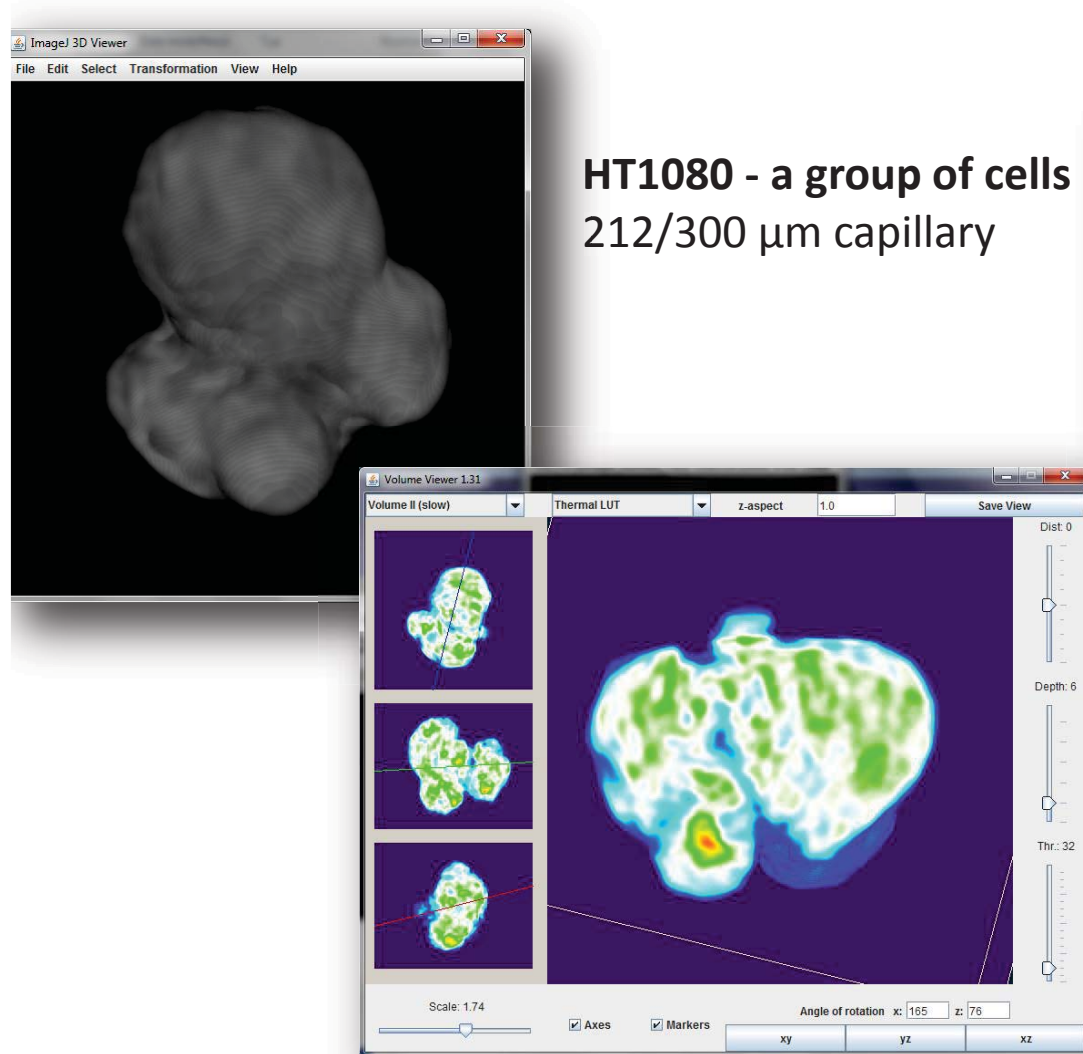


Results

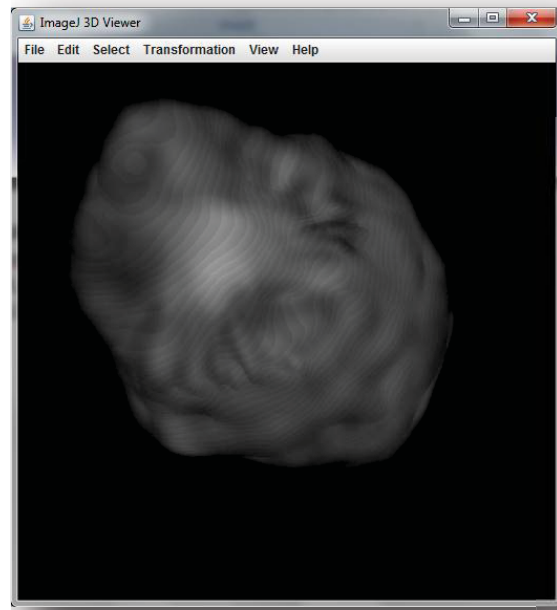
HT1080 Fibrosarcoma
212/300 μm capillary



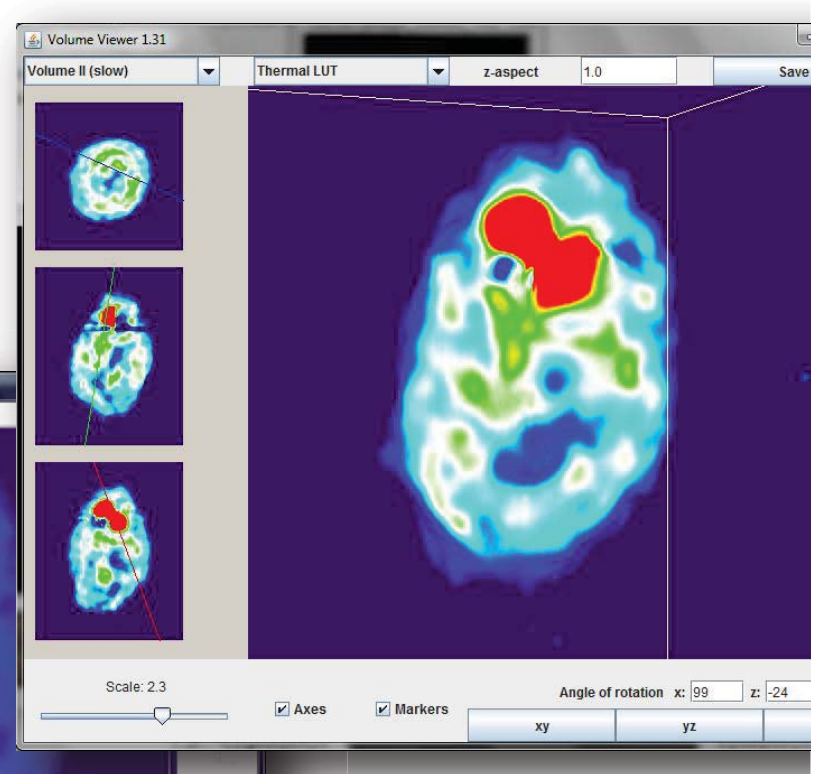
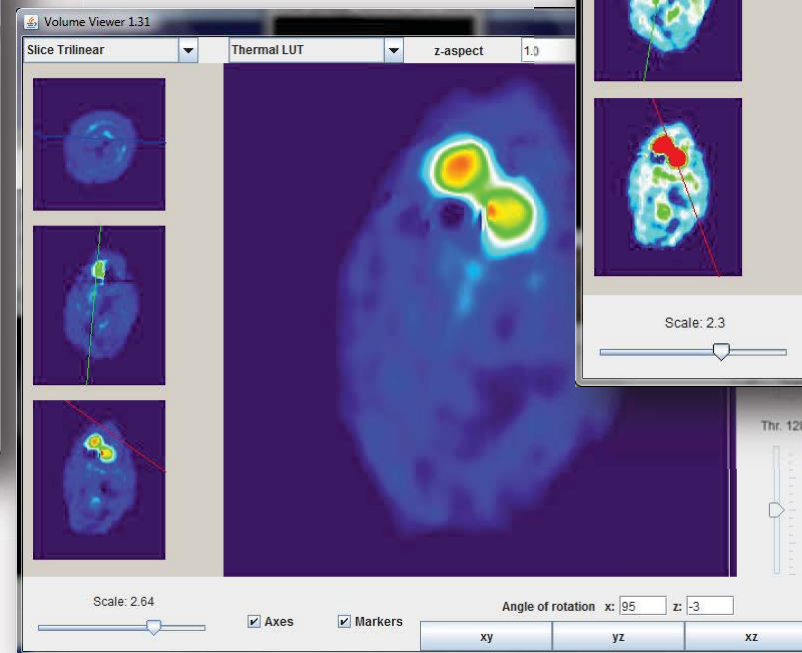
Results



Results



**HT1080 fibrosarcoma,
incorporated silica beads
 $\varnothing=3,44\mu\text{m}$; $n=1,435$
128/340 μm capillary**



Future work

- Resolve the matter of calibration and absolute refractive index value determination
- Reduce noise and diffraction artifacts
- Improve the algorithms for bigger phase gradients
- Improve algorithms for rec. with limited angle projections
- Introduce optical manipulation
- Adapt system for dynamic measurements

Final goal – one shot tomographic camera system for dynamic processes such as infections

References

1. Wedberg T. C., Stamnes J. J., and Singer W., Comparison of the filtered backpropagation and the filtered backprojection algorithms for quantitative tomography, *Appl. Opt.* 34 6575-6581 (1995)
2. Esmersoy C. and Miller D., Backprojection versus backpropagation in multidimensional linearized inversion, *Geophysics* 54 921-926 (1989)
3. Verhoeven D., Limited-data computed tomography algorithms for the physical sciences, *Appl. Opt.* 32 3736-3754 (1993)
4. Tam K. C. and Perez-Mendez V., Tomographical imaging with limited-angle input, *J. Opt. Soc. Am.* 71 582-592 (1981)
5. Medoff B. P., Brody W. R., Nassi M., and Macovski A., Iterative convolution backprojection algorithms for image reconstruction from limited data, *J. Opt. Soc. Am.* 73 1493-1500 (1983)
6. Sung Y., Choi W., Fang-Yen C., Badizadegan K., Dasari R. R., and Feld M. S., Optical diffraction tomography for high resolution live cell imaging, *Opt. Express* 17 266-277 (2009)
7. Kemper B. and von Bally G., Digital holographic microscopy for live cell applications and technical inspection, *Appl. Opt.* 47 A52-A61 (2008)
8. Dholakia, K. & Reece, P., 2006. Optical micromanipulation takes hold. *Nano today*, 1(1), pp.18-27.
9. Å, X.-cheng Y.A.O. & Hang, D.-zhong Z., 2004. Micro-Rotation by Flow-Induced Torque in an Optical Trap. *Optical Review*, 11(1), pp.4-6.

References

10. Ashok, P.C. & Dholakia, K., 2012. Optical trapping for analytical biotechnology. *Current opinion in biotechnology*, 23(1), pp.16-21.
11. Curtis, J. & Grier, D., 2003. Structure of Optical Vortices. *Physical Review Letters*, 90(13), pp.13-16.
12. Bingelyte, V. et al., 2003. Optically controlled three-dimensional rotation of microscopic objects. *Applied Physics Letters*, 82(5), p.829.
13. Carmon, G. & Feingold, M., 2011. Controlled alignment of bacterial cells with oscillating optical tweezers. *Journal of Nanophotonics*, 5(1), p.051803.
14. http://biologica.concord.org/webtest1/view_3D_cells.htm
15. http://ibidi.com/products/disposables/D_8013X_Dish35mm_low.html
16. Kreysing, M.K. et al., 2008. The optical cell rotator, *Optics express*, 16(21), pp.912-914.
17. Ziolkowska, K.,et al. Long-termthree-dimensional cell culture and anticancer druga ctivity evaluation in a microfluidic chip. *BiosensorsandBioelectronics*(2012)
18. Green, E. R. et al., Comparison of refractive index estimated from single-cell and bulk optical properties,
19. Charrière, F. et al. Cell refractive index tomography by digital holographic microscopy, *Optics Letters* 31(2), 2006
20. Choi W, Yu CC, Fang-Yen C, Badizadegan K, Dasari RR, Feld MS. Field-based angle-resolved light-scattering study of single live cells. *Opt. Lett.* 2008;33:1596–1598